VTRC
Virginia Transportation Research Council

We Bring Innovation to Transportation

Influence of Aggregate Morphology and Grading on the Performance of 9.5-mm Stone Matrix Asphalt Mixtures

http://www.virginiadot.org/vtrc/main/online_reports/pdf/19-r15.pdf

Yufeng Liu
Teaching Assistant
Virginia Tech

Harikrishnan Nair, Ph.D., P.E.
Senior Research Scientist
Virginia Transportation Research Council

D. Stephen Lane
Associate Principal Research Scientist
Virginia Transportation Research Council

Linbing Wang, Ph.D., P.E.
Professor
Virginia Tech

Wenjuan Sun, Ph.D.
Research Associate
Lehigh University

Final Report VTRC 19-R15

VIRGINIA TRANSPORTATION RESEARCH COUNCIL
530 Edgemont Road, Charlottesville, VA 22903-2454
vtrc.virginiadot.org

Standard Title Page - Report on Federally Funded Project

1. Report No.: FHWA/VTRC 19-R15	2. Government Accession No.:	3. Recipient's Catalog No.:
4. Title and Subtitle: Influence of Aggregate Morphology and Grading on the Performance of 9.5-mm Stone Matrix Asphalt Mixtures		5. Report Date: May 2019 6. Performing Organization Code:
7. Author(s): Yufeng Liu, Harikrishnan Nair, Ph.D., P.E., D. Stephen Lane, Linbing Wang, Ph.D., P.E., and Wenjuan Sun, Ph.D.		8. Performing Organization Report No.: VTRC 19-R15
9. Performing Organization and Address: Virginia Transportation Research Council 530 Edgemont Road Charlottesville, VA 22903		10. Work Unit No. (TRAIS): 11. Contract or Grant No.: 101905
12. Sponsoring Agencies' Name and Address: Virginia Department of Transportation 1401 E. Broad Street Richmond, VA 23219 Federal Highway Administration 400 North 8th Street, Room 750 Richmond, VA 23219-4825		13. Type of Report and Period Covered: Final 14. Sponsoring Agency Code:
15. Supplementary Notes: This is an SPR-B report.		

16. Abstract:

Stone matrix asphalt (SMA) is a gap-graded hot mix asphalt with a high percentage of coarse aggregate and a high asphalt content. SMA is the typical gap-graded mixture used in Virginia that is intended to maximize rutting resistance and durability with a stable stone-on-stone skeleton held together by a rich mixture of asphalt binder. The field performance of SMA in Virginia has been generally excellent. However, several SMA pavements have undergone premature failure, and factors related to both pavement structure and materials have been identified as causes for the poor performance. A detailed forensic study recommended a specification change for gradation of SMA-9.5 mixtures to provide improved stability. The Virginia Department of Transportation adopted a new aggregate gradation in 2012 for these mixtures. Aggregate morphological characteristics, including sphericity, flatness ratio, elongation ratio, angularity, and texture, have been recognized as major factors influencing the performance of aggregate and asphalt mixtures. The current study demonstrated via laboratory methods the stability of mixtures conforming to the Virginia Department of Transportation's new grading specification and the effects of aggregate morphology and asphalt binder properties on stability.

SMA mixtures designed and produced by different contractors using aggregates from different quarries in Virginia were included in the study. SMA mixtures and samples of the aggregates used in production were obtained for laboratory evaluation of the structural stability and aggregate characteristics of the mixtures. All mixtures met the criterion of $VCA_{MIX} < VCA_{DRC,}$ indicating good stone-on-stone contact and a denser coarse aggregate fraction. Flow number and asphalt pavement analyzer results showed better rutting resistance of all mixtures with revised gradation. In both confined and unconfined flow number tests, polymer-modified binders (PG 64E-22 or PG 76-22) showed a lower flow number slope compared to that of PG 70-22 (PG 64H-22) binders, indicating better rutting resistance. SMA mixtures with polymer-modified binder also showed excellent fatigue performance. All mixtures showed a maximum number of cycles of 1,200 in the Texas overlay test, showing the excellent reflection crack resistance of these mixtures. Regression analyses were conducted between weighted mean morphological characteristics and performance parameters. Aggregate morphological characteristics were found to play an important role in the mechanical performance of SMA mixtures and the uncompacted void content of the coarse aggregates. Results showed that using more spherical (equant), angular, or better-crushed rough coarse aggregate particles in SMA mixtures can improve the resistance of the SMA to rutting. In addition, aggregates with fewer flat and elongated aggregate particles can contribute to better rutting performance of SMA mixtures. Results also showed that better rutting resistance can be obtained using polymer-modified binders even if the aggregate morphological characteristics are slightly less favorable.

17 Key Words: SMA, aggregate morphology, dynamic modulus, fatigue test, rutting test, performance grade, polymer-modified binder	18. Distribution Statement: No restrictions. This document is available to the public through NTIS, Springfield, VA 22161.		
19. Security Classif. (of this report): Unclassified	20. Security Classif. (of this page): Unclassified	21. No. of Pages: 77	22. Price:

FINAL REPORT

INFLUENCE OF AGGREGATE MORPHOLOGY AND GRADING ON THE PERFORMANCE OF 9.5-MM STONE MATRIX ASPHALT MIXTURES

Yufeng Liu
Teaching Assistant
Virginia Tech

Harikrishnan Nair, Ph.D., P.E.
Senior Research Scientist
Virginia Transportation Research Council

D. Stephen Lane
Associate Principal Research Scientist
Virginia Transportation Research Council

Linbing Wang, Ph.D., P.E.
Professor
Virginia Tech

Wenjuan Sun, Ph.D.
Research Associate
Lehigh University

In Cooperation with the U.S. Department of Transportation
Federal Highway Administration

Virginia Transportation Research Council
(A partnership of the Virginia Department of Transportation
and the University of Virginia since 1948)

Charlottesville, Virginia

May 2019
VTRC 19-R15

DISCLAIMER

The contents of this report reflect the views of the authors, who are responsible for the facts and the accuracy of the data presented herein. The contents do not necessarily reflect the official views or policies of the Virginia Department of Transportation, the Commonwealth Transportation Board, or the Federal Highway Administration. This report does not constitute a standard, specification, or regulation. Any inclusion of manufacturer names, trade names, or trademarks is for identification purposes only and is not to be considered an endorsement.

ABSTRACT

Stone matrix asphalt (SMA) is a gap-graded hot mix asphalt with a high percentage of coarse aggregate and a high asphalt content. SMA is the typical gap-graded mixture used in Virginia that is intended to maximize rutting resistance and durability with a stable stone-on-stone skeleton held together by a rich mixture of asphalt binder. The field performance of SMA in Virginia has been generally excellent. However, several SMA pavements have undergone premature failure, and factors related to both pavement structure and materials have been identified as causes for the poor performance. A detailed forensic study recommended a specification change for gradation of SMA-9.5 mixtures to provide improved stability. The Virginia Department of Transportation adopted a new aggregate gradation in 2012 for these mixtures. Aggregate morphological characteristics, including sphericity, flatness ratio, elongation ratio, angularity, and texture, have been recognized as major factors influencing the performance of aggregate and asphalt mixtures. The current study demonstrated via laboratory methods the stability of mixtures conforming to the Virginia Department of Transportation's new grading specification and the effects of aggregate morphology and asphalt binder properties on stability.

SMA mixtures designed and produced by different contractors using aggregates from different quarries in Virginia were included in the study. SMA mixtures and samples of the aggregates used in production were obtained for laboratory evaluation of the structural stability and aggregate characteristics of the mixtures. All mixtures met the criterion of $VCA_{MIX} < VCA_{DRC,}$ indicating good stone-on-stone contact and a denser coarse aggregate fraction. Flow number and asphalt pavement analyzer results showed better rutting resistance of all mixtures with revised gradation. In both confined and unconfined flow number tests, polymer-modified binders (PG 64E-22 or PG 76-22) showed a lower flow number slope compared to that of PG 70-22 (PG 64H-22) binders, indicating better rutting resistance. SMA mixtures with polymer-modified binder also showed excellent fatigue performance. All mixtures showed a maximum number of cycles of 1,200 in the Texas overlay test, showing the excellent reflection crack resistance of these mixtures. Regression analyses were conducted between weighted mean morphological characteristics and performance parameters. Aggregate morphological characteristics were found to play an important role in the mechanical performance of SMA mixtures and the uncompacted void content of the coarse aggregates. Results showed that using more spherical (equant), angular, or better-crushed rough coarse aggregate particles in SMA mixtures can improve the resistance of the SMA to rutting. In addition, aggregates with fewer flat and elongated aggregate particles can contribute to better rutting performance of SMA mixtures. Results also showed that better rutting resistance can be obtained using polymer-modified binders even if the aggregate morphological characteristics are slightly less favorable.

FINAL REPORT

INFLUENCE OF AGGREGATE MORPHOLOGY AND GRADING ON THE PERFORMANCE OF 9.5-MM STONE MATRIX ASPHALT MIXTURES

Yufeng Liu
Teaching Assistant
Virginia Tech

Harikrishnan Nair, Ph.D., P.E.
Senior Research Scientist
Virginia Transportation Research Council

D. Stephen Lane
Associate Principal Research Scientist
Virginia Transportation Research Council

Linbing Wang, Ph.D., P.E.
Professor
Virginia Tech

Wenjuan Sun, Ph.D.
Research Associate
Lehigh University

INTRODUCTION

Hot mix asphalt (HMA) concrete is composed of up to approximately 90% to 95% mineral aggregates by weight and up to 80% to 90% aggregates by volume. The mineral aggregate predominantly plays a vital role in the mechanical performance of asphalt concrete. According to the basic material properties and composition of the aggregate skeleton, asphalt concrete mixtures can be classified as dense graded or gap graded. Dense-graded mixtures, also known as Superpave mixtures in Virginia, are asphalt mixtures with a uniform distribution of aggregate sizes along the maximum density line. Stone matrix asphalt (SMA) is a gap-graded HMA with a high percentage of coarse aggregate and a high asphalt content. Gap-graded mixtures are characterized by a non-uniform distribution of aggregate sizes. These mixtures contain aggregates retained on the larger and smaller sieves but with little aggregate retained on the middle sieves. As with dense-graded mixtures, gap-graded mixtures are identified based on nominal maximum aggregate size.

SMA is the most common gap-graded mixture used in Virginia and is composed of a gap-graded aggregate that is intended to maximize rutting resistance and durability with a stable stone-on-stone skeleton held together by a rich mixture of asphalt binder, mineral filler, and cellulose fibers. SMAs are recommended only for placements in heavy traffic conditions

because of their higher cost. From a production and placement standpoint, a fiber feeder machine is required, material transfer vehicles are mandatory, and paver speeds are generally slower to ensure that density requirements are met (McGhee et al., 2010). The rut resistance of SMA is achieved through stone-on-stone contact by specifying the coarse aggregate fraction of the mixture to be between 70% and 80%; durability is enhanced through the rich asphalt mastic. To ensure durability of SMA mixtures, a stiff mastic containing a high liquid asphalt content (6.3% minimum specified in Virginia for SMA-9.5), a high amount of mineral filler (9% to 11%), and a small amount of cellulose fibers (minimum of 0.3%) is typically specified.

SMA mixtures have been used extensively by the Virginia Department of Transportation (VDOT) throughout Virginia since 2003. The field performance of SMA in Virginia has been generally excellent, with reported service lives of 15 to 18 years (McGhee et al., 2010). However, several SMA pavements have undergone premature failures. McGhee et al. (2010) identified factors related to both pavement structure and material as causes for the poor performance of some VDOT SMA-surfaced pavements. Material-related failures including flushing, rutting, and surface distortions were observed at intersections for an SMA-9.5 mixture with a Performance Grade (PG) 70-22 binder (Figure 1). SMA mixtures with finer aggregates appeared to perform worse than SMA mixtures with larger coarse aggregates (SMA-12.5). The SMA-9.5 mixture is a surface mixture with a fine to medium nominal maximum aggregate size (3/8 in [9.5 mm]) generally placed at 1½ in of thickness. Apeagyei et al. (2011) conducted a detailed forensic study and concluded that a combination of traffic characteristics (slow moving, turning, or stopped); aggregate packing (higher voids in the coarse aggregate in the mixture [VCA_{MIX}], lower fineness modulus, higher percent passing the No. 4 sieve); and binder amount may have contributed to the observed poor SMA field performance. The study recommended a specification change for the gradation of SMA-9.5 mixtures to provide improved stability.

Figure 1. Flushing, Rutting, and Shoving in SMA-9.5 Pavement on US 17 Near Opal, Virginia. SMA = stone matrix asphalt. *Source:* McGhee et al. (2010).

VDOT adopted a new gradation for SMA-9.5 mixtures in 2012. The new gradation along with the previous gradation is shown in Table 1. The primary change was the reduction of the maximum percent passing the No. 4 sieve from 40% to 32%. In addition, minor changes were made with regard to the 3/8 in and No. 200 sieves. The purpose of changing percent passing for the 3/8 in and No. 4 sieves was to coarsen the mixture and improve stone-on-stone contact.

An additional requirement placed on coarse aggregates for use in SMA mixtures was a limitation on the percentage of particles with a high aspect ratio (e.g., >3:1, >5:1), commonly referred to as flat and elongated (F&E) particles. The purpose of this requirement was to avoid extreme shapes that could impair the ability of the aggregate to pack into a stone-on-stone skeleton or break easily during compaction, changing the aggregate gradation. Compliance with the F&E requirements is currently determined by manual measurement of individual particles. Advanced imaging technology with a computer-automated system is a promising tool in providing precise data for aggregate morphological characteristics. With the ability to characterize the aggregate morphology objectively and quantitatively, without tedious human interaction, more effort can be focused on simple performance tests and wheel tracking tests. The laboratory performance–based results can be analyzed to link better the aggregate morphological characteristics with the mechanical performance of asphalt mixtures. A better and more scientific understanding of the effect of aggregate morphology on the performance of asphalt mixtures is needed to reduce the production costs for mixtures and improve long-term pavement performance.

Table 1. Stone Matrix Asphalt (SMA) Design Gradation Range

VDOT Specification	Percent by Weight Passing Sieve							
	1 in	**¾ in**	**½ in**	**3/8 in**	**No. 4**	**No. 8**	**No. 30**	**No. 200**
New SMA-9.5 specification[a]	---	100	90-100	65-75	25-32	15-25	---	9-11
Previous SMA-9.5 specification[b]	----	100	90-100	70-85	25-40	15-25	---	10-12

--- = No requirement

[a] VDOT 2016 *Road and Bridge Specifications.*

[b] VDOT 2007 *Road and Bridge Specifications.*

PURPOSE AND SCOPE

The purpose of this study was to examine VDOT's revised grading specifications for the design of SMA mixtures with smaller aggregates and the impact of aggregate morphology on the structural stability of the mixture. A limited suite of aggregates representing the range of particle morphology typical of Virginia sources was characterized using an image analysis system. SMA mixtures designed and produced by different contractors using aggregates from different quarries in Virginia were included in the study. SMA mixtures and samples of the aggregates used in production were obtained for a laboratory evaluation of the structural stability and aggregate characteristics of the mixtures.

The study had the following objectives:

1. Assess the volumetric properties, binder properties, and laboratory performance of SMA mixtures produced under the revised gradation specification.

2. Quantify coarse aggregate morphological characteristics, including sphericity, flatness ratio, elongation ratio, F&E ratio, angularity, and texture, using an image analysis system and the uncompacted void content.

3. Correlate aggregate morphological characteristics captured by image analysis techniques with the mechanical performance of SMA mixtures obtained from the laboratory performance–based tests.

4. Correlate aggregate morphological characteristics captured by image analysis techniques with the uncompacted void content of coarse aggregates.

5. Assess the field performance of these mixtures using data from VDOT's Pavement Management System (PMS).

METHODS

Literature Review

A literature review was conducted by searching various transportation-related databases such as Transport Research International Documentation (TRID), the catalog of Transportation Libraries (TLCat), the Catalog of Worldwide Libraries (WorldCat), and the Transportation Research Board Research in Progress (RiP) and Research Needs Statements (RNS) databases.

Materials and Mix Design

SMA-9.5 mixtures were collected from field projects that were paved in 2013, 2014, and 2015. SMA mixtures were produced in accordance with VDOT's specifications for SMA mix design (VDOT, 2016). Virginia aggregates used for mixtures quarried at Bealeton, Stuarts Draft, Piney River, Leesburg, Goose Creek, Chantilly, and Garrisonville were also collected. Table 2 presents the mix designs for all SMA mixtures, including the size, type, fiber content, recycled asphalt pavement (RAP) content, and asphalt binder content. As shown, SMA mixtures marked as 13-1070, 13-1081, 14-1021, 14-1047, and 15-1012 were prepared using four aggregate fractions. SMA mixtures marked as 15-1068, 15-1080, and 15-1084 included three aggregate fractions. Three types of asphalt binder were selected: PG 70-22, PG 76-22, and PG 76-28 High Polymer (HP). The asphalt binder content in each SMA mixture varied around 6.3% to 6.4% by weight except for one mixture in which it was 6.8%. There was a total of 23 types of coarse aggregates in the SMA mixtures. These aggregates mainly included the following rock types: aplite, limestone (No. 10 screenings only), quartzite, arkose, diabase, and amphibolite. Table 3 shows aggregate properties including aggregate material type, size, and origin and the crushers used to process the aggregates.

Table 2. Mix Designs

Material	SMA-9.5 (70-22)	SMA-9.5 (70-22)	SMA-12.5 (76-22)	SMA-9.5 (76-22)	SMA-9.5 (64E-22)	SMA-9.5 (76-28HP)	SMA-9.5 (64H-22)	SMA-9.5 (64E-22)
Mix ID **Aggregate ID**	**13-1070** **13-1071**	**13-1081** **13-1073**	**14-1021** **14-1019**	**14-1047** **14-1048**	**15-1012** **15-1013**	**15-1068** **15-1069**	**15-1080**	**15-1084**
No. 78	30% Diabase (Traprock)	10% Quartzite	29% Diabase (Traprock)	30% Diabase (Traprock)	61% Diabase (Traprock)	52% (Amphibolite)	52% (Amphibolite)	52% (Amphibolite)
No. 8	34% Diabase (Traprock)	50% Aplite	24% Diabase (Traprock)	34% Diabase (Traprock)	12% (No. 28) Diabase (Traprock)	23% (Amphibolite)	23% (Amphibolite)	23% (Amphibolite)
No. 30 (No. 57 scalped of + 19 mm)	13% Diabase (Traprock)	---	23% Diabase (Traprock)	13% Diabase (Traprock)	---	---	---	-
No. 68		20% Aplite	---	---	---	---	---	---
No. 10 Screenings	-	11% Limestone	---	---	---	---	---	---
Filler	10% Diabase (Traprock)	8% Limestone	12%	11% Diabase (Traprock)	13%	10%	10%	10%
Additives (Fiber)	0.3%	0.4%	0.3%	0.3%		0.3%	0.3%	0.3%
Recycled Asphalt Pavement, -½ in	12%	-	12%	12%	10%	15%	15%	15%
Asphalt Binder	6.3% (PG 70-22)	6.8% (PG 70-22)	6.3% (PG 76-22)	6.3% (PG 76-22)	6.3% (PG 76-22)	6.4% (PG 76-28HP)	6.4% (PG 70-22)	6.4% (PG 76-22)
VCA_{DRC}	41.8%	42.2%	42.6%	41.8%	47.1%	41.9%	41.9%	41.9%

--- = **n**ot used.

Table 3. Aggregate Materials Information

Aggregate ID	Label on Container	Aggregate Material Type	Size[a]	Origin	Crusher
1	13-1073 Staunton #8	Aplite	No. 8	Piney River	Jaw crusher
2	13-1073 Staunton #10	Limestone	No. 10	Rockydale (Staunton Lime)	Impact crusher
3	13-1073 Staunton #68	Aplite	No. 68	Piney River	Impact crusher
4	13-1073 Staunton #78	Quartzite, Arkose	No. 78	Stuarts Draft	Impact crusher
5	13-1071 Bealeton #30	Diabase	No. 57 with +3/4 in removed	Bealeton-13	Cone crusher
6	13-1071 Bealeton #60	Diabase	No. 8	Bealeton-13	Cone crusher
7	13-1071 Bealeton #78	Diabase	No. 78	Bealeton-13	Cone crusher
8	13-1071 Bealeton RAP	RAP	-1/2 in	Stockpiled at Bealeton-13	---
9	14-1048 Bealeton #30	Diabase	No. 57 with +3/4 in removed	Bealeton-14	Cone crusher
10	14-1048 Bealeton #60	Diabase	No. 8	Bealeton-14	Cone crusher
11	14-1048 Bealeton #78	Diabase	No. 78	Bealeton-14	Cone crusher
12	14-1048 Bealeton RAP	Diabase	-1/2 in	Bealeton-14	Cone crusher
13	14-1019 Leesburg #8	Diabase	No. 8	Leesburg	Cone crusher
14	14-1019 Leesburg #78	Diabase	No. 78	Leesburg	Cone crusher
15	14-1019 Leesburg RAP	RAP	-1/2 in	Leesburg	---
16	14-1019 Goose Creek #30	Diabase	No. 57 with +3/4 in removed	Goose Creek	Impact crusher
17	15-1012 Chantilly #28	Diabase	No. 57 with +½ in removed	Chantilly	Cone crusher
18	15-1012 Chantilly #78	Diabase	No. 78	Chantilly	Cone crusher
19	15-1012 Chantilly #10	Diabase	No. 10	Chantilly	Cone crusher
20	15-1012 Chantilly RAP	RAP	-1/2 in	Chantilly	---
21	15-1069[b] Garrisonville #8	Amphibolite	No. 8	Garrisonville	Gyratory crusher
22	15-1069 Garrisonville #78	Amphibolite	No. 78	Garrisonville	Gyratory crusher
23	15-1069 RAP	RAP	Recycled, 1/2 in	Garrisonville	---

RAP = recycled asphalt pavement; --- = crusher not used.

[a] Aggregate size No. 8 is nominal size 3/8 to 0.094 in (No. 8 sieve) (9.5 to 2.36 mm); aggregate size No. 10 is nominal size No. 4 to 0 (2.36 to 0 mm); aggregate size No. 68 is nominal size 3/4 in to No. 8 (19 to 2.36 mm); aggregate size No. 78 is nominal size 1/2 in to No. 4 (12.5 to 4.75 mm); No. 57 aggregate ranges from 1 to 0.19 in (25 to 4.75 mm); Bealeton-13 means aggregates were selected from Bealeton in 2013; Bealeton-14 means aggregates were selected from Bealeton in 2014.

[b] Aggregates of 15-1069 in SMA-9.5 are the same as aggregates of 15-1080 and 15-1084.

Volumetric analyses were performed for all mixtures. Gyratory pills 150 mm in diameter were compacted to 75 gyrations for volumetric determination in accordance with VDOT specifications. Data collected included asphalt content for each type of mixture and gradations of all types of aggregates; bulk and Rice specific gravities (G_{mb} and G_{mm}); voids in total mixture (VTM); voids in mineral aggregate (VMA); voids filled with asphalt (VFA); aggregate bulk and effective specific gravities (G_{sb} and G_{se}); dust/asphalt ratio; percent binder absorbed (P_{ba}); and effective binder content (P_{be}).

Aggregate Tests

Morphological Characteristics

The improved Fourier transform interferometry (FTI) image analysis system (FTI system) was used to measure the morphological properties of coarse aggregates, which were retained on a 2.36 mm sieve after passing a 12.5 mm sieve. All coarse aggregate samples were sieved into four size ranges: 2.36 to 4.75 mm; 4.75 to 9.5 mm; 9.5 to 12.5 mm; and 12.5 to 19 mm (No. 8 to No. 4; No. 4 to 3/8 in; 3/8 in to 1/2 in; and 1/2 in to ¾ in). In this investigation, a total of 120 particles were scanned for each type of aggregate.

The Improved FTI System

The improved FTI system is considered an important tool to characterize aggregate morphologies. It is based on the FTI system (Lally, 2010), which is also a three-dimensional (3-D) surface profilometer with a simple fiber optic coupler in order to form a Young's double-pinhole interferometer. In the improved FTI system, the following improvements were made: (1) a new charge-coupled device (CCD) camera replaced the original CCD camera in the FTI system, improving the image resolution from 35.4 μm per pixel to 28.47 μm per pixel in the horizontal plane; and (2) computational time was reduced via the application of new programs with a more user-friendly graphical interface.

The improved FTI system can capture images in either single-particle mode or multiple-particle mode. Laser lights with wave lengths of 675 nm and 805 nm were input through the fiber optic switch. A 45 degree-angled mirror was used to reflect the fringe projection on the aggregate surface. A higher-resolution CCD camera was used to capture the aggregate surface image. The image was then analyzed through the Fourier transform method. The surface profile of each aggregate was reconstructed using the phases of the fringe pattern on the aggregate surface. The 3-D coordinates of the top surface of the aggregate can be obtained through three images: one image taken with visible light and two images taken with laser lights with wavelengths of 675 nm and 805 nm, respectively. In the improved FTI system, the image resolutions in the x-axis and y-axis are 28.47 μm per pixel, and the z-axis resolution is 20 μm.

Figure 2 shows the improved FTI system. Additional details about the FTI system are available (Sun et al., 2012; Wang et al., 2012). The surface of the aggregate is represented by a matrix z(x, y), the elements of which represent the height of each coordinate pair (x, y) in the horizontal plane. With the improved image resolution, the output z(x, y) matrix changes from a 1,019 × 1,371 matrix in the FTI system to a 2448 × 2046 matrix in the improved FTI system.

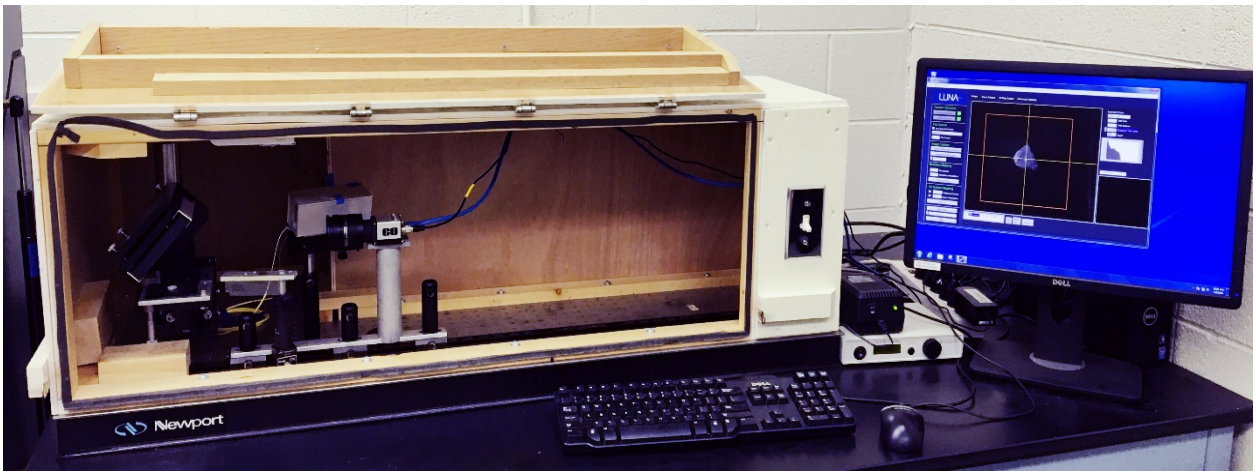

Figure 2. The Improved FTI System

Procedures for Scanning

Aggregate samples selected for the study were scanned individually or collectively depending on their size. First, the fiber-optic switch was turned on. Second, each aggregate was placed on the platform, where the height was adjusted initially. A clear image of an aggregate can be seen from the graphical user interface of the improved FTI system. Aggregates were moved on the tray to adjust their positions so that they could be scanned with the best resolution in the improved FTI software.

Three images were taken separately to generate the 3-D coordinates for the surface of an aggregate: one image taken with white light, and two images taken with laser lights. The white light image was captured first, and then the fiber-optic switch was turned off; the two laser light images were captured under laser lights with wavelengths of 675 nm and 805 nm, respectively. Boundary mapping and surface mapping were performed sequentially, and then the 3-D contour plot of an aggregate surface was output. The image of an aggregate can be output via the graphical user interface in the improved FTI system. A MATLAB program processes the image to 3-D coordinates, and the two-dimensional (2-D) Fourier transform method (FFT2) is used to analyze the 3-D coordinates for computing morphological characteristics. Figure 3 shows the boundary and surface mapping and a 3-D contour plot of an aggregate.

Two-Dimensional Fourier Transform Method for Characterizing Aggregate Morphology

The FFT2 is used in the improved FTI system to quantify aggregate morphology, including sphericity, flatness ratio, elongation ratio, angularity, and surface texture. It is derived from the one-dimensional Fourier transform method (Wang et al., 2005). The improved FTI system uses a better camera and improves the operation automaticity and computational efficiency of the FTI software.

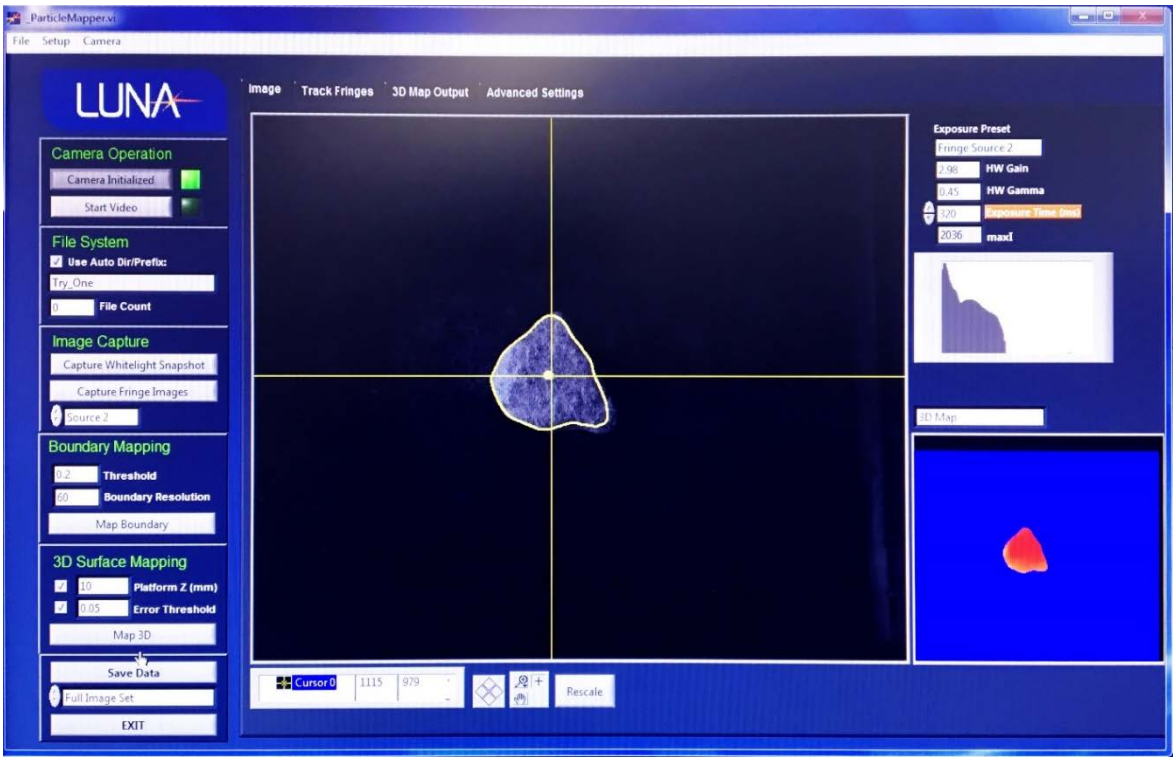

(a)

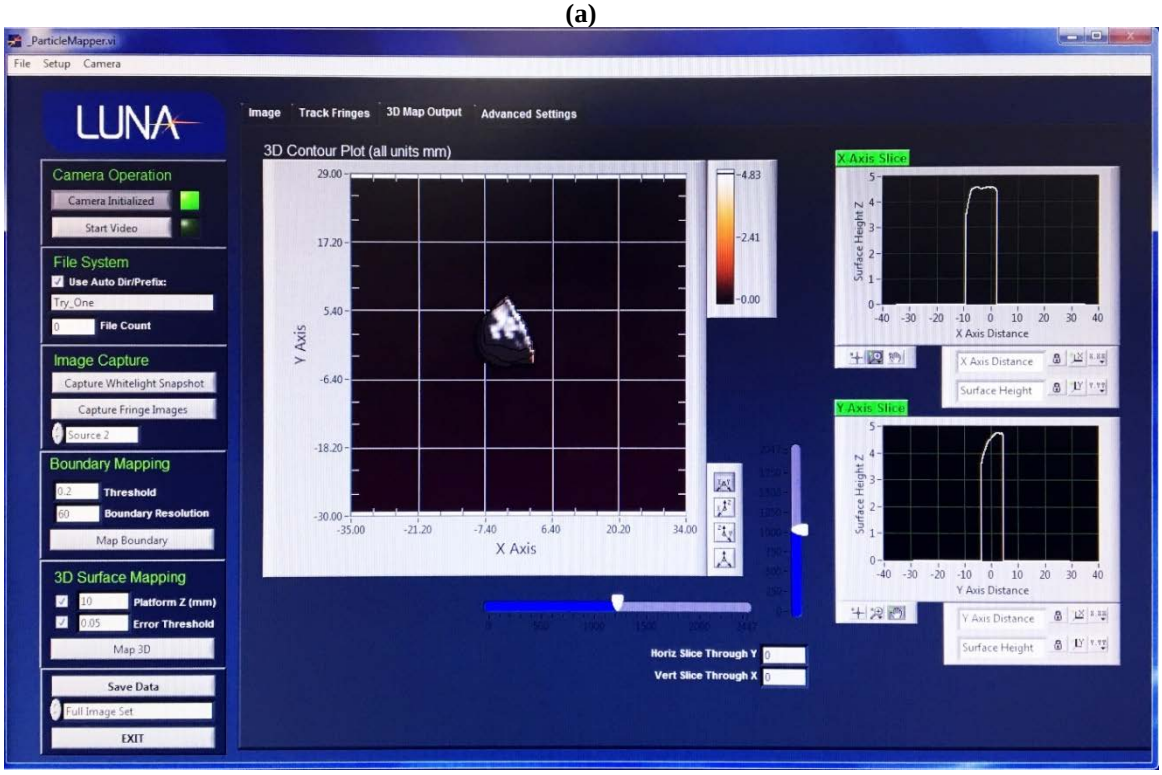

(b)

Figure 3. Aggregate scanning using FTI system: (a) boundary mapping and surface mapping; (b) 3-D contour plot of an aggregate.

The morphological characteristics of aggregates are represented by variations of asperities at multiple dimensional scales, including shape, angularity, and texture. Shape is described by sphericity, flatness ratio, and elongation ratio. Sphericity represents the overall three-dimensional shape of an individual aggregate. Sphericity is defined by Equation 1 and ranges from 0 to 1. A sphericity value of 1 indicates that an aggregate is equidimensional (i.e., cubical or spherical).

$$\text{Sphericity } (S) = \sqrt[3]{\frac{D_s D_m}{D_l^2}} \quad \text{[Eq. 1]}$$

where

S = sphericity
D_s = the shortest dimension of an aggregate
D_m = the intermediate dimension of an aggregate
D_l = the longest dimension of an aggregate.

The flatness ratio is defined by Equation 2, and the elongation ratio is defined by Equation 3. A greater flatness ratio or elongation ratio indicates that the analyzed aggregate is platy and elongated.

$$\text{Flatness Ratio (FR)} = \frac{D_s}{D_m} \quad \text{[Eq. 2]}$$

$$\text{Elongation Ratio (ER)} = \frac{D_m}{D_l} \quad \text{[Eq. 3]}$$

According to ASTM D4791 (ASTM International [ASTM], 2010) and Virginia Test Method 121 (VDOT, 2015), the F&E ratio of coarse aggregate particles is described as a ratio of length to thickness, which is the ratio of the longest dimension of a coarse aggregate particle to the shortest dimension as follows:

$$\text{Flat and Elongated Ratio (F\&E Ratio)} = \frac{D_l}{D_s} \quad \text{[Eq. 4]}$$

The described parameter F&E ratio for a particle can be defined in terms of the flatness ratio and elongation ratio obtained from the improved FTI system, which is expressed as follows:

$$\text{Flat and Elongated Ratio (FE Ratio)} = \frac{1}{(FR)(ER)} = \frac{D_l}{D_s} \quad \text{[Eq. 5]}$$

The improved FTI system provides an easy and convenient way of calculating the F&E ratio of coarse aggregates instead of performing a complete F&E test. The determination of the percentage of F&E coarse aggregates through the improved FTI system is more efficient than the manual measurements using a caliper device, where the particles are weighed or counted to determine the percentage of F&E particles in a sample.

The two-dimensional discrete Fourier transform (DFT) is used to quantify angularity and texture from a discrete function *z(x,y)* that represents the aggregate's surface, and *z(x,y)* is nonzero over the finite region $0 \le x \le N$ -1 and $0 \le y \le N$ -1. The DFT transforms spatial domain data into frequency domain data. The relationship between the DFT and the inverse DFT is given by Equations 6 through 9 (Wang, 2007):

$$Z(p,q) = \sum_{x=0}^{N-1}\sum_{y=0}^{N-1} z(x,y) e^{-j(\frac{2\pi}{N}xp+\frac{2\pi}{N}yq)} \quad \text{[Eq. 6]}$$

$$z(x,y) = \sum_{p=0}^{N-1}\sum_{q=0}^{N-1} Z(p,q) e^{j(\frac{2\pi}{N}xp+\frac{2\pi}{N}yq)} \quad \text{[Eq. 7]}$$

$$f_x = \frac{2\pi}{N}x \quad \text{[Eq. 8]}$$

$$f_y = \frac{2\pi}{N}y \quad \text{[Eq. 9]}$$

where

N = the size of the $z(x, y)$ matrix
$Z(p, q)$ = the DFT coefficient matrix in the frequency domain
$z(x, y)$ = the z coordinate of an aggregate surface
j = the imaginary root
f_x and f_y = frequencies in x and y directions, respectively.

The angularity factor (AF) and texture factor (TF) of an aggregate are defined in Equations 10 and 11, respectively.

$$\text{Angularity Factor (AF)} = \sum_{p=1}^{N_A}\sum_{q=1}^{N_A}[(\frac{a(p,q)}{a_0})^2 + (\frac{b(p,q)}{a_0})^2] \quad \text{[Eq. 10]}$$

$$\text{Texture Factor (TF)} = \sum_{p=1}^{N}\sum_{q=1}^{N}[(\frac{a(p,q)}{a_0})^2 + (\frac{b(p,q)}{a_0})^2] - \text{AF} \quad \text{[Eq. 11]}$$

where

a_0 = the average height of $z(x, y)$

a and b = the real and imaginary parts of the coefficients for the FFT2, respectively
N = the size of the $z(x, y)$ matrix
N_A = a threshold frequency.

The determination of the threshold frequency is a critical step that differentiates angularity from texture. More detailed information that demonstrates how to separate texture from angularity on an aggregate surface by the FFT2 method can be found in Sun et al. (2012) and Wang et al. (2012). A 3-D surface is reconstructed using the inverse of FFT2 coefficients that have frequencies smaller than $2 \pi N_A / N$ in either the x-direction or the y-direction. A set of square matrix z (x, y) varying the matrix size N is sampled on the measured aggregate surface. The FFT2 coefficients are considered to contribute only to angularity if the mean value of distance between the original surface and the reconstructed surface using the inverse of FFT2 is greater than 0.2 mm (Brandon and Kaplan, 1999). The other FFT2 coefficients are considered to contribute to texture only.

The relationship between AF and the size of roughness matrix is plotted for every aggregate particle. All points in the AF and size of roughness plot exactly follow a linear relationship for the same type of aggregate within a certain size range, and the aggregate with more irregularities has a steeper slope in the plot. Therefore, the angularity is defined as the slope in the plot of AF and roughness matrix size. Similarly, texture is defined as the slope in the plot of TF and roughness matrix size. Further information on the elucidation of the definitions of angularity and texture can be found in Wang et al. (2012).

Uncompacted Void Content

The uncompacted void content of aggregates provides an indication of morphological characteristics such as sphericity, angularity, and surface texture. The test is considered an indirect method for measuring morphology. The uncompacted void content of individual aggregate fractions was measured in accordance with AASHTO T 326 (American Society of State Highway and Transportation Officials [AASHTO], 2005a) (coarse aggregate) or AASHTO T 304 (AASHTO, 2005b) (fine aggregate) depending on the particle size. In addition, the uncompacted voids of particles in the 4.75 to 2.36 mm fraction were obtained using equipment sized between that used for coarse particles and that used for fine particles. The coarse aggregates were tested by allowing the material to flow through an orifice 105 mm in diameter into a cylindrical metal measure with a diameter of 152 mm and a height of 160 mm. For fine aggregate, the orifice is 12.7 mm in diameter and the container has a volume of approximately 100 ml. The equipment used to measure the 4.75 to 2.36 mm fraction has an orifice of 28 mm and a vessel volume of 400 ml. The uncompacted void content is calculated as the difference between the volume of the calibrated cylindrical measure and the absolute volume of the aggregate filling the cylinder. The size fractions tested were 12.5 to 9.5 mm, 9.5 to 4.75 mm, 4.75 to 2.36 mm, Nos. 8 to 16, Nos. 16 to 30, and No. 50100 when sufficient material was available.

Aggregate Mineral Content

Mineral compositions of aggregate particles were determined using an Olympus BTX X-

Ray Diffractometer (XRD), a portable and low power (10 W) unit that is capable of quickly analyzing a small amount of powdered sample. Whole aggregate particles were crushed to pass a 150-micrometer sieve. A small amount of the powder sample was placed in a cell that vibrated in the unit causing the particles to move, presenting different orientations as they were exposed to the radiation beam. Reflections were recorded using a CCD detector. The unit is equipped with a cobalt X-ray tube, and the analysis was conducted through a 2-theta range from 5° to 55°. Diffraction patterns were analyzed using XPowder Ver. 2010.01.26, with the American Mineralogist Crystal Structure Database (Downs and Hall-Wallace, 2003) to identify the minerals and estimate their content by weight.

Laboratory Performance Tests for SMA Mixtures

To evaluate further the influence of aggregate morphological characteristics on the mechanical performance of SMA mixtures, laboratory tests were performed on SMA mixtures. Laboratory performance–based tests such as dynamic modulus test, flow number test, asphalt pavement analyzer (APA) rut test, beam fatigue test, and modal mobile load simulator **(**MMLS) tests were conducted, and the test results were compared to aggregate morphological properties.

Dynamic Modulus Test

Dynamic modulus tests were performed with an asphalt mixture performance tester generally in accordance with AASHTO T 342 (AASHTO, 2014) Tests were performed on specimens prepared from gyratory compacted asphalt samples (100 mm in diameter by 150 mm deep). An air void content of 7% ± 0.5% was obtained for each test specimen. Four testing temperatures ranging from 4.4 ºC to 54 °C and six testing frequencies ranging from 0.1 to 25 Hz were used. Tests were performed from the coldest to the warmest temperature. At each test temperature, the tests were performed from the highest to the lowest frequency. Load levels were selected in such a way that at each temperature-frequency combination, the applied strain was in the range of 75 to 100 microstrain. All tests were conducted in the uniaxial mode without confinement. Stress versus strain values were captured continuously and used to calculate dynamic modulus. The results at each temperature-frequency combination for each mixture type are reported for three replicate specimens.

Flow Number Test

The repeated load permanent deformation test (also known as the flow number test) is used to evaluate the rutting resistance of asphalt mixtures. An asphalt mixture performance tester with a 15 kN loading capacity was used to conduct tests. Tests were performed on specimens 100 mm in diameter by 150 mm high (7% air voids). Tests were conducted at 54 °C based on LTPPBind software that represents the 50% reliability maximum high pavement temperature at locations in central Virginia. A repeated haversine axial compressive load pulse of 0.1 sec per every 1.0 sec was applied to the specimens. The repeated load permanent deformation tests were performed in both the unconfined and confined modes, which are commonly used in the laboratory. For the unconfined mode, a deviator stress of 600 kPa was applied. The tests were performed in the confined mode by using a confining stress of 10 psi and a deviator stress of 70 psi. The tests were continued for 10,000 cycles or a permanent strain of

10%, whichever came first. During the test, permanent strain (εp) versus the number of loading cycles was recorded automatically, and the results were used to estimate the flow number. The flow number was determined numerically as the cycle number at which the strain rate was at a minimum based on the Francken model (Roy et al., 2015). The general relationship between the cumulative permanent strain and the loading cycles includes three stages: primary, secondary, and tertiary, as shown in Figure 4.

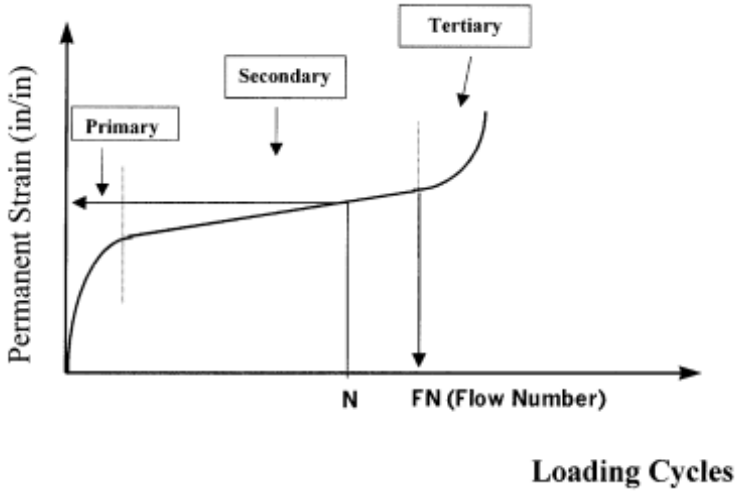

Figure 4. General Relationship Between Permanent Strain and Loading Cycles. N = Number of cycles.

In addition to calculations of the flow number, the slope and intercepts of the secondary portion of the cycle versus permanent strain curve were estimated in log-log space by applying a power law function:

$$\varepsilon_p = aN^b \quad \text{[Eq. 12]}$$

where

ε_p = permanent strain
a = intercept in log-log space
N = cycle number
b = slope in log-log space.

The slope of this line is indicative of the plastic strain rate of the mixture. A higher slope relative to other mixtures indicates a mixture that is likely more susceptible to rutting.

APA Test

The APA test was conducted in accordance with Virginia Test Method 110 (VDOT, 2009). Three beam specimens 3 in thick by 5 in wide by 12 in long (75 mm by 125 mm by 300 mm) were tested in the APA at a test temperature of 49 ^{o}C (120 ^{o}F) for each type of SMA mixture. The specimens were compacted in the laboratory to ensure an air void content of 8.0% ± 0.5%. All three specimens for each type of mixture were tested simultaneously. A vertical load of 120 lbf (533N) was applied through a rubber hose filled with compressed air at a pressure of 120 psi (830 kPa). The loading wheel speed was 2 ft/sec, and a total of about 135 min was

required to complete 8,000 cycles of load application. The recorded rut depth results after 8,000 cycles of load applications include left, middle, right, and average rut depth of the three replicate beams for each mixture type.

Beam Fatigue Test

Beam fatigue tests were performed in accordance with AASHTO T 321 (AASHTO, 2007) using three replicate specimens at three strain levels for a total of nine beams for each mixture type. For the fatigue tests, compacted beams measuring approximately 75 mm thick by 125 mm wide by 381 mm long were fabricated. From these compacted beams, the 50.8 mm by 63.5 mm by 381 mm specimens required for the fatigue testing were saw cut. The target air void level for the fatigue beams was 7% ± 0.5%. All tests were conducted at a single temperature of 20 °C. The tests were conducted in the strain-controlled mode. Applied tensile strain levels ranging from 300 to 600 microstrain were used so that fatigue curves describing strain versus number of cycles to failure could be developed. During the test, repeated loading to induce the specified strain was continued until failure occurred in the test specimen. Specimen failure was defined as the number of cycles at which beam stiffness degraded to 50% of the initial flexural stiffness.

Texas Overlay Test

The Texas overlay test was performed to assess the susceptibility of each mixture to cracking. Testing was performed using a universal testing machine with a 25 to 100 kN loading capacity generally in accordance with TX-248-F (Texas Department of Transportation, 2009). Testing was performed at a temperature of 25 °C ± 0.5 °C. Loading was applied for a total 1,200 cycles or until a reduction of 93% or more of the maximum load was reached.

MMLS Test

The MMLS can evaluate the rutting and fatigue susceptibility of HMA under different environmental and trafficking conditions. In this study, the MMLS3 was used to analyze the fatigue resistance of SMA mixtures. The MMLS3 fatigue testing was carried out at an intermediate temperature of 20 °C. The MMLS3 used in this study was a one-third scale accelerated pavement testing system with four single wheel bogies for simulating realistic dynamic wheel load application to SMA specimens. The MMLS3 has four axles and an electric motor. Each axle is equipped with a single tire 30 cm diameter, and the electric motor provides power for circulating each axle in a vertical closed loop in such a way that the loads can be applied to the specimens. Each axle of the MMLS3 applies a load of 2.7 kN, and the tire pressure is set to 0.7 MPa. The loads were applied with a loading frequency of 2 Hz, indicating 7,200 loading repetitions were finished per hour. The MMLS3 was run on SMA mixtures until a total of 1 million loading cycles were applied for fatigue resistance evaluation. The size of each SMA beam specimen was 12 in in length, 5 in in width, and 3 in in depth (i.e., 30 cm by 12.5 cm by 7.5 cm).

The portable seismic pavement analyzer (PSPA), a nondestructive device, was used to measure the seismic modulus of the SMA samples. The seismic modulus difference between the initial loading cycle and the 1 million loading cycles is indicative of the integrity change of the

SMA. The PSPA has become a tool for evaluation of the ability of SMA to resist fatigue during the trafficking process. More detailed information about the PSPA can be found in Jurado et al. (2012).

Asphalt Binder Testing

Binder grading was performed in accordance with AASHTO M 320 (AASHTO, 2017). The multiple stress creep recovery test was performed in accordance with AASHTO T 350 (AASHTO, 2017).

Extraction of Field Performance Data From VDOT's Pavement Management System

The field performance of the SMA mixtures was extracted from VDOT's PMS. VDOT's Maintenance Division acquires and maintains the results of an annual condition survey of all interstates, all primaries, and approximately 20% of secondary pavements. The survey collects and summarizes detailed distress data for each 0.1 mile of right-lane or principal direction pavement surface. Condition is reported on a scale from 0 to 100, completely failed to new or like new, respectively. The overall section rating, the critical condition index, is the lower of two ratings that summarize the load-related and non-load related distresses for a pavement. PMS data also give the rutting performance of the sections.

RESULTS AND DISCUSSION

Literature Review

Numerous studies have been conducted to characterize the morphological properties of aggregates and to analyze the effect of aggregate morphology on the mechanical performances of asphalt mixtures and pavement. The mechanical performance of asphalt mixtures can be measured using laboratory experiments, such as simple performance tests and wheel tracking tests. With regard to the quantification of aggregate morphology, both direct and indirect methods have been used. Among these methods, imaging analysis techniques have been widely used as a promising tool to quantify geometric characteristics (i.e., form, angularity, texture, etc.) of aggregates at high speed objectively and accurately. To identify further the effects of aggregate morphological characteristics on the mechanical performance of asphalt mixtures and pavements, numerous laboratory performance–based tests have been conducted to measure the mechanical behavior and assess the fatigue and rutting resistance ability of asphalt mixtures.

Methods for Measuring Aggregate Morphology

There are three types of measurement methods for the quantification of aggregate morphology: manual measurement, image analysis, and indirect measurement. Manual measurement uses a caliper to measure three dimensions of aggregates (ASTM D3398) (ASTM, 2006) and a proportional caliper device to measure the flatness ratio and elongation ratio (ASTM D4791) (ASTM, 2010). The common indirect method measures the void content of

uncompacted aggregate particles to infer the angularity and texture of aggregates (ASTM D5821) (ASTM, 2013). However, both methods are time-consuming, tedious, inaccurate, and subjective (Fletcher et al., 2003; Rao and Tutumluer, 2000).

Motivated by advancements in digital imaging techniques and the availability of cost-effective image processing software, image analysis techniques have been widely employed to quantify aggregate morphological characteristics effectively and accurately (Al-Rousan et al., 2007; Fletcher et al., 2003; Masad and Button., 2000;Rao et al., 2001). Various mathematical algorithms and experimental setups have been developed to quantify the size, shape, angularity, surface texture, surface area, and volume of aggregates (Fernlund, 2005; Fletcher et al., 2003; Rao and Tutumluer, 2000; Sime and Ferguson, 2003; Wang et al., 2005). Image processing techniques often determine aggregate morphological characteristics based on 2-D images, which cannot represent the 3-D characteristics accurately (Wang et al., 2005). Therefore, the improved FTI system, which was developed based on the Fourier transform interferometry (FTI) system (Lally et al., 2010; Wang et al., 2005), was adopted to measure aggregate morphological properties, based on 3-D coordinates of aggregate surfaces that are determined from digital images. The reliability and accuracy of the improved FTI measurements, including sphericity, flatness ratio, elongation ratio, angularity, and texture, were validated in previous research (Lally et al., 2010; Liu et al., 2016; Wang et al., 2012).

Effects of Aggregate Morphologies on HMA Performance

Aggregate morphological characteristics such as shape factors (i.e., sphericity, flatness ratio, and elongation ratio), angularity, and surface texture significantly affect physical properties and the mechanical performance of asphalt mixtures (Francisco et al., 2016; Kandhal and Parker, 1998; Meininger, 1998; Naidu and Adiseshu, 2011; Pan et al., 2006; Saeed et al., 2001; Unal and Mimaroglu, 2014; Wang et al., 2016). Aggregate shape significantly influences mechanical properties (Akbuluta et al., 2011; Bessa et al., 2014; Chen et al., 2005; Krumbein, 1941), such as permanent deformation, fatigue, and friction resistance. It was found that spherical (equant) particles are preferable for providing proper aggregate internal friction and improving rutting performance (Chen et al., 2013). F&E aggregates tend to break down and reduce the particle-to-particle interlock, which mostly contributes to the mechanical properties of aggregate structure (Buchanan, 2000). In addition, because aggregate angularity is crucial for this interlocking effect, asphalt mixtures with angular aggregates exhibit stronger shear resistance than those without (Kim and Souza, 2009; Mahmoud and Ortiz, 2014; Souza, 2009). The angularity and surface texture of aggregates affect mutual interactions between aggregates and interactions of aggregates with stabilizers (i.e., asphalt, cement and lime) (Al-Rousan et al., 2006; Tafesse et al., 2013), playing a vital role in durability, rheological properties, bonding potential, and interlocking strength of cement concrete and asphalt concrete (Masad et al., 2001; Smith and Collis, 1993). In summary, it is preferable to have more equal-dimensional, rougher, and more angular aggregates than F&E aggregates in mixtures for better mechanical performance. To evaluate quantitatively the influence of aggregate morphological characteristics on the mechanical performance of asphalt mixtures, some studies have linked shape properties by various imaging techniques with the performance of asphalt mixtures (Al-Rousan, 2005; Janoo, 1998; Little et al., 2003; Masad, 2003; Rao et al., 2002).

Laboratory Performance–Based Tests for Measuring the Mechanical Performance of Asphalt Mixtures

Fatigue and rutting are the most common distresses that occur in asphalt mixtures. For SMA mixtures, rutting occurs early in service life. Numerous laboratory tests can be used to measure mechanical performances of asphalt mixture, such as simple performance tests like the static creep test, dynamic modulus test, flow number test, indirect tensile test, beam fatigue test, Marshall stability test, and wheel tracking tests such as the APA test, MMLS test, Hamburg test, and accelerated pavement tests (Huang et al., 2009; Mohammad et al., 1999; Pan, 2005; Prowell et al., 2009; Stiady et al., 2001). The dynamic modulus test has been used widely for measurement of resilient modulus, which characterizes the elastic part of the stiffness of the asphalt mixture under repeated loading, therefore reflecting the stiffness of asphalt mixtures (Pan et al., 2005; Tutumluer et al., 2005). Flow number test is also a popular simple performance test for measuring the rutting performance of asphalt mixtures, thereby assessing the resistance of the mixtures to permanent deformation (Francisco et al., 2016; Pan et al., 2006). The beam fatigue test is a strain-controlled test to determine the fatigue life of asphalt mixtures subjected to repeated flexural bending until failure (Shu et al., 2008). In the beam fatigue test, fatigue life is traditionally defined as the number of cycles corresponding to a 50% reduction of initial stiffness.

Wheel tracking devices such as the APA and MMLS have been shown to be promising testing methods for measuring the rutting and fatigue resistance ability of SMA mixtures. The APA and MMLS are two important tools for simulating traffic and environmental conditions in field. APA is one of the most common and popular loaded wheel testers for evaluating the rutting resistance of HMA mixtures (VDOT, 2009). The MMLS also has been used widely for effective evaluation of permanent deformation or rutting and fatigue failure of scaled asphalt concrete pavement (Huang et al., 2016; Walubita et al., 2000). Rut depth obtained from the APA typically is indicative of permanent deformation on the pavement surface at high temperatures.

Materials and Mix Design

The volumetric properties of an SMA mixture are key indicators of production and placement quality, as well as long-term performance. Volumetric properties of field sampled mixtures are shown in Table 4. Volumetric properties were determined using a design gyration level of 75 per VDOT's SMA specification (VDOT, 2017). All mixtures were SMA-9.5 mixtures except for 14-1021, which was an SMA-12.5 mixture.

SMA requires good stone-on-stone contact of the coarse aggregate to be able to function as a durable and rut-resistant mixture. A common qualitative method suggests that approximately 30% passing the 4.75 mm (No. 4) sieve, 20% passing the 2.36 mm (No. 8) sieve, and 10% passing the 0.075 mm (No. 200) sieve may help ensure stone-on-stone contact (Brown and Haddock, 1997). All mixtures met this criterion. A more quantitative method for ensuring stone-on-stone contact suggests limiting the voids in coarse aggregate (VCA) of the SMA mixture (VCA_{MIX}) to be less than the VCA in the dry-rodded condition (VCA_{DRC}). The VCA was determined for the coarse aggregate fraction of the mixture by a dry rodding procedure in

accordance with AASHTO T 19 (AASHTO, 2017) and VCA_{MIX} were determined by Virginia Test Method 99 (VDOT, 2014). VCA_{MIX} for all mixtures is shown in Table 4, and VCA_{DRC} for all mixtures are shown in Table 2. All mixtures met the criterion of $VCA_{MIX} < VCA_{DRC}$, indicating presence of good stone-on-stone contact (using a breakpoint sieve of 2.38 mm) and a denser coarse aggregate fraction (if $VCA_{MIX} > VCA_{DRC}$, the fine aggregate fraction and asphalt in the mixture have pushed the coarse aggregate particles apart and would create extra voids above VCA_{DRC}). VCA_{MIX} for all mixtures ranged from 33.6% to 39.8%, and VCA_{DRC} of all mixture ranged from 41.8% to 47.1%. The fineness modulus for the gradation (in accordance with ASTM C125 [ASTM, 2017]) was determined for all mixtures and is shown in Table 4. The fineness modulus for the mixtures ranged from 5.08 (Mix 13-1081) to 5.38 (Mix 14-1021). The fineness modulus is an empirical factor obtained by adding the total percent of a sample of the aggregate retained on each of a specified series of sieves and dividing the sum by 100. Even though different particle size distributions may result in the same value for the fineness modulus, in general, a smaller value indicates a finer material and a larger value indicates a coarser material. Apeagyei et al. (2011) indicated that mixtures performed poorly in rutting when the fineness modulus was less than 5.0.

Most of the SMA-9.5 mixtures also met the VDOT gradation requirement for SMA-12.5 mixtures (12.5 mm: 83% to 93%; 9.5 mm: 80% maximum; 4.75 mm: 22% to 28%; 2.36 mm: 16% to 24%; No. 30: 15% to 30%; No. 200: 9% to 11%), which shows that by using certain gradations, a producer can meet the requirements for both SMA-9.5 and SMA-12.5 mixtures. SMA is very sensitive to changes in the material passing the respective breakpoint sieve (4.75 mm and 2.38 mm are breakpoint sieves for SMA-12.5 and SM-9.5 mixtures, respectively). The significance of the breakpoint sieve is that it identifies the point at which the gap in the gradation begins. Excessive material passing the breakpoint sieve (reduction in coarse aggregate fraction) will cause the mixture to lose stone-on-stone contact. Since some of the SMA-9.5 mixture also met the gradation requirement for the SMA-12.5 mixture, VCA_{MIX} was calculated based on a 4.75 mm breakpoint sieve and is also shown in Table 4. Comparing the VCA_{DRC} values (Table 2, based on a 2.38 mm breakpoint sieve) with the VCA_{MIX} values (using a 4.75 mm breakpoint sieve), three mixtures (i.e., SMA 13-1081, SMA 15-1012, and SMA 15-1084) did not meet the criterion of $VCA_{MIX} < VCA_{DRC}$, indicating loss of stone-on-stone contact.

Table 5 summarizes the volumetric properties (minimum, maximum, average, and standard deviation) as measured by the producer and VDOT districts for all mixtures. For two of the mixtures, average asphalt content did not meet the minimum specification requirement of 6.3%; all mixtures met the VMA specification requirement. However, during production, the asphalt content can be as low as 6.1% and still be within specification. Figures 5 and 6 show plots of percent passing the 4.75 mm sieve with VMA and VCA_{MIX}, respectively. From Figure 5 it can be seen that all the mixtures met the VMA criteria for the gradation change requirement for the 4.75 mm sieve (25% to 32%). The trend in three of the mixtures shows that as percent passing the 4.75 mm sieve increases, the VMA of the mixture decreases. From Figure 6 it can be seen that as percent passing increases, VCA_{MIX} also increases. Mixture 14-1021 shows higher VCA_{MIX} values because it is an SMA-12.5 mixture and VCA_{MIX} is calculated based on the breakpoint sieve of 4.75 mm.

Table 4. Volumetric Results for All Mixtures (VTRC Results)

Property	SMA 13-1070	SMA 13-1081	SMA 14-1021	SMA 14-1047	SMA 15-1012	SMA 15-1068	SMA 15-1080	SMA 15-1084	2016 VDOT Spec
% AC	6.45	6.91	6.29	6.7	6.02	6.58	6.2	6.45	6.3 (Min)
Rice Specific Gravity (G_{mm})	2.655	2.48	2.669	2.639	2.695	2.615	2.627	2.614	
Binder Specific Gravity (G_b)	1.03	1.03	1.03	1.03	1.03	1.03	1.03	1.03	
% Air Voids (V_a)	3.2	3.3	3	2.5	3.8	2	4.2	2.7	2%-4%
% VMA	19.2	19.1	18	19.1	18.7	18	18.9	18.2	18 (Design Min) 17 (Production Min)
% VFA	83.6	82.7	77.1	87.1	79.8	88.7	78	85.4	
$VCA_{MIX\ (\%)}$	34.6	36.6	39.8	36.7	33.6	33.6	33.9	34.9	$<VCA_{DRC}$
Dust/Ac	1.49	1.41	2.38	1.8	1.53	1.5	1.61	1.71	1.2-2
Bulk Specific Gravity (G_{mb})	2.572	2.398	2.59	2.574	2.594	2.562	2.518	2.544	
Effective Specific Gravity (G_{se})	2.979	2.769	2.989	2.973	3.006	2.933	2.927	2.924	
Aggregate Specific Gravity (G_{sb})	2.976	2.759	2.789	2.97	2.998	2.919	2.913	2.91	
% Binder Absorbed (P_{ba})	0.03	0.13	2.47	0.04	0.09	0.17	0.17	0.17	
Effective % Binder (P_{be})	6.42	6.78	3.97	6.66	5.93	6.42	6.04	6.29	
Effective Film Thickness, (F_{be})	9.6	10.3	5.9	8.5	9.2	9.7	9.1	8.6	
Sieve Size	**Average Percent Passing**								
3/4 in (19.0 mm)	100	100	100	100	100	100	100	100	
1/2 in (12.5 mm)	88.9	92.4	83.9	89.5	92.9	88.7	89.6	90.8	90-100
3/8 in (9.5 mm)	66.9	78.2	61.4	70.3	71.1	70.7	71.2	72.4	65-75
No. 4 (4.75 mm)	26.7	32.9	26.7	29.4	31.5	28.4	26.8	29	25-32
No. 8 (2.36 mm)	19.5	21.8	18.1	21.9	18.7	19.2	18.4	20.3	15-25
No. 16 (1.18 mm)	17.2	18.1	16	19.5	16.4	17.1	16.4	18.4	
No. 30 (600 µm)	15.8	15.8	14.5	17.8	15.1	15.5	15	16.9	
No. 50 (300 µm)	14.5	13.9	13.3	16.3	13.9	14	13.8	15.5	
No. 100 (150 µm)	12.8	11.8	12.1	14.7	12	12.4	12.3	13.9	
No. 200 (75 µm)	9.56	9.59	9.45	11.97	9.09	9.65	9.71	10.78	9-11
	100	100	100	100	100	100	100	100	
Fineness Modulus (FM)	5.27	5.08	5.38	5.10	5.21	5.23	5.23	5.14	
$VCA_{MIX\ (\%)}$ (4.75 mm breakpoint sieve)	40.4	45.6	39.8	42.7	44.1	41.7	40.7	42.0	
VCA_{DRC}	41.8	42.2	42.6	41.8	47.1	41.9	41.9	41.9	

VTRC = Virginia Transportation Research Council; AC = asphalt content, VMA = voids in mineral aggregate, VFA = voids filled with asphalt.

Table 5. Volumetric Results for All Mixtures (From VDOT Districts and Producers)

Mix Type	Property																			
	% AC				% VMA				% VFA				VCA_{MIX} (%)				FAR	Pbe	Gmm	VTM %
	Min	Max	Avg	SD	Min	Max	Avg	SD	Min	Max	Avg	SD	Min	Max	Avg	SD	Avg	Avg	Avg	Avg
SMA 13-1070	6.05	7.02	6.4	0.26	17.5	20.90	18.70	0.87	82	87	84.83	1.75	33	36.20	34.90	0.84	1.5	6.33	2.65	2.83
SMA 13-1081	6.71	6.97	6.84	0.08	17.90	19.40	18.72	0.42	79	88	83.20	2.4	34.10	36.80	35.44	0.82	1.25	6.71	2.46	3.16
SMA 14-1021	5.96	6.5	6.20	0.13	16.50	18.80	17.68	0.65	83	94	87.93	3.22	39	41.80	40.60	0.70	1.52	6.17	2.65	2.15
SMA 14-1047	6.14	6.55	6.34	0.16	17.80	19.30	18.43	0.65	84	88	85.75	1.70	34.70	35.70	35.35	0.44	1.47	6.34	2.63	2.65
SMA 15-1012	5.84	6.49	6.24	0.19	17.90	19.30	18.55	0.41	79	90	84.08	2.75	33.10	35	34.19	0.59	1.50	6.17	2.67	2.98
SMA 15-1068	6.07	6.62	6.36	0.12	17.60	20.10	18.57	0.75	74	88	82	4.15	32.90	34.60	33.82	0.56	1.48	6.21	2.61	3.36
SMA 15-1080	6.21	6.67	6.42	0.20	18.10	19.10	18.55	0.41	79	84	82.25	2.36	32.40	34.20	33.53	0.99	1.47	6.26	2.60	3.25
SMA 15-1084	6.31	6.70	6.45	0.11	17.30	18.90	18.34	0.56	79	91	84	4.09	33.90	36.10	34.73	0.70	1.62	6.27	2.60	2.94
2016 VDOT Spec	6.3 (Min)				18 (Design Min) 17 (Production Min)								$<VCA_{DRC}$				1.2-2			2%-4%

VDOT = Virginia Department of Transportation; AC = asphalt content, VMA = voids in mineral aggregate, VFA = voids filled with asphalt. FAR= fine to asphalt ratio, Pbe= effective binder content, VTM= voids in total mix. Gmm = rice specific gravity.

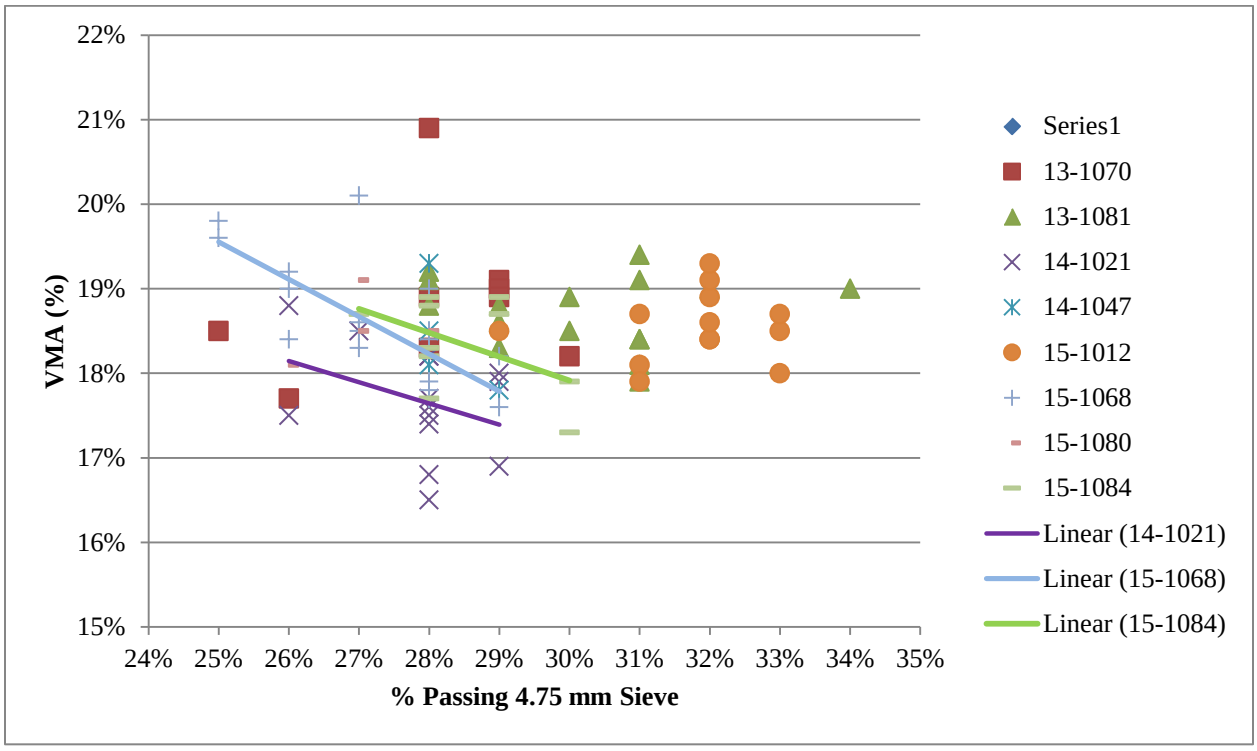

Figure 5. VMA vs. Percent Passing 4.75 mm Sieve for All Mixtures. VMA = voids in mineral aggregate.

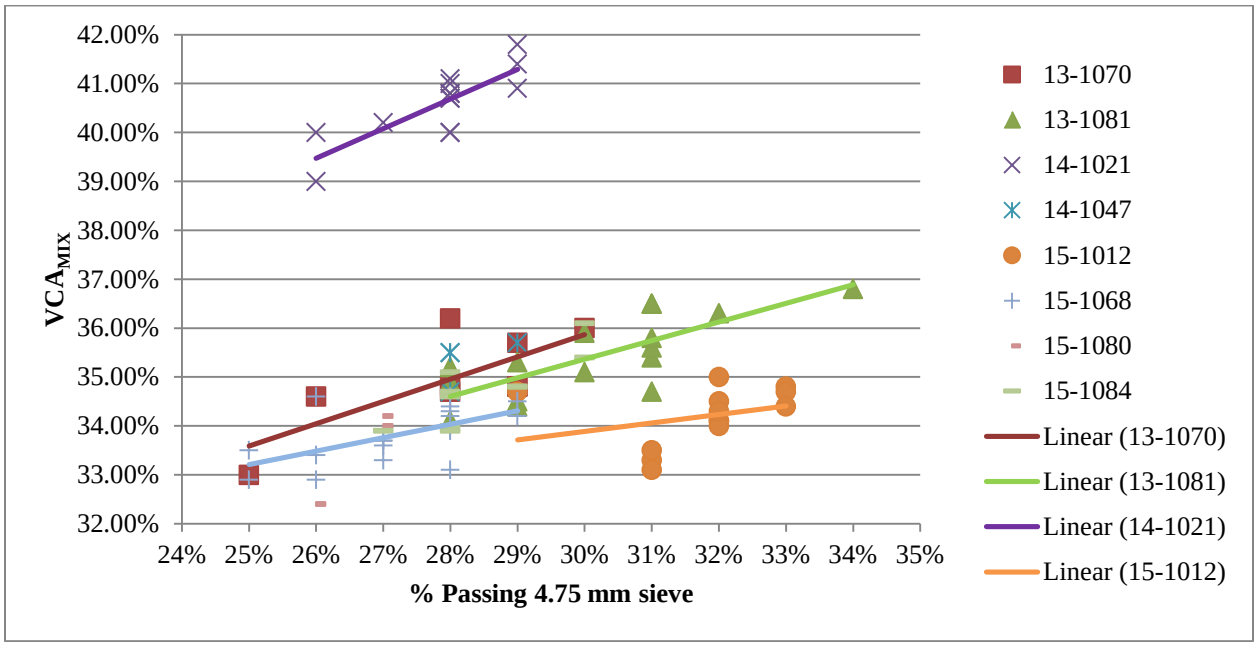

Figure 6. VCA_{MIX} vs. Percent Passing 4.75 mm Sieve for All Mixtures. The VCA_{MIX} value of 14-1021 is calculated based on a breakpoint sieve of 4.75 mm. VCA = voids in coarse aggregate.

Aggregate Morphological Characteristics

Selection of Aggregate Particles

The first 16 types of aggregates were selected for statistical analysis to determine the rational aggregate sample size. Figure 7 shows the sample aggregates selected for the first 16 types of aggregates. These 16 aggregate fractions contain aggregates ranging in size from No. 8 (2.36 mm) to 1 in (25.4 mm), mostly between 4.75 mm and 19 mm. The only fine aggregate fraction was 13-1071 Staunton #10. Aggregates from each type of aggregate fraction were randomly selected.

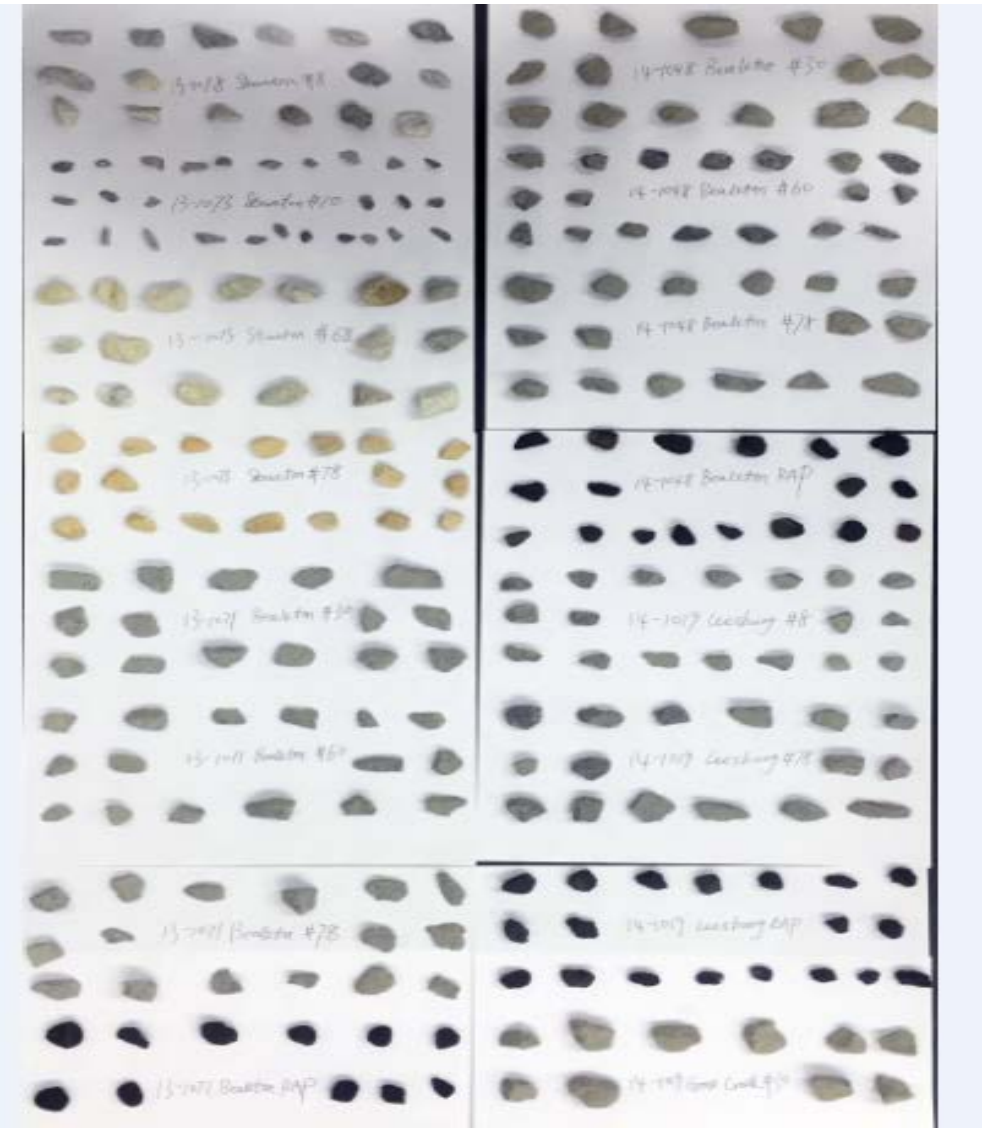

Figure 7. Photographs of 16 Aggregate Fractions

Statistical analysis of aggregate morphological characteristics was performed to validate that the sample population was adequate for all 16 aggregate fractions. A sample size of 120 particles was randomly selected for each aggregate fraction to ensure that the sample population was large enough to reach statistically stable results of aggregate morphological characteristics. All aggregates were imaged and analyzed using the improved FTI system. Five morphological parameters, including sphericity, flatness ratio, elongation ratio, F&E ratio, angularity, and texture, were measured for each aggregate particle.

Quantile-quantile (QQ) plots were generated using Rstudio. If the data are normally distributed, the points in the QQ-normal plot line lie on a straight diagonal line (Ford, 2015). It can be seen from Figures 8 and 9 that all the QQ-normal plots almost follow straight lines, which provides the evidence that the distributions of sphericity and elongation ratio for all aggregate fractions follow normal distributions.

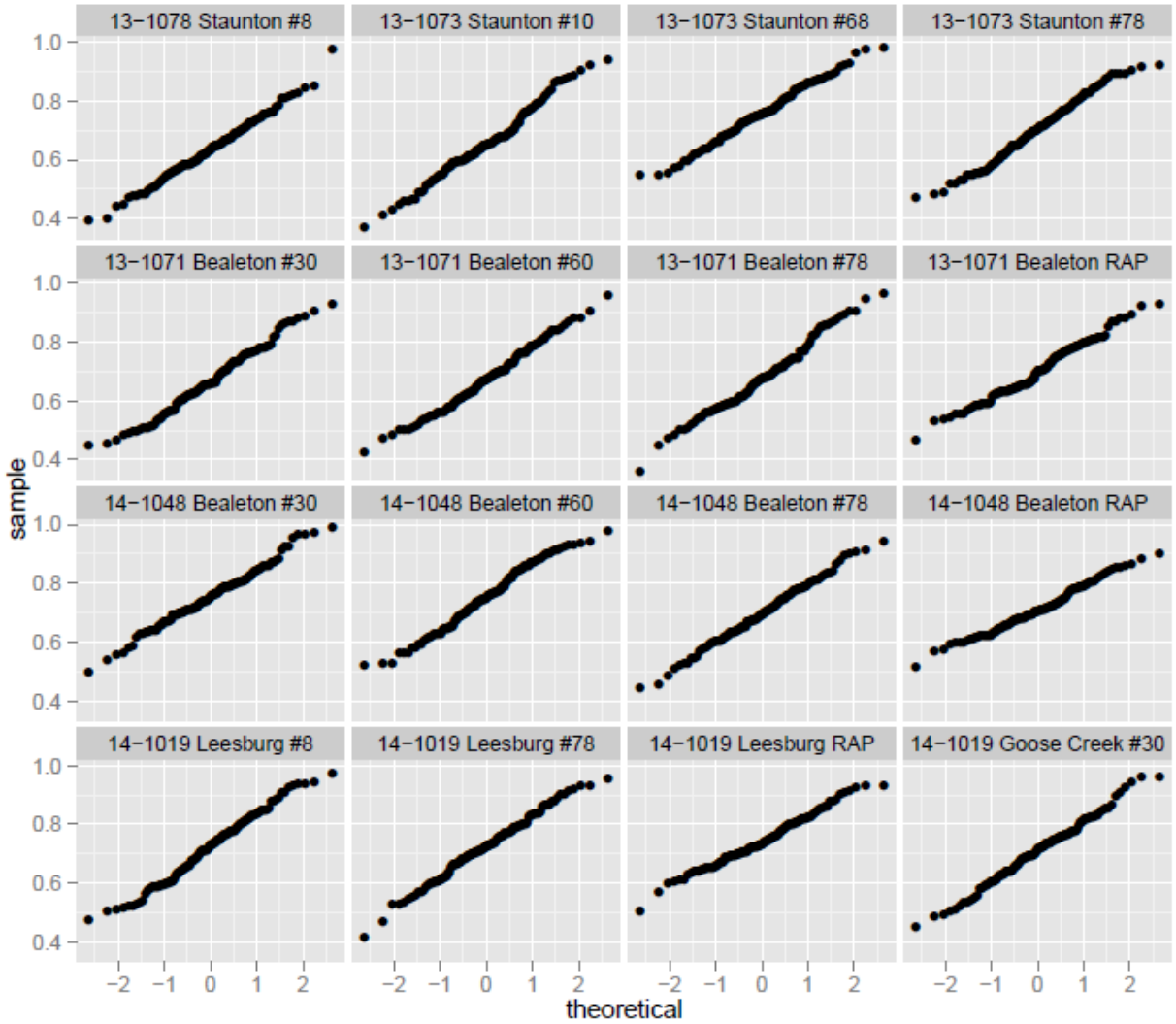

Figure 8. Quantile-Quantile Plot of Sphericity for 16 Aggregate Fractions. y-axis = sample quantile, x-axis = theoretical quantile. RAP = recycled asphalt pavement.

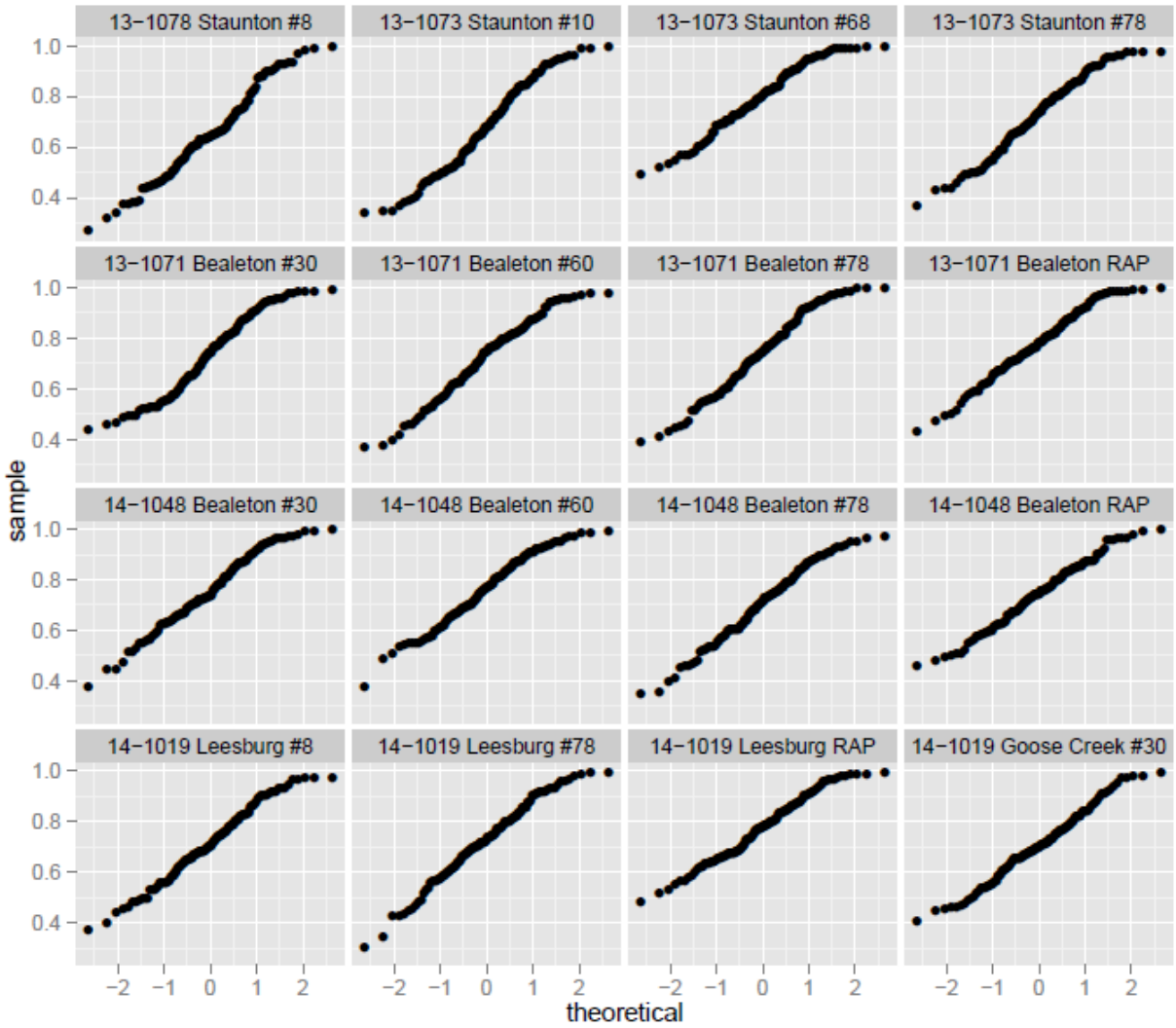

Figure 9. Quantile-Quantile Plot of Elongation Ratio for 16 Aggregate Fractions. y-axis = sample quantile; x-axis = theoretical quantile. RAP = recycled asphalt pavement.

Statistical analysis of the other morphological characteristics also showed similar linear trends in QQ-normal plots, indicating that the other morphological characteristics closely follow normal distributions. As a consequence, representing an entire population with 120 particles for each aggregate fraction is sufficient. Therefore, 120 aggregates were imaged for each aggregate fraction. The literature also showed that the selection of 120 aggregate particles for scanning was appropriate (Mahmoud and Ortiz, 2014).

The F&E aggregate particles may tend to lock up more readily during compaction and have a tendency to break up easily; as a consequence, the percentage of F&E particles is commonly limited to ensure the quality of aggregates and the performance of asphalt concrete pavements, although the actual impact of F&E particles at the 3:1 ratio on asphalt performance has been questioned (Watson and Julian, 2017). The F&E ratio at which the aggregate is considered too flat and elongated differs from specification to specification. The Superpave mix design specification allows less than 10% by weight of particles having an F&E ratio greater than 5:1 for aggregate blends in asphalt mixtures. In VDOT's SMA specification (VDOT,

2017), the amount of aggregates having an F&E ratio greater than 3:1 is limited to 20% and the amount of aggregates having an F&E ratio greater than 5:1 is limited to 5%. Celaya and Haddock (2006) noted that meeting F&E requirements is typically not an issue for coarse aggregates because of current crushing techniques (crushing techniques used for the aggregates used in this study are noted in Table 3) and further suggested that the F&E test should be retained in the specification to ensure that coarse aggregates selected for use in SMA mixtures are properly crushed. Watson and Julian (2017) and Brown and Cooley (1999) found that VMA increases as the percentage of F&E increases and further suggested that the high asphalt demand for the mixtures with high F&E values may limit their use even if satisfactory mixtures can be designed. Figure 8 plots the cumulative percentage versus the F&E ratio obtained from the improved FTI system for 16 types of aggregates. As shown in Figure 10, the percentage of aggregates having F&E ratios greater than 3:1 is less than 20% and the percentage of aggregates having F&E ratios greater than 5:1 is less than 5%, indicating that the requirement for the allowable percentage of F&E aggregates with F&E ratios greater than 3:1 and 5:1 is mostly satisfied as specified by VDOT's specification. This demonstrates an easier way of assessing the F&E ratio of an aggregate than the conventional manual measurements.

Comparison Between the Shape Results With the Improved FTI System and Manual Measurements

For the verification of the accuracy and reliability of the improved FTI system, three dimensions of the first eight types of aggregates (960 particles) were manually measured using a vernier caliper for further comparison with the results from the improved FTI system. The mean values of shape descriptors measured by the improved FTI system were very close to those obtained from manual measurements for every fraction of each type of aggregate. Figures 11 and 12 present the relationship between the shape descriptors calculated by the improved FTI system and the manually measured shape descriptors, including the sphericity and elongation ratio, respectively. The manually measured shape descriptors are labeled *x*, and the shape descriptors quantified using the improved FTI system are labeled *y* for the same aggregate. As shown in Figures 11 and 12, the relationship between the shape results with the improved FTI system shape and the manual measurements for the eight aggregate fractions showed good agreement between the improved FTI results and the manual measurements. The consistency of shape descriptors measured by the improved FTI system and the manual measurement method validates the accuracy and reliability of the improved FTI system.

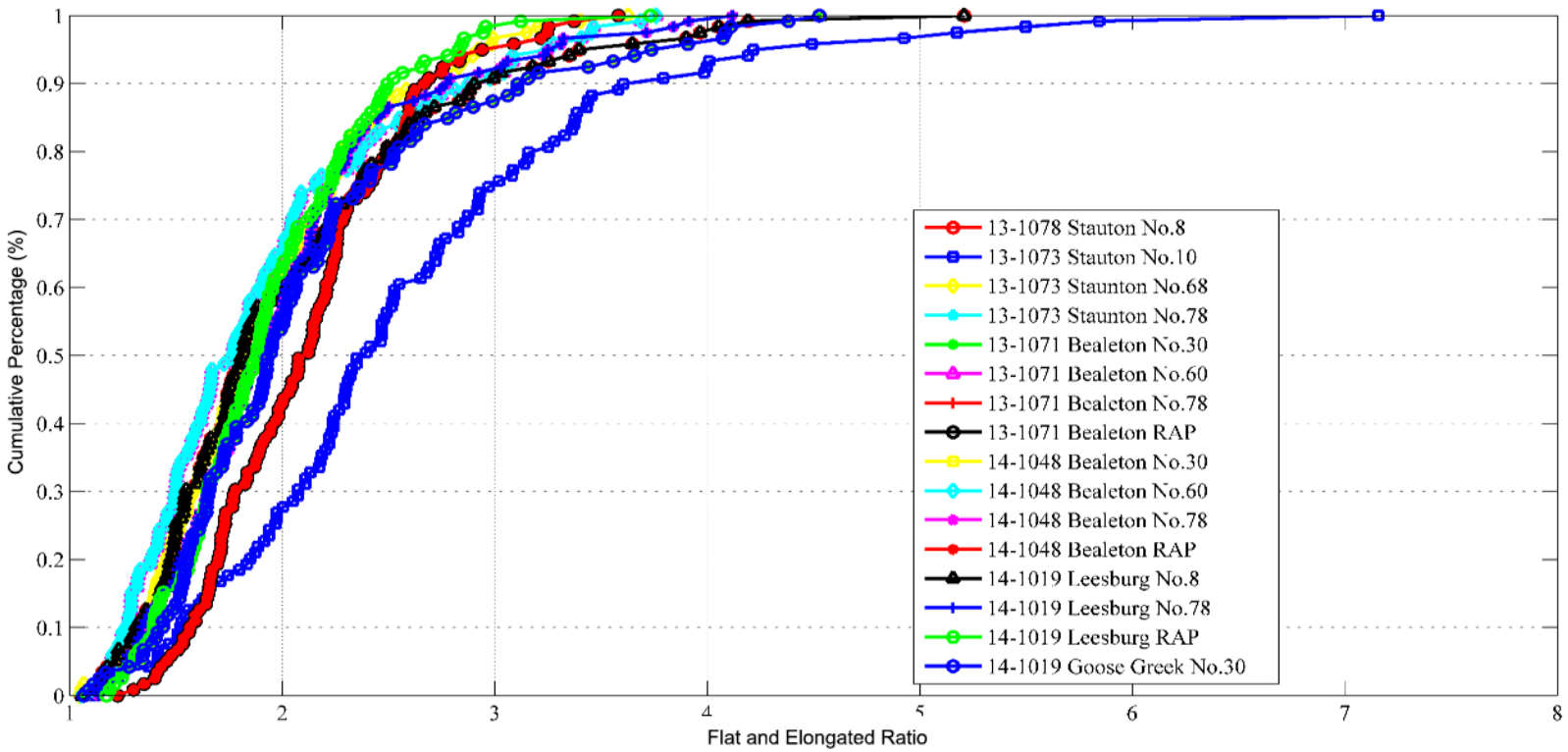

Figure 10. FTI Flat and Elongated Ratio Distributions of 16 Aggregate Fractions. FTI = Fourier transform interferometry; RAP = recycled asphalt pavement.

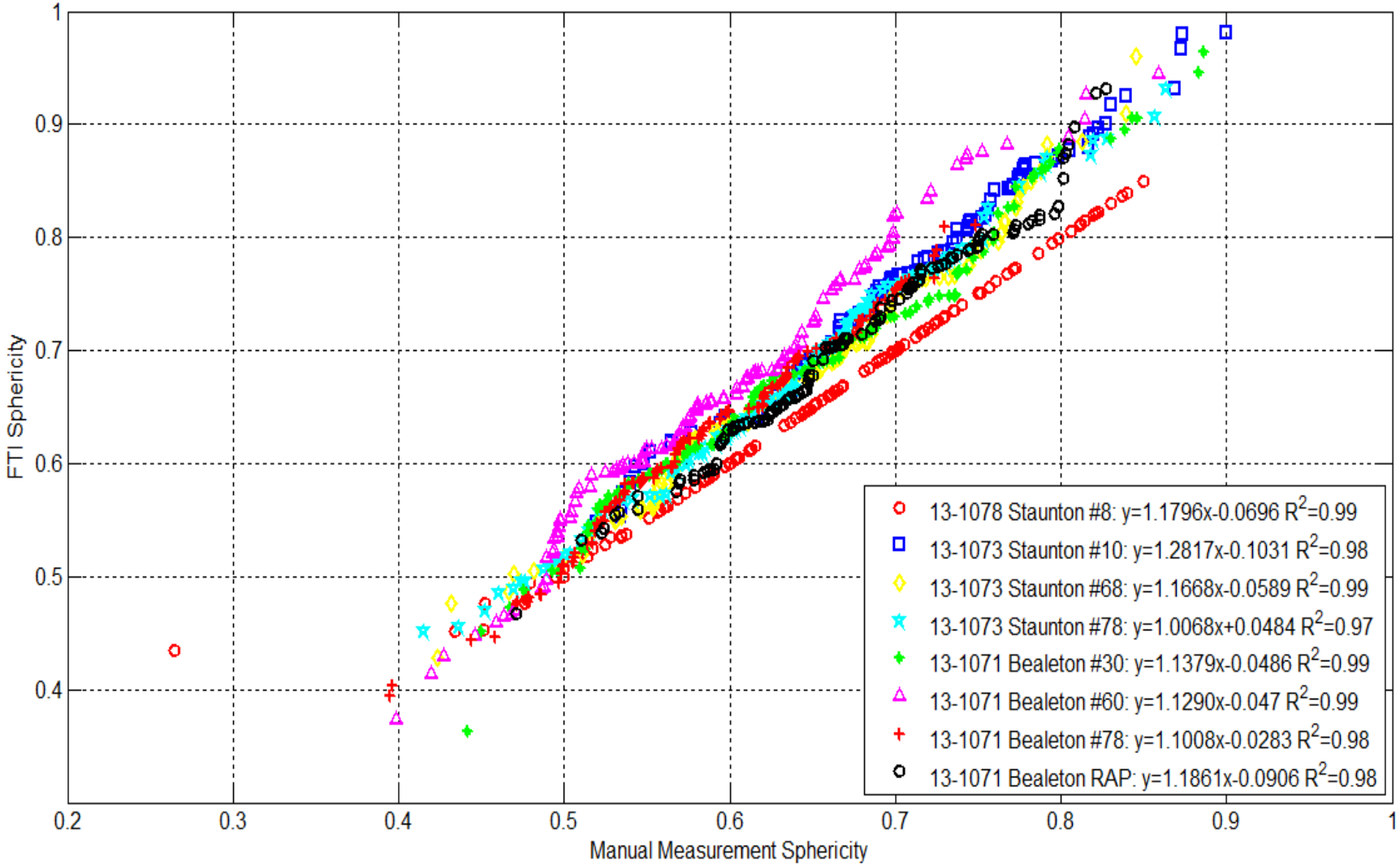

Figure 11. Manually Measured Sphericity vs. Improved FTI Sphericity. FTI = Fourier transform interferometry; RAP = recycled asphalt pavement.

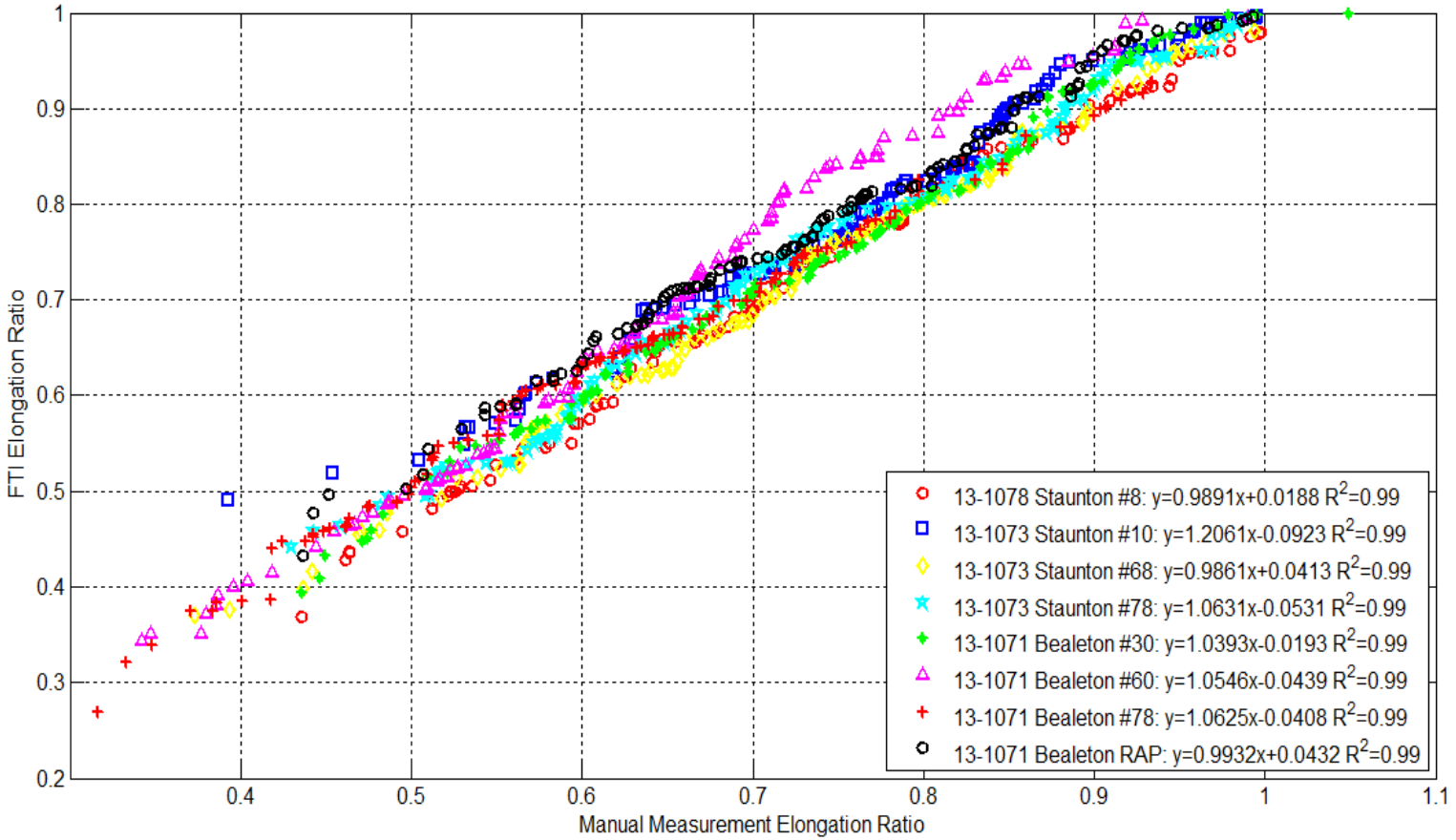

Figure 12. Manually Measured Elongation Ratio vs. Improved FTI Elongation Ratio. FTI = Fourier transform interferometry; RAP = recycled asphalt pavement.

Morphological Characteristics by the Improved FTI System

Morphological characteristics were measured for each coarse aggregate using the improved FTI system in terms of sphericity, flatness ratio, elongation ratio, angularity, and texture. Considering various blends of coarse aggregate fractions used in each type of SMA mixture, the weighted mean aggregate morphological index is proposed to account for the relative weight percentages of constituted coarse aggregate fractions in the SMA mixture:

$$\text{Weighted mean index} = \sum_{i=1}^{n} [(p_i)\,(\text{index}_i)] \qquad \text{[Eq. 13]}$$

where

Weighted mean index = the composite aggregate morphological index for each coarse aggregate blend used in a certain SMA mix design

p_i = the percentage by weight of the ith coarse aggregate fraction used in the mix design, as shown in Table 5

index_i = the mean morphological characteristic value of the corresponding ith coarse aggregate fraction

n = the number of coarse aggregate fraction in each SMA mixture.

For example, there are four aggregate fractions in the first five types of SMA mixtures and *n* is 4; similarly, *n* is 3 for the last three types of SMA mixtures, as shown in Table 6. The mean morphological value index_i determined for each type of aggregate fraction is listed in Table 6, followed by the weighted mean index for each aggregate blend. The results indicate that different blends of aggregate fractions show distinct morphological characteristics in terms of the weighted mean index. The weighted mean values were based on the weight fraction from gradation, without counting fillers.

Uncompacted Void Content Test

Tables 7 and 8 show the uncompacted void test results for aggregates of the coarse aggregate fractions. Table 9 shows the uncompacted void content of fine aggregate fractions. The uncompacted void content of aggregate fractions passing the 12.5 mm and retained on the 9.5 mm sieves ranged from 46.8 to 53.8, and aggregate fractions retained on the 4.75 mm sieve ranged from 46.8 to 54.4. The uncompacted void content of fine aggregate fractions (finer than the 4.75 mm sieve size**)** ranged from 46.9 to 53.5.

Table 6. Mean Morphological Value and Weighted Mean Index for Coarse Aggregates Used in Each SMA Mixture

SMA Mix ID	Aggregate Fractions	D_s	D_m	D_l	Sphericity	Flatness Ratio	Elongation Ratio	Flat and Elongated Ratio	Angularity	Texture
SMA-9.5/13-1070	13-1071 No. 30	6.9574	12.6669	18.2666	0.6425	0.5683	0.7067	2.4899	0.02	0.0206
	13-1071 No. 60	5.7763	9.4302	13.3975	0.6675	0.6108	0.7143	2.2920	0.018	0.0216
	13-1071 No. 78	5.6941	9.8892	13.4935	0.6717	0.5716	0.7469	2.3423	0.0171	0.0216
	13-1071 RAP	5.8412	10.2698	13.4045	0.6952	0.5831	0.7716	2.2226	0.0185	0.0285
	Weighted Mean Value	5.2776	9.0521	12.5864	0.5954	0.523	0.6514	2.9353	0.0161	0.0199
SMA-9.5/13-1081	13-1073 No. 8	5.2758	9.7004	13.863	0.6405	0.5491	0.7142	2.5499	0.0187	0.0227
	13-1073 No. 10	2.7047	6.4275	8.7809	0.6078	0.4312	0.7479	3.1008	0.0134	0.0159
	13-1073 No. 68	8.1832	12.9927	16.6504	0.7309	0.6489	0.7878	1.9562	0.0259	0.0286
	13-1073 No. 78	5.6228	9.6254	12.979	0.6807	0.5809	0.7525	2.2877	0.017	0.0235
	Weighted Mean Value	5.1343	9.1183	12.5254	0.6014	0.5098	0.6722	2.9181	0.0177	0.0212
SMA-12.5/14-1021	14-1019 No. 8	5.91	9.0686	11.9335	0.7142	0.6449	0.7678	2.0196	0.0216	0.026
	14-1019 No.30	8.0731	12.0999	16.519	0.7129	0.6796	0.747	1.9698	0.0254	0.0252
	14-1019 No. 78	6.0874	9.6079	13.1671	0.6923	0.6335	0.7411	2.1300	0.0208	0.0244
	14-1019 RAP	6.4378	9.8916	12.2562	0.7501	0.6534	0.8136	1.8811	0.0226	0.033
	Weighted Mean Value	5.8131	8.9327	11.9526	0.6262	0.5732	0.6686	2.6093	0.0198	0.0231
SMA-9.5/14-1047	14-1048 No. 30	7.5897	12.0489	17.2611	0.6787	0.6364	0.7182	2.1879	0.0214	0.0232
	14-1048 No. 60	6.0334	9.8848	13.3285	0.6937	0.6191	0.7536	2.1434	0.0203	0.025
	14-1048 No. 78	5.8255	9.7063	13.4785	0.6701	0.6	0.7278	2.2900	0.0203	0.0238
	14-1048 RAP	6.1235	10.1016	12.7041	0.7221	0.6048	0.803	2.0591	0.0222	0.03
	Weighted Mean Value	5.5205	9.0513	12.3437	0.6118	0.5458	0.6643	2.7581	0.0184	0.0223
SMA-9.5/15-1012	15-1013 No. 28	4.2717	9.1398	12.4166	0.6209	0.4608	0.7443	2.9157	0.0178	0.0203
	15-1013 No. 78	7.5084	10.2491	12.9949	0.7626	0.7223	0.794	1.7437	0.0269	0.0276
	15-1013 No. 10	2.4468	6.9657	9.2224	0.5837	0.3546	0.7708	3.6586	0.0106	0.0155
	Weighted Mean Value	5.1906	7.6273	9.7858	0.563	0.5101	0.6045	3.2430	0.019	0.0199
SMA-9.5/15-1068[a]	15-1069 No. 8	5.4936	8.3257	11.1504	0.7022	0.6507	0.749	2.0518	0.0234	0.0251
	15-1069 No. 78	6.6165	10.6196	14.0412	0.691	0.6007	0.7617	2.1855	0.0264	0.0244
	15-1069 RAP	6.8625	12.43	15.5994	0.697	0.5496	0.7984	2.2789	0.0215	0.0255
	Weighted Mean Value	5.7335	9.3016	12.2059	0.6253	0.5444	0.6881	2.6695	0.0223	0.0223

SMA = stone matrix asphalt; Ds = short dimension, D_m = medium dimension, D_l = long dimension; RAP = recycled asphalt pavement.

[a] SMA 15-1080 and SMA 15-1085 used the same aggregate blend as SMA 15-1068, as shown in Table 1.

Table 7. Uncompacted Void Contents of Aggregate Fractions Passing the 12.5 mm and Retained on the 9.5 mm Sieve

Aggregate Fraction	Sample 1 (mass/g)	Sample 2 (mass/g)	UCV of Sample 1 (%)	UCV of Sample 2 (%)	Average UCV (%)
13-1071 No. 30	4401.3	4369.2	49.45868	49.92729	49.6
13-1071 No. 60	4524.4	4560.4	48.04509	47.63169	47.8
13-1073 No. 8	3782.9	3781.9	53.74727	53.75949	53.8
13-1073 No. 68	4121	4200.5	49.61339	48.64136	49.1
13-1073 No. 78	3972.4	3912.5	46.41913	47.22708	46.8
14-1019 No. 8	4533.4	4516.5	47.94174	48.13581	48.0
14-1019 No. 30	4431.6	4410.3	49.28208	49.52585	49.4
14-1019 No. 78	4520.8	4551.3	48.08643	47.73619	47.9
14-1048 No. 30	4431.6	4410.3	49.11074	49.35533	49.2
14-1048 No. 60	4458.2	4465.3	48.80528	48.72375	48.8
14-1048 No. 78	4593.8	4544.3	47.24815	47.81657	47.5
15-1013 No. 28	4609.8	4573.3	47.59554	48.01048	47.8
15-1013 No. 78	4198.8	4216.4	52.26781	52.06774	52.2
15-1069 No. 8	4464.9	4486.3	47.12052	46.86707	47.0
15-1069 No. 78	4348.6	4373	49.20584	48.92083	49.1

UCV = uncompacted void content.

Table 8. Uncompacted Void Contents of Aggregate Fractions Retained on the 4.75 mm Sieve

Aggregate Fraction	Sample 1 (mass/g)	Sample 2 (mass/g)	UCV of Sample 1 (%)	UCV of Sample 2 (%)	Average UCV (%)
13-1071 No. 60	4391.2	4369.6	49.57466	49.8227	49.7
13-1073 No. 8	3755.3	3703.9	54.08473	54.71318	54.4
13-1073 No. 68	4188.2	4200.5	48.79175	48.64136	48.7
13-1073 No. 78	3840	3833.2	48.20498	48.2967	48.3
14-1019 No. 8	4453.5	4466.2	48.85925	48.71341	48.8
14-1019 No. 78	4407.9	4432.8	49.38289	49.09696	49.2
14-1048 No. 60	4253.7	4279.9	51.15361	50.85275	51.0
14-1048 No. 78	4342.7	4388.7	50.1316	49.60337	49.9
15-1013 No. 28	4552.2	4593.1	48.25034	47.78539	48.0
15-1013 No. 78	4066.7	4072.9	53.76953	53.69905	53.7
15-1069 No. 8	4484.6	4502.8	46.88721	46.67166	46.8
15-1069 No. 78	4230.8	4221.6	50.58181	50.68927	50.6

UCV = uncompacted void content.

Table 9. Uncompacted Void Contents of Aggregate Fractions Finer Than the 4.75 mm Sieve

Aggregate Fraction	Sample 1 (mass/g)	Sample 2 (mass/g)	UCV of Sample 1 (%)	UCV of Sample 2 (%)	Average UCV (%)
13-1071 No. 60, 8-16	151.2	151.0	48.332	48.706	48.5
13-1073 No. 10, 8-16	132.7	132.4	51.290	51.400	51.3
13-1073 No. 10, 16-30	129.5	130.1	52.464	52.244	52.4
13-1073 No. 10, 30-50	126.3	126.9	53.639	53.419	53.5
13-1073 No. 78, 30-50	133.4	132.9	46.952	47.151	47.1
14-1019 No. 8, 8-16	150.2	150.0	48.629	4848.629	48.6
14-1019 No. 8 ,+78, 16-30	145.4	146.3	50.524	50.218	50.4
14-1019 No. 78, 8-16	153.6	154.2	47.999	47.795	47.9
14-1048 No. 60, 8-16	146.1	146.1	50.370	50.370	50.4
14-1048 No. 60, 4-8	570.8	585.5	51.627	50.381	51.0
14-1048 No. 78, 4-8	600.8	590.5	49.082	449.958	49.5
15-1013 No. 28, 4-8	631.2	639.6	47.224	46.522	46.9
15-1013 No. 78, 4-8	556.8	563.0	52.612	52.926	52.8
15-1013 No. 78, 8-16	145.5	146.6	51.235	50.867	51.1
15-1069 No. 8, 8-16	148.9	150.1	48.009	48.629	48.3
15-1069 No. 8, 4-8	576.9	583.6	50.438	49.863	50.2
15-1069 No. 78, 4-8	577.5	580.1	49.695	49.469	49.6

UCV = uncompacted void content.

Aggregate Mineral Content

Figure 13 plots an example XRD analysis result of the Bealeton aggregates. The XRD analysis shows that the Bealeton diabase consists of plagioclase, pyroxene, and quartz. Compared with the Bealeton diabase, quartz diabase from Leesburg and Goose Creek includes an additional mineral of montmorillonite, a clay mineral resulting from weathering of the plagioclase. The dominant mineral in quartzite from Stuarts Draft is quartz. Amphibolite from Garrisonville primarily consists of hornblende, pargasite, quartz, and chlorite. The three lithologies of aplite from Piney River mainly include the same mineral composition of albite, quartz, epidote, and muscovite at varying percentages by weight. The mineral composition of the aggregates is presented in Table 10.

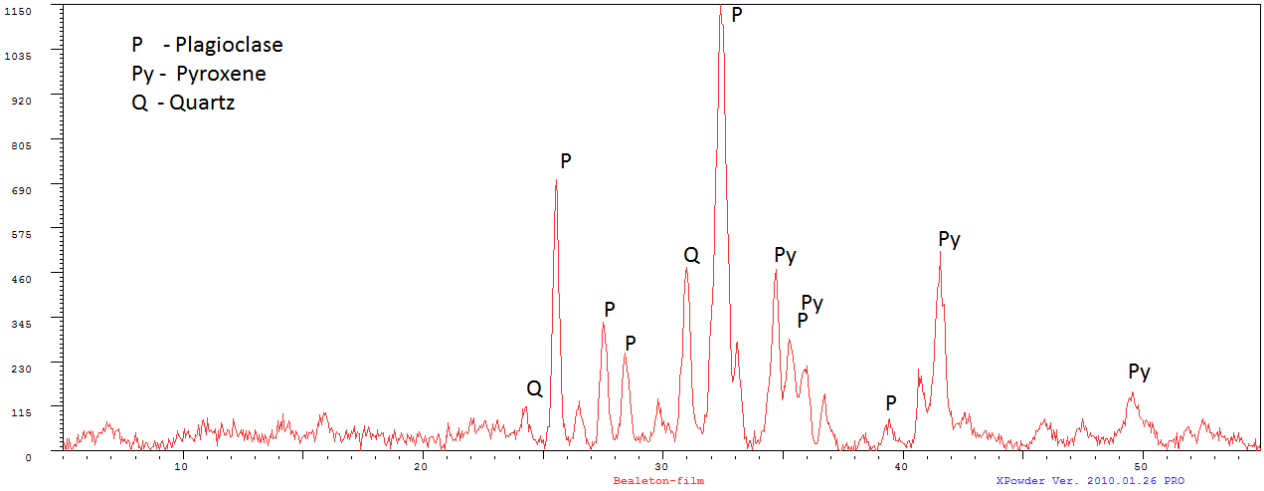

Figure 13. XRD Analysis of Bealeton Aggregates. XRD = e-ray diffraction.

Laboratory Performance–Based Tests

Dynamic Modulus

The dynamic modulus is used as a major input for the Mechanistic-Empirical Pavement Design (MEPDG) software. The dynamic modulus master curves of all SMA mixtures are shown in Figure 14. It can be seen that overall there is no major difference in dynamic modulus values between different mixtures. Tables 11 and 12 list the dynamic modulus test results at temperatures of 21.1 °C and 54.4 °C for all types of SMA mixtures, respectively.

Table 10. Rock Type and Fractional Mineral Composition of Aggregates[a]

Rock Type	Origin	Crusher Type	Plagioclase	Pyroxene	Quartz	Montmorillonte	Albite	Epidote	Muscovite	Hornblende	Pargasite	Chlorite
Diabase	Bealeton Diabase	Cone	0.55	0.24	0.21	---	---	---	---	---	---	---
Quartz Diabase	Leesburg Diabase	Cone	0.49	0.20	0.27	0.05	---		---	---	---	---
Quartz Diabase	Goose Creek Diabase	Impact	0.46	0.22	0.25	0.07	---	---	---	---	---	---
Quartzite	Stuarts Draft Quartzite	Impact	---	---	1.0000	---	----	---	---	---	---	---
Granite	Garrisonville Amphibolite	Cone	0.27	---	0.22	---	---	---	---	0.33	0.12	0.06
Aplite	Piney River Aplite	Impact	---	---	0.18	---	0.53	0.18	0.11	---	---	---
			---	---	0.20	---	0.61	0.16	0.03	---	---	---
			---	---	0.52	---	0.26	0.12	0.10	---	---	---

--- = no value.

[a] There are unresolved minerals in each type of aggregate in the XRD analysis. Unresolved minerals were not considered in the determination of mineral content.

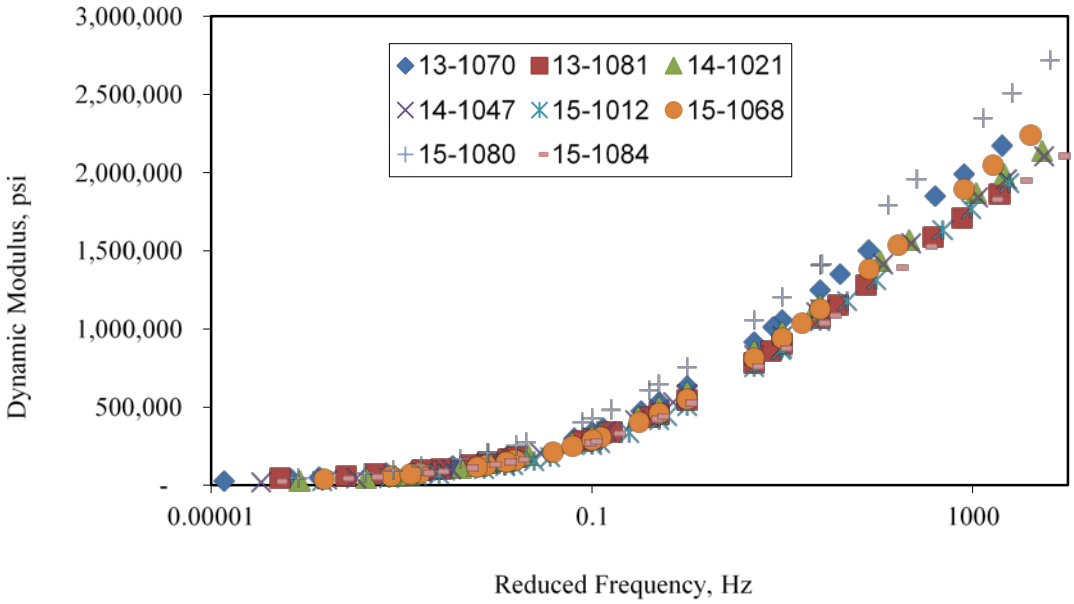

(a)

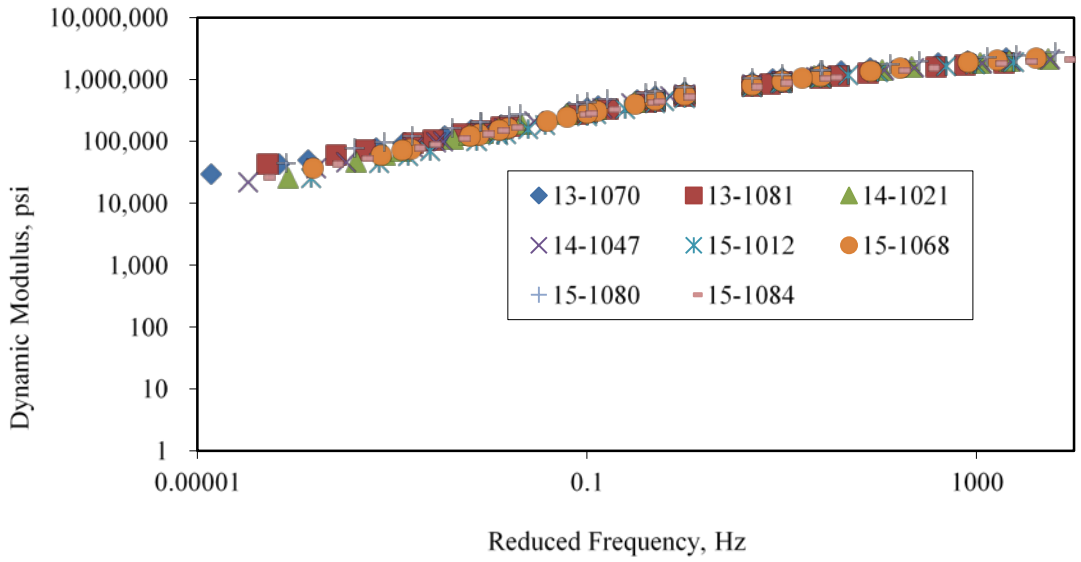

(b)

Figure 14. Dynamic Modulus Results: (a) for SMA mixtures; (b) for SMA mixtures (log-log Scale). SMA = stone matrix asphalt.

Table 11. Dynamic Modulus Test Results Under a Temperature of 21.1 °C

Mix ID	Average Dynamic Modulus |E*| (psi)						φ	sin φ	|E*| sin φ
	25 Hz	10 Hz	5 Hz	1 Hz	0.5 Hz	0.1 Hz	10 Hz	10 Hz	10 Hz
13-1070	1238815	1044464	906195	627288	529967	350169	19.10	0.33	341600
13-1081	1069798	901989	782430	537654	456481	301001	19.40	0.33	299459
14-1021	1147634	970688	844506	590738	500621	322032	18.60	0.32	309458
14-1047	1109151	937088	818689	575896	491049	320098	18.40	0.32	295646
15-1012	1039098	863941	746025	500186	420174	261938	20.60	0.35	303823
15-1068	1124283	936411	805394	547710	460639	296843	20.50	0.35	327779
15-1080	1404980	1199026	1054520	752407	647786	436708	18.00	0.31	370337
15-1084	1029284	864231	750715	519525	441833	289495	19.30	0.33	285501

Table 12. Dynamic Modulus Test Results Under a Temperature of 54.4 °C

Mix ID	Average Dynamic Modulus (psi)						φ	sin φ	|E*| /sin φ
	25 Hz	10 Hz	5 Hz	1 Hz	0.5 Hz	0.1 Hz	10 Hz	10 Hz	10 Hz
13-1070	187920	144491	117113	65034	57681	44560	26.2	0.44	327423
13-1081	172788	132941	107521	65233	58875	45396	26.1	0.44	302324
14-1021	195945	139270	107526	57826	45725	25840	32.1	0.53	262200
14-1047	144331	101594	78687	44202	36157	22567	31.4	0.52	195083
15-1012	187775	133226	102372	55679	44521	26058	32.2	0.53	250127
15-1068	222052	160895	128034	74302	61249	37405	29.9	0.5	322915
15-1080	279729	206292	163167	94540	76715	46557	29.6	0.49	417836
15-1084	153541	110794	87187	50995	42297	27030	30.3	0.5	219700

Flow Number Test

Flow number was determined numerically as the cycle number at which the permanent strain rate is at a minimum based on the Francken model (Roy et al., 2015). Figure 15 presents an example plot of change of permanent strain versus loading cycles for the flow number test under the unconfined condition for the 13-1081 SMA mixture. Figure 16 represents the flow number results under the unconfined condition. A higher flow number indicates better rutting resistance. SMA 15-1068 has the largest flow number because the high-polymer modified asphalt binder was used in this type of SMA mixture. Only Mixtures 13-1070 and 13-1081 showed a low flow number compared to other mixtures in the unconfined condition. Both of these mixtures used PG 70-22 binders. Tables 13 and 14 provide the flow number results for the unconfined and confined conditions, respectively. The flow number results under the unconfined condition varied greatly, indicating the different rutting resistance potentials of these SMA mixtures; flow numbers for the confined condition for all types of SMA mixtures were the same.

Flow number slope (FNS) is the slope of the secondary stage, as shown in Figure 15. The estimation of the slope parameter is determined from a regression analysis of the linear portion of the permanent strain versus number of cycles curve on a log-log scale. FNS has a close relation with simulated rutting in pavement. Tables 15 and 16 provide the FNS results for the unconfined and confined conditions, respectively. A higher slope number indicates a higher rutting susceptibility. In both the confined and unconfined flow number tests, polymer-modified binders showed a lower slope compared to PG 70-22 binders, indicating better rutting resistance.

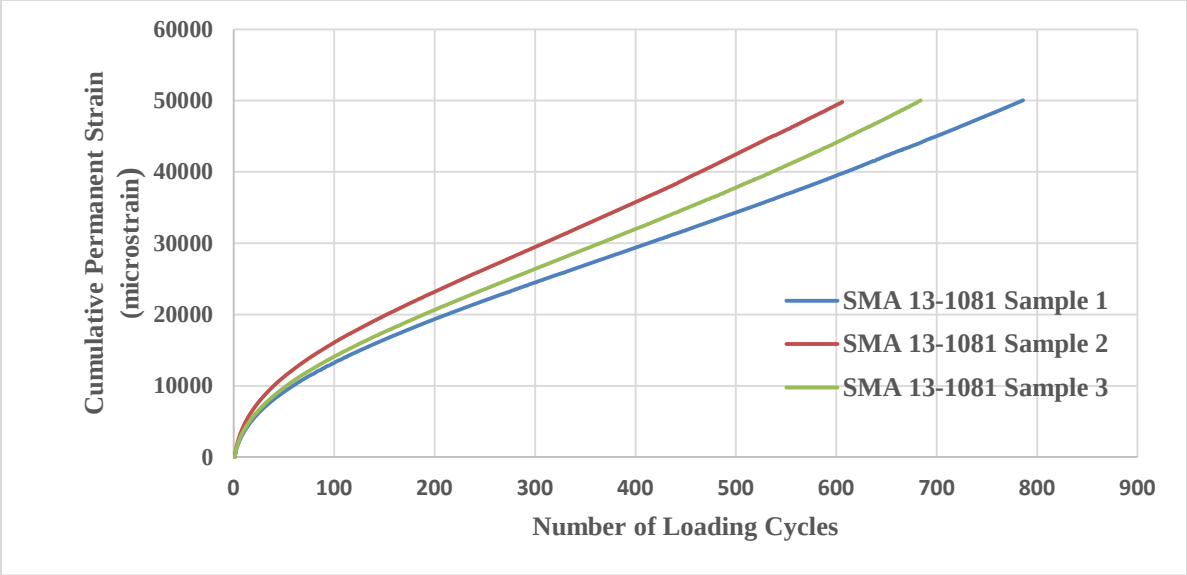

Figure 15. Plots of Cumulative Permanent Strain vs. Number of Loading Cycles for Flow Number Test Under the Unconfined Condition for Each Type of SMA Mixture (13-1081). SMA = stone matrix asphalt.

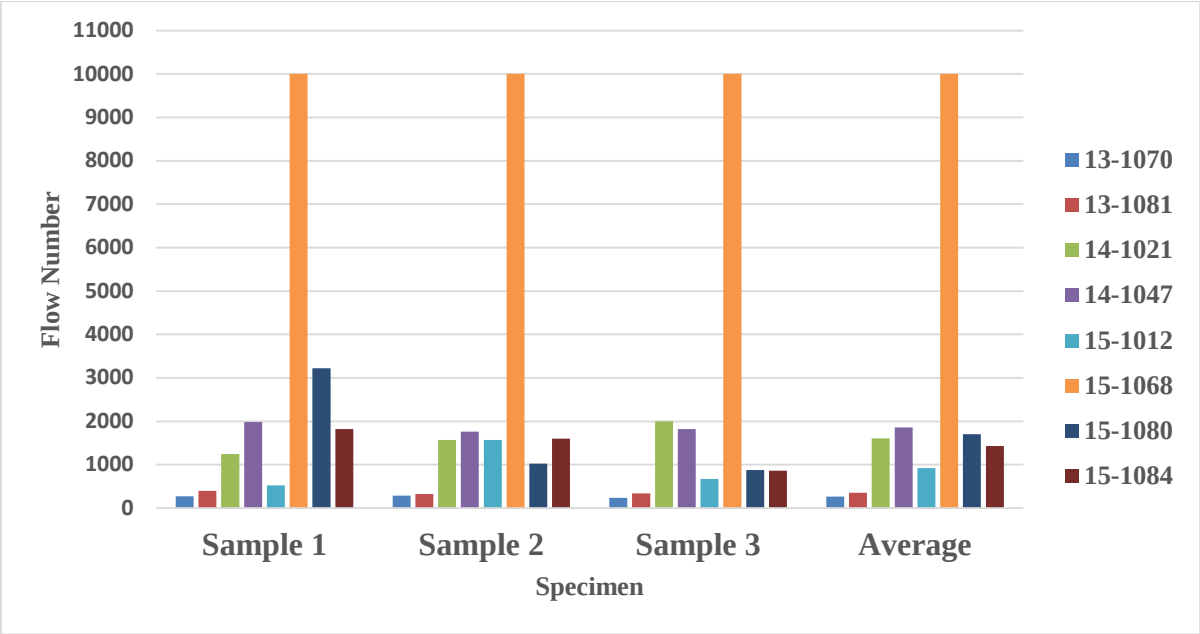

Figure 16. Flow Numbers of SMA Mixtures Under the Unconfined Condition. SMA = stone matrix asphalt.

Table 13. Flow Numbers of SMA Mixtures Under the Unconfined Condition

Mix ID	Unconfined Flow Number (cycles/microstrain at flow point)			
	Sample 1	Sample 2	Sample 3	Average
13-1070	275 (30039)	289 (28529)	238 (33185)	267 (30584)
13-1081	400 (29431)	323 (30989)	341 (28712)	355 (29711)
14-1021	1249 (38894)	1572 (28865)	1994 (31491)	1605 (33083)
14-1047	1981 (27857)	1760 (37589)	1823 (36705)	1855 (34050)
15-1012	527 (36032)	1568 (24112)	670 (36988)	922 (32377)
15-1068	10000 (27373)	10000 (25218)	10000 (27032)	10000 (26541)
15-1080	3218 (22778)	1025 (29019)	876 (26078)	1706 (25958)
15-1084	1823 (39302)	1596 (25695)	861 (41469)	1426 (35489)

SMA = stone matrix asphalt.

Table 14. Flow Numbers of SMA Mixtures Under the Confined Condition

Mix ID	Confined Flow Number (cycles/microstrain at flow point)			
	Sample 1	Sample 2	Sample 3	Average
13-1070	10000 (26376)	10000 (24947)	10000 (16825)	10000 (22716)
13-1081	10000 (17357)	10000 (19661)	9472 (49849)	9824 (28956))
14-1021	10000 (79254)	10000 (24662)	10000 (33279)	10000 (45732)
14-1047	10000 (21414)	10000 (27983)	10000 (21280)	10000 (23559)
15-1012	10000 (20395)	10000 (29148)	-	10000 (24772)
15-1068	10000 (18725)	10000 (20376)	10000 (17652)	10000 (18918)
15-1080	10000 (14920)	10000 (22210)	10000 (15691)	10000 (17607)
15-1084	7414 (25385)	10000 (24459)	10000 (18982)	9138 (22942)

SMA = stone matrix asphalt.

Table 15. Flow Number Slopes of SMA Mixtures Under the Unconfined Condition

Mix ID	Unconfined Flow Number Test			
	Flow Number Slope			
	Sample 1	Sample 2	Sample 3	Average
13-1070	6.07E-01	5.94E-01	6.14E-01	0.6052
13-1081	5.48E-01	5.29E-01	5.49E-01	0.5420
14-1021	3.41E-01	3.44E-01	3.50E-01	0.3452
14-1047	3.75E-01	3.49E-01	3.55E-01	0.3596
15-1012	4.32E-01	4.33E-01	4.44E-01	0.4361
15-1068	2.54E-01	2.05E-01	2.17E-01	0.2255
15-1080	3.79E-01	3.95E-01	4.63E-01	0.4124
15-1084	3.53E-01	3.70E-01	4.29E-01	0.3839

SMA = stone matrix asphalt.

Table 16. Flow Number Slopes of SMA Mixtures Under the Confined Condition

Mix ID	Confined Flow Number Test			
	Flow Number Slope			
	Sample 1	Sample 2	Sample 3	Average
13-1070	1.67E-01	2.13E-01	1.98E-01	0.1926
13-1081	1.73E-01	2.72E-01	2.86E-01	0.2435
14-1021	2.14E-01	1.26E-01	1.70E-01	0.1700
14-1047	1.87E-01	2.13E-01	1.45E-01	0.1816
15-1012	1.81E-01	1.04E-01	1.93E-01	0.1595
15-1068	1.30E-01	1.64E-01	1.24E-01	0.1392
15-1080	2.36E-01	2.84E-01	9.74E-02	0.2059
15-1084	1.77E-01	1.76E-01	2.21E-01	0.1914

SMA = stone matrix asphalt.

APA Test

APA test results are shown in Table 17. Previous work by Prowell et al (2002) proposed a criterion of 4.0 mm for Virginia's SMA. All mixtures showed lower rut values than the criterion. The air-void content was measured for every SMA replicate sample in the APA tests, and the average value is listed in Table 17. The APA test results did not show a clear distinction between neat binders and polymer-modified binders. This may be due to the lower APA test temperature (49 ^{o}C).

Figure 17 shows the APA rut depth versus the asphalt content for different mixtures used in this study. It can be seen that rut depth is not increased when asphalt content higher than specification minimum of 6.3% was used.

Table 17. APA Rut Depth Results After 8,000 Loading Cycles

	Rut Depth (mm) (49 ^{o}C)				
Mix ID	**Left**	**Middle**	**Right**	**Mean**	**Average Air Void Content (%)**
13-1070	2.01	1.72	1.34	1.69	7.9
13-1081	1.19	1.30	1.40	1.30	8.4
14-1021	1.22	1.37	1.38	1.32	7.5
14-1047	2.44	2.63	2.63	2.57	7.7
15-1012	2.85	3.09	3.57	3.17	7.8
15-1068	1.18	1.43	1.69	1.43	7.8
15-1080	2.34	2.38	2.65	2.46	8.2
15-1084	1.12	1.54	1.34	1.33	8.0

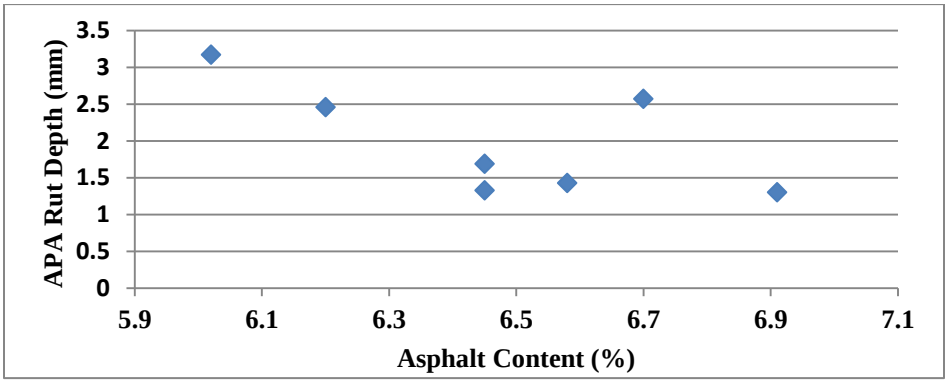

Figure 17. Asphalt Content vs. APA Rut Depth for SMA Mixtures. APA = Asphalt Pavement Analyzer; SMA = stone matrix asphalt.

Beam Fatigue Test

Table 18 presents the fatigue test results of all SMA mixtures under three different strain levels. Figure 18 shows the number of loading cycles to failure versus the applied strain curves for the eight types of SMA mixtures. It can be seen that mixtures with polymer-modified binder showed excellent fatigue performance.

Table 18. Fatigue Test Results of Stone Matrix Asphalt (SMA) Mixtures

Mix ID	Fatigue Test Results (cycles)								
	300 microstrain			450 microstrain			600 microstrain		
Air Voids (%)	7.1	6.6	6.7	6.8	6.9	6.4	6.8	6.7	6.2
13-1070	1,440,250	1,826,920	1,121,160	189,220	198,520	140,260	42,280	28,320	23,730
Air Voids (%)	6.9	5.2	5.3	6.2	5.3	5.2	5.2	5.9	5.2
13-1081	3,158,360	3,973,570	3,303,000	231,900	220,860	379,820	48,510	62,980	74,400
Air Voids (%)	6.6	6.5	-	6.2	-	-	7.3	6.7	-
14-1021	4,803,880	6,168,820	-	238,970	-	-	73,420	39,560	-
Air Voids (%)	7.0	7.1	7.5	7	7.1	7.1	7.1	7.2	-
14-1047	6,646,010	8,166,320	5,986,030	414,030	576,020	556,370	116,280	104,200	-
Air Voids (%)	6.6	6.8	-	8	6.7	7.3	6.6	8.3	7.2
15-1012	10,000,000	4,512,300	-	305,790	256,480	179250	69,730	64,650	51,610
Air Voids (%)	6.9	6.7	6.8	6.6	6.8	-	6.8	7.2	7.2
15-1068	10,000,000	10,000,000	6,760,000	2,948,900	2,828,500	-	855,000	507,920	264,580
Air Voids (%)	6.5	-	-	7.0	6.9	7.2	7.0	7.0	6.9
15-1080	2,757,390	-	-	277,160	251,650	332,130	41,960	49,700	47,720
Air Voids (%)	6.6	6.8	7.2	7.5	7.1	7.3	6.7	6.8	6.7
15-1084	3,211,820	5,924,760	5,940,140	-	286,540	274,920	49,690	57,740	90,270

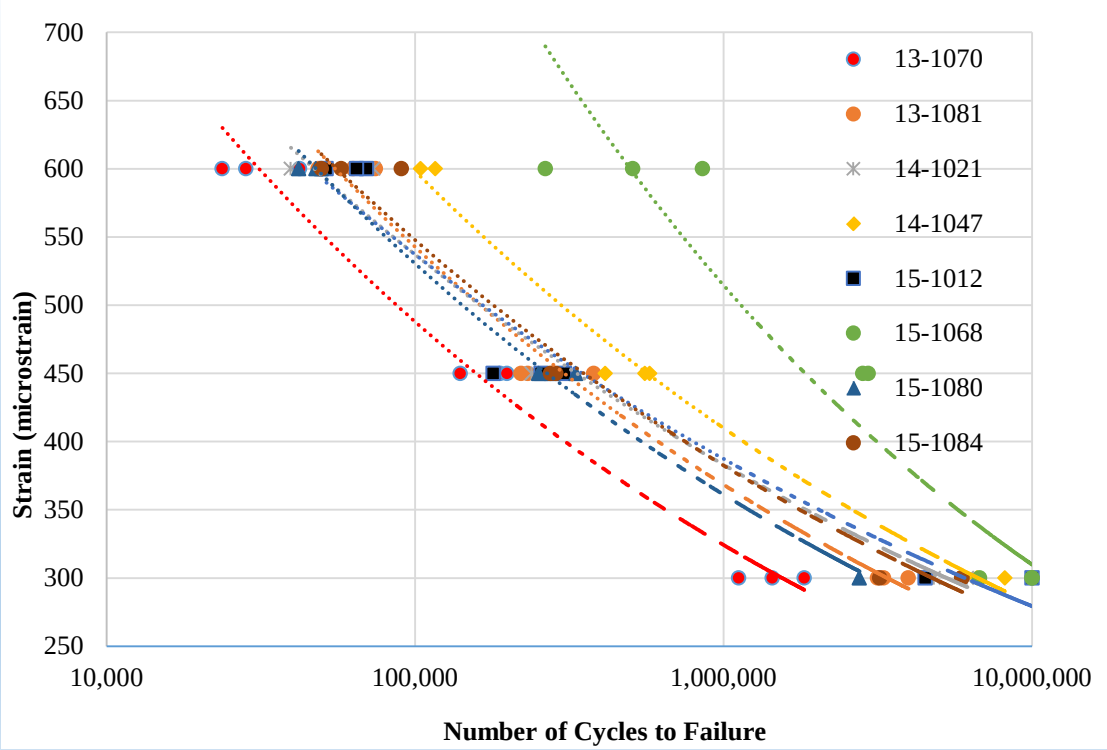

Figure 18. Fatigue Curves of SMA Mixtures. SMA = stone matrix asphalt.

Texas Overlay Test

Overlay test results are shown in Table 19. All mixtures showed the maximum number of cycles of 1,200, suggesting better reflection crack resistance.

Table 19. Overlay Test Results

Mix ID	Overlay Cycles (mean)	Air Voids (%)	No. of Specimens
13-1070	1,200	6.5	4
13-1081	1,200	6.7	4
14-1021	---	---	---
14-1047	---	---	---
15-1012	1,200	7.0	6
15-1063	1,200	7.3	6
15-1068	1,200	5.9	6
15-1080	1,200	8.5	5
15-1084	1,200	4.4	5

--- = not available.

MMLS Test

Table 20 shows the difference in seismic modulus of each specimen after 1 million loading cycles. After the application of 1 million loading cycles in the MMLS3 test, SMA mixtures 13-1081, 14-1047, 15-1068, 15-1080, and 15-1084 showed decreasing trends in seismic

modulus. Conversely, there were some increases of seismic modulus in SMA mixtures 13-1070, 13-1081, and 15-1080. The moduli would typically be expected to decrease as a result of anticipated traffic damage. However, material densification during trafficking may offset the effects of traffic damage. Such decreases and increases in normalized PSPA modulus were also found in other MMLS tests (Walubita et al., 2000).

Table 20. Summary of Change of Seismic Modulus After 1 Million Loading Cycles

	Seismic Modulus (GPa)(20 °C)								
	Initial			After 1 Million Loading Cycles			Difference (%)		
Mix ID	1	2	3	1	2	3	1	2	3
13-1070	6.2	5.67	7	6.67	6.867	8.27	7.53	21.17	18.09
13-1081	6.53	7.03	6.23	7.8	5.6	5.43	19.39	-20.38	-12.83
14-1047	9.17	8.00	10.80	5.03	5.37	4.83	-45.09	-32.91	-55.25
15-1068	10.13	9.70	7.57	5.37	4.97	4.67	-47.04	-48.80	-38.33
15-1080	10.05	9.28	8.50	8.57	8.97	9.10	-18.44	-4.79	5.06
15-1084	8.96	8.43	10.48	9.10	4.17	10.13	-2.14	-47.03	-19.87

Asphalt Binder Testing

Performance grading was conducted on the virgin binder samples collected. Table 21 summarizes the grading results for all binders. VDOT's specification allows up to 20% RAP for PG 70-22 binder and up to 15% when PG 76-22 binder is used. RAP content used in different mixtures ranged from 0% to 15%. Extracted binder grading for all mixtures was not conducted because of low RAP contents. Rutting parameter G*/Sin delta is high for polymer-modified binders, indicating better performance against rutting. Modified asphalt also showed low non-recoverable creep compliance (Jnr) values, indicating better performance of these binders against rutting and for accommodating temperature variations and extreme loading conditions. Studies have shown that non-recoverable creep compliance based on the MSCR test is better correlated to pavement rutting (Anderson, 2011).

Table 21. Asphalt Binder Testing results

		G*/Sin Delta						Non-Recoverable Creep Compliance	
		Original AASHTO T 315 Criterion: >1.00 kPa			RTFO AASHTO T 315 Criterion: >2.20 kPa				
Mix ID	PG	70	76	82	70	76	82	100 Pa	3200 Pa
13-1070	70-22	1.559	0.7756	---	4.057	1.957		0.822	0.9035
13-1081	70-22	1.542	0.7674	---	4.003	1.924		0.8727	0.9633
14-1021	76-22	---	1.582	0.9091	---	3.074	1.833	0.174	0.1799
14-1047	76-22	---	1.68	0.9851		3.012	1.813	0.1731	0.1739
15-1012	76-22	1.681	0.9539	---	2.439	1.27	---	0.3572	0.4939
15-1068	82-28	---	4.498	3.246			4.907	0.0299	0.03063
15-1080	70-22	1.165	0.5843	---	3.399	1.642	---	0.9432	1.073
15-1084	76-22	---	1.41	0.7629	---	3.736	2.0260	0.1526	0.1892

RTFO = rolling thin film oven aging; PG = performance grade; --- = no data.

Comparison of Morphological Characteristics With Performance-Based Tests

Flow Number Test

To quantify the permanent deformation behavior of SMA mixtures and correlate it with the aggregate morphological characteristics, the flow number and FNS were considered as two major indicators of asphalt mixtures to evaluate the rutting potential.

Flow Number

Regression analyses were performed between aggregate morphologies and the logarithms of the flow numbers, which are denoted as Log(FN). A total of four regression pairs between the four morphological characteristics and the flow number test parameters Log(FN) were analyzed statistically. The descriptive statistics of the aggregate morphological characteristics and the permanent deformation parameter (Log(FN)) are listed in Table 22. The regression pairs that have a p-value higher than the specified significance level of 5% ($\alpha = 0.05$) were considered to have a poor correlations between the response and the predictor variables. Regression analyses were performed only on the regression pairs in bold type, since they had the meaningful p-values that indicate statistical significance.

Figures 19 through 22 show the linear regression analyses conducted between the weighted mean morphological characteristics (sphericity [S], flat and elongation ratio [FER], angularity factor [AF], and texture factor [TF]) and the measured permanent deformation parameters Log(FN) of all SMA mixtures. As shown in Figures 19 through 22, Log(FN) increases with increased weighted mean S, AF, and TF values. It is generally accepted that the higher the FN, the lower the rutting susceptibility. Therefore, using more of the spherical, angular, or better-crushed rough coarse aggregate particles in SMA mixtures, as indicated by higher S, AF, and TF values, can improve the resistance of the SMA to rutting. More angular aggregates in the mixtures improved rutting resistance potential because of better interlocking in the aggregate skeleton. Rougher textured aggregates in the mixtures improved rutting performance because of stronger aggregate structures and higher stability. In Figure 20, Log(FN) also increases with decreased weighted mean FER values. Likewise, aggregates with fewer F&E aggregate particles, as indicated by lower FER values, can promote the rutting performance of the SMA mixtures. F&E particles tend to break up easily and are considered undesirable in SMA mixtures. The SMA mixtures with more spherical, less flat and elongated aggregates that also exhibit more angular, rougher-textured surfaces have better rutting resistance.

Table 22. Statistical Results of Regression Analyses Between Aggregate Morphologies and Flow Numbers

Regression Pair	T Stat	p-value
Log(FN)-S	2.801	**0.01041**
Log(FN)-FER	-2.868	**0.008938**
Log(FN)-AF	4.889	**6.889E-05**
Log(FN)-TF	3.741	**0.001133**

Bold type indicates statistical significance. FN = flow number, S = sphericity, FER = flat and elongated ratio, AF = angularity factor, TF = texture factor.

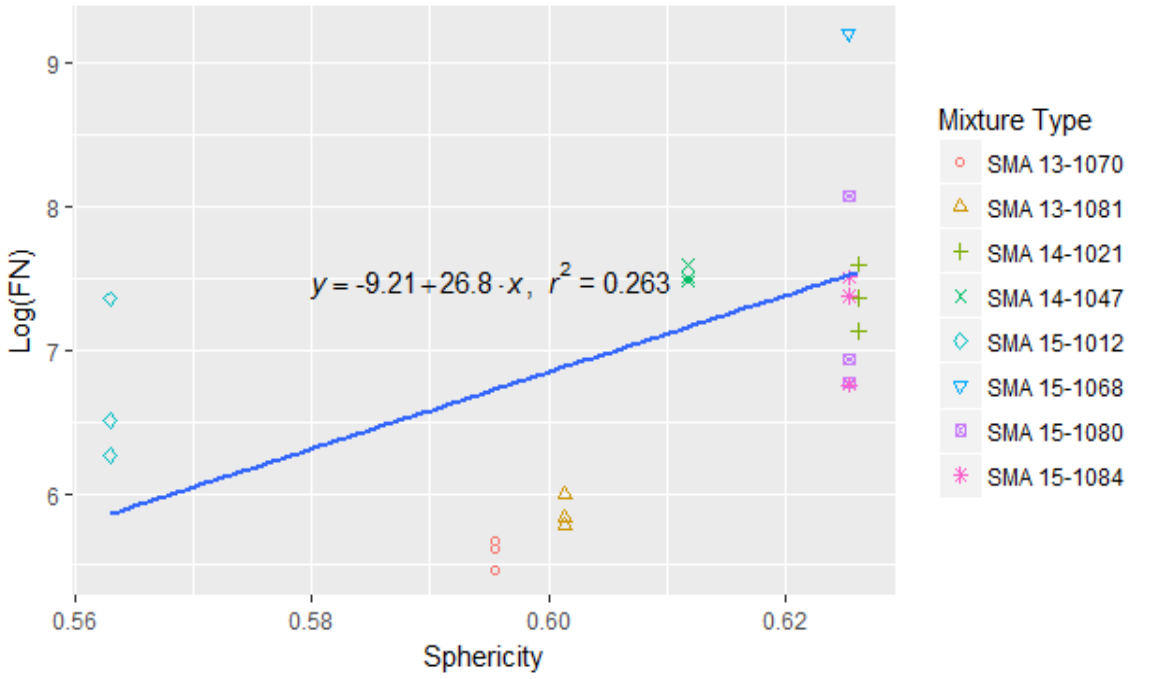

Figure 19. Sphericity vs. Log(FN) for All SMA Mixtures. FN = flow number; SMA = stone matrix asphalt.

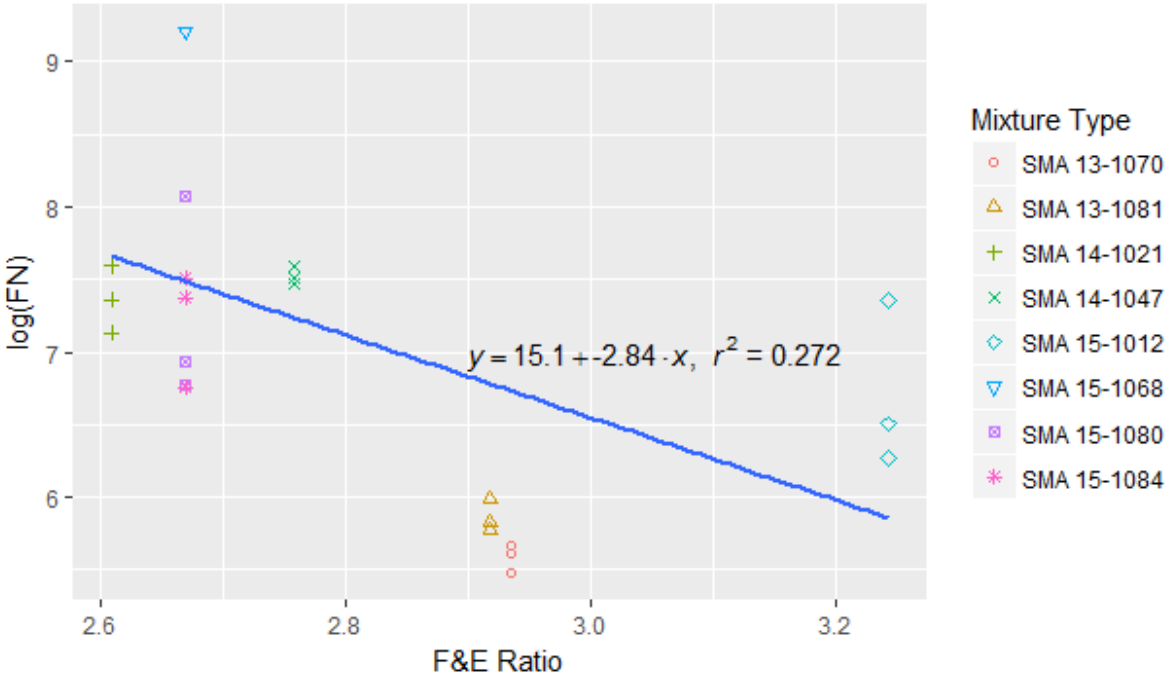

Figure 20. F&E Ratio vs. Log(FN) for All SMA Mixtures. F&E = flat and elongated; FN = flow number; SMA = stone matrix asphalt.

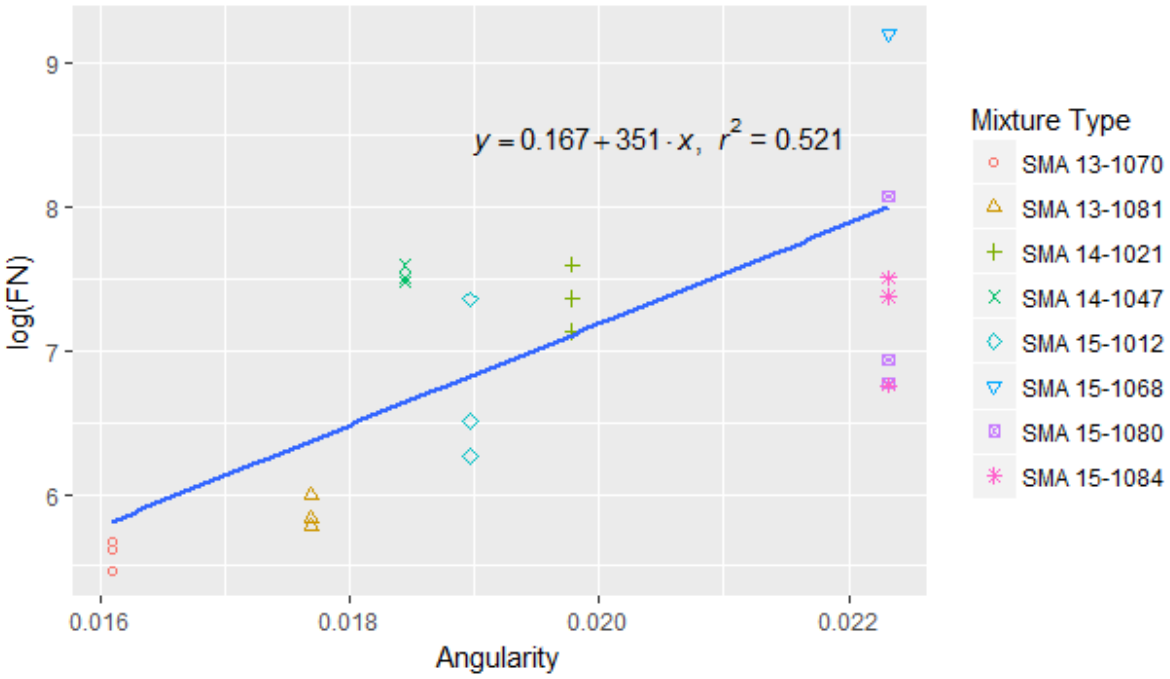

Figure 21. Angularity vs. Log(FN) for All SMA Mixtures. FN = flow number; SMA = stone matrix asphalt.

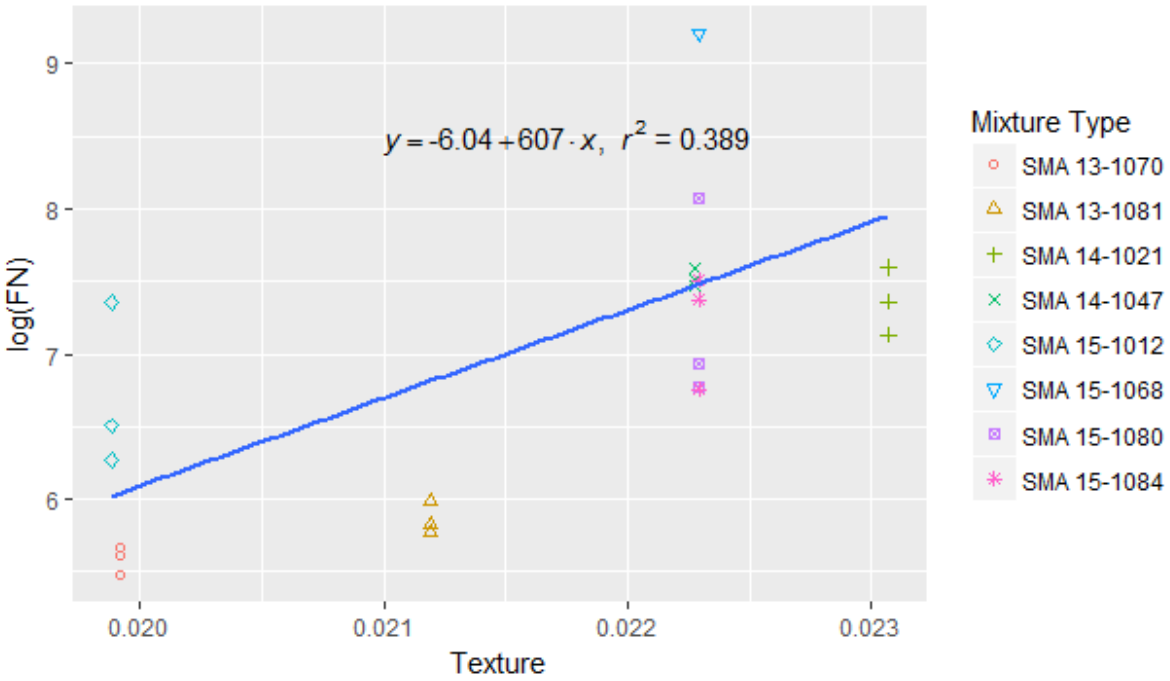

Figure 22. Texture vs. Log(FN) for All SMA Mixtures. FN = flow number; SMA = stone matrix asphalt.

Flow Number Slope

The FNS characterizes the rate of change of cumulative permanent deformation under the repeated loading condition and was found to relate well to the rutting performance of asphalt mixture pavements. To investigate how aggregate morphology would affect the rate of change of vertical permanent deformation, FNS was used as another important indicator that could be affected by the aggregate morphological characteristics. Statistical analyses between the FNS and both the asphalt content and performance grades of the eight asphalt mixtures are provided in Table 23. The lower p-value in bold indicates that FNS had correlations with the performance grade of the asphalt binder. Figure 23 presents the plot of FNS versus the performance grade of the asphalt binder. As seen in Figure 23, the stiffer the asphalt binder, the lower the FNS and the better the rutting resistance. The FNS data were then grouped based on different asphalt binder stiffnesses (PG 70 and PG 76); two separate sets of regression analyses were performed for the different categorized SMA mixtures. The descriptive statistics of the aggregate morphological characteristics and the FNS are listed in Tables 24 and 25. The regression pairs with a p-value higher than the specified significance level of 5% ($\alpha = 0.05$) were considered to have poor correlations between the response and the predictor variables. Regression analyses were performed only on the regression pairs in bold type, since they had the meaningful p-values that indicate statistical significance.

Figures 24 through 27 show the linear regression analyses conducted between the weighted mean morphological characteristics (S, FER, AF, and TF) and the measured permanent deformation parameter FNS for all SMA mixtures with or without grouping of the FNS data based on PG grade. As shown in Figure 25, FNS increases with increased weighted mean FER values. FNS decreases with increased weighted mean S, AF, and TF values. It is generally accepted that the lower the FNS, the better the rutting resistance. Therefore, using more of the spherical, angular, or better-crushed rough less flaky coarse aggregate particles in SMA mixtures, as indicated by higher S, AF, and TF values and lower FER values, can improve the resistance of the SMA to rutting. From Figures 24 through 27 it can also be seen that with polymer-modified binder, better rutting resistance can be obtained even if the aggregate morphological characteristics are slightly less favorable.

Table 23. Statistical Results of Regression Analyses Between Flow Number Slope and Asphalt Content and Performance Grade

Regression Pair	T Stat	p-value
FNS-AC	0.447	0.6591
FNS-PG	-5.043	**4.746e-05**

Bold type indicates statistical significance. FNS = flow number slope; AC = asphalt content; PG = performance grade.

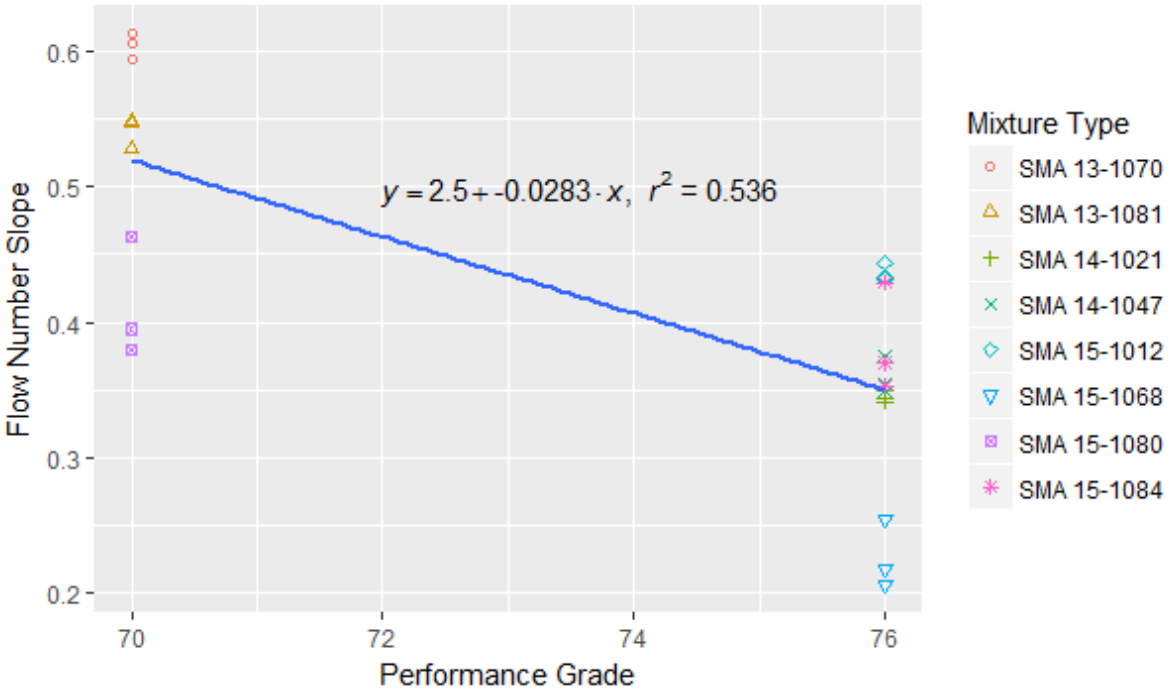

Figure 23. Performance Grade of Asphalt Binder vs. Flow Number Slope. SMA = stone matrix asphalt.

Table 24. Statistical Results of Regression Pairs Between Aggregate Morphologies and Flow Number Slopes

Regression Pair	T Stat	p-value
FNS-S	-2.786	**0.01077**
FNS-FER	2.947	**0.007458**
FNS-AF	-5.132	**3.828e-05**
FNS-TF	-4.603	**0.0001383**

Bold type indicates statistical significance. FNS = flow number slope; S = sphericity; FER = flat and elongated ratio; AF = angularity factor; TF = texture factor.

Table 25. Statistical Results of Regression Pairs Between Aggregate Morphologies and Flow Number Slopes When Categorized Based on Asphalt Binder Stiffness

Regression Pair	T Stat	p-value
FNS-S (PG = 70)	-8.482	**6.263e-05**
FNS-FER (PG = 70)	6.660	**0.0002879**
FNS-AF (PG = 70)	-9.182	**3.743e-05**
FNS-TF (PG = 70)	-7.053	**0.0002018**
FNS-S (PG = 76)	-2.933	**0.01165**
FNS-FER (PG = 76)	2.758	**0.0163**
FNS-AF (PG = 76)	-2.238	**0.04333**
FNS-TF (PG = 76)	-2.335	**0.03622**

Bold type indicates statistical significance. FNS = flow number slope; S = sphericity; PG = performance grade; FER = flat and elongated ratio; AF = angularity factor, TF = texture factor.

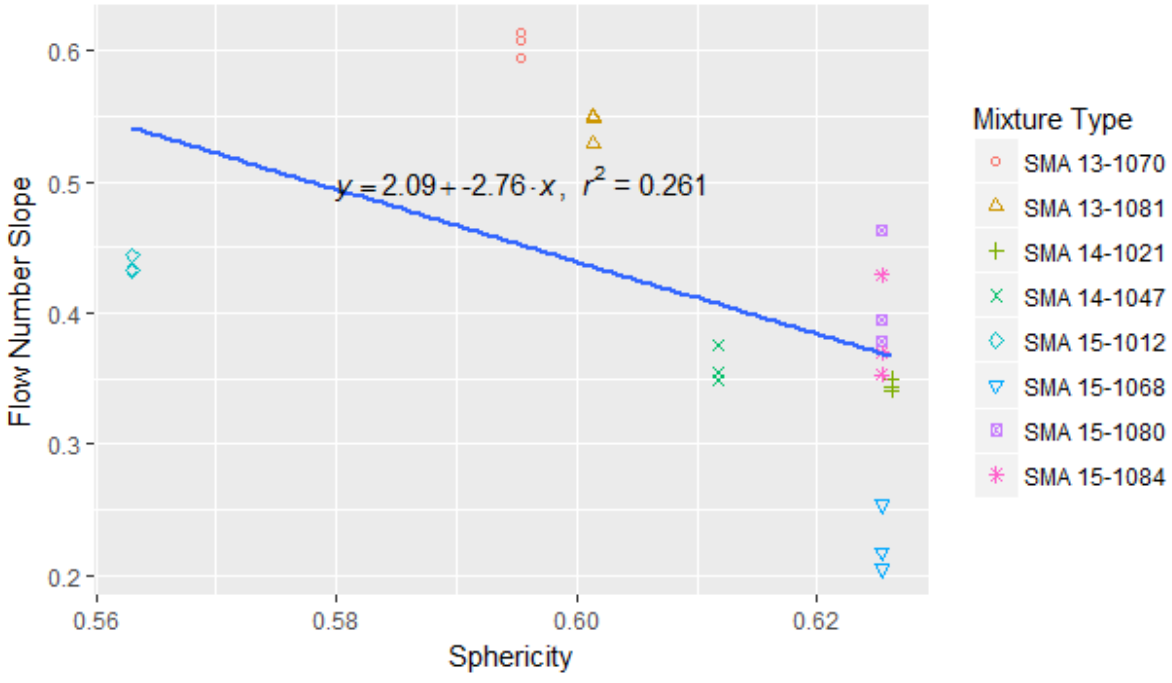

(a)

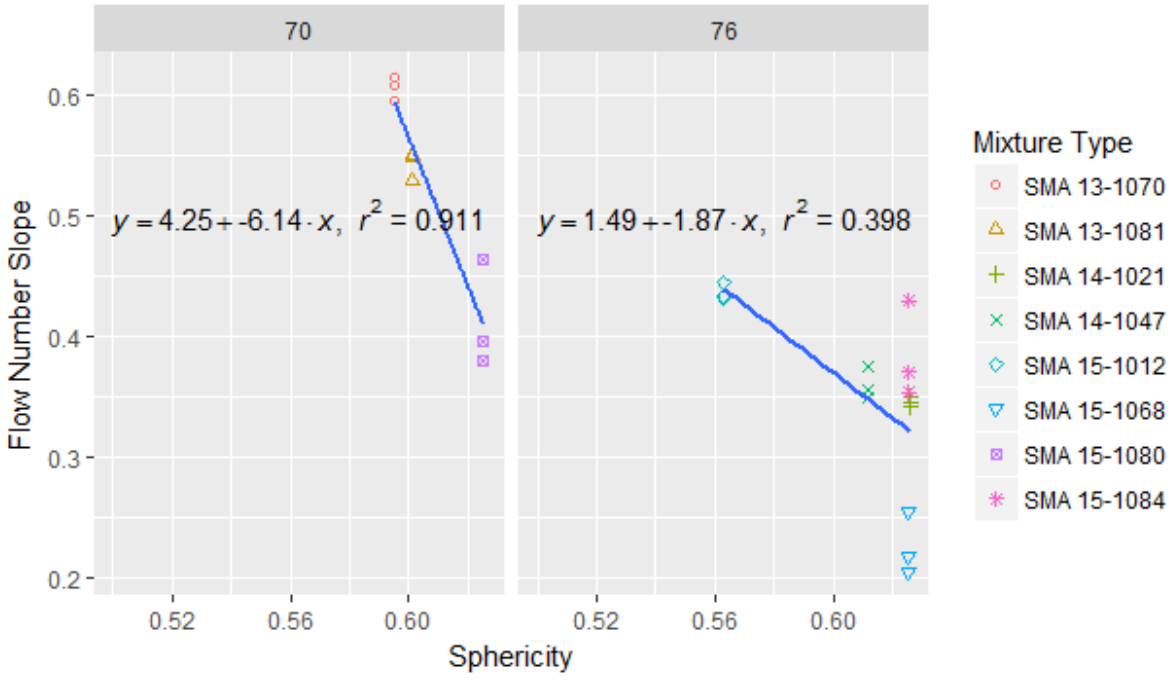

(b)

Figure 24. Sphericity vs. FNS: (a) for all SMA mixtures; (b) for SMA mixtures with PG 70-22 (*left*) and PG 76-22 (*right*) binder. FNS = flow number slope; SMA = stone matric asphalt.

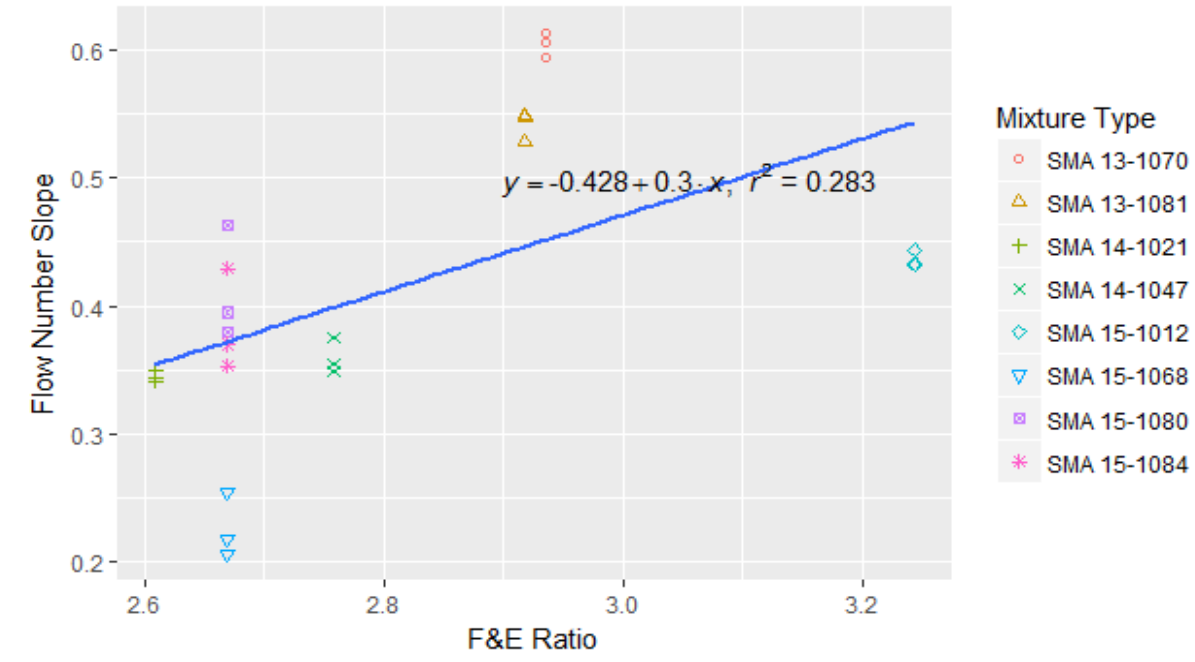

(a)

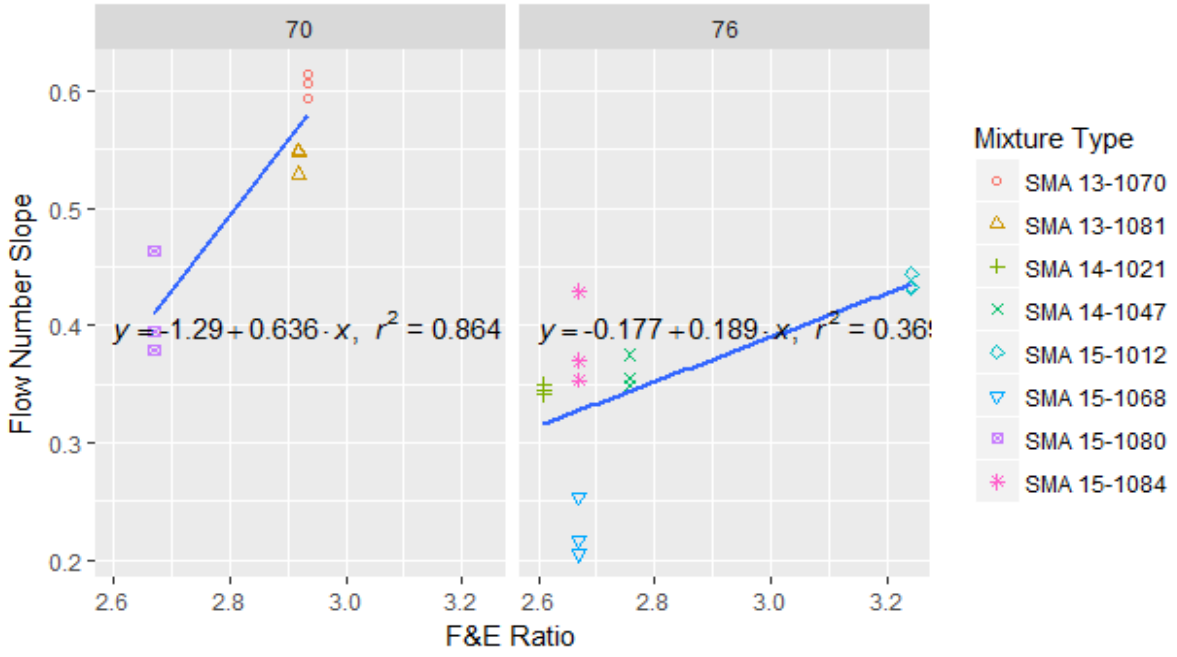

(b)

Figure 25. F&E Ratio vs. FNS: (a) for all SMA mixtures; (b) for SMA mixtures with PG 70-22 (*left*) and PG 76-22 (*right*) binder. F&E = flat and elongated; FNS = flow number slope; SMA = stone matrix asphalt.

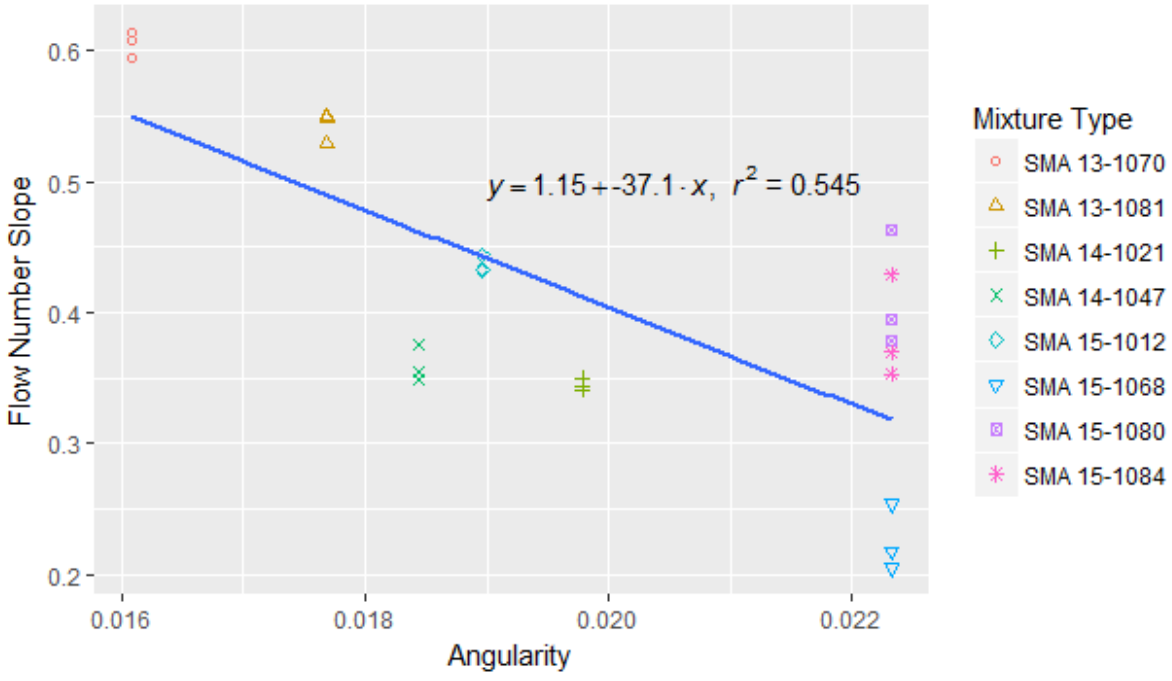

(a)

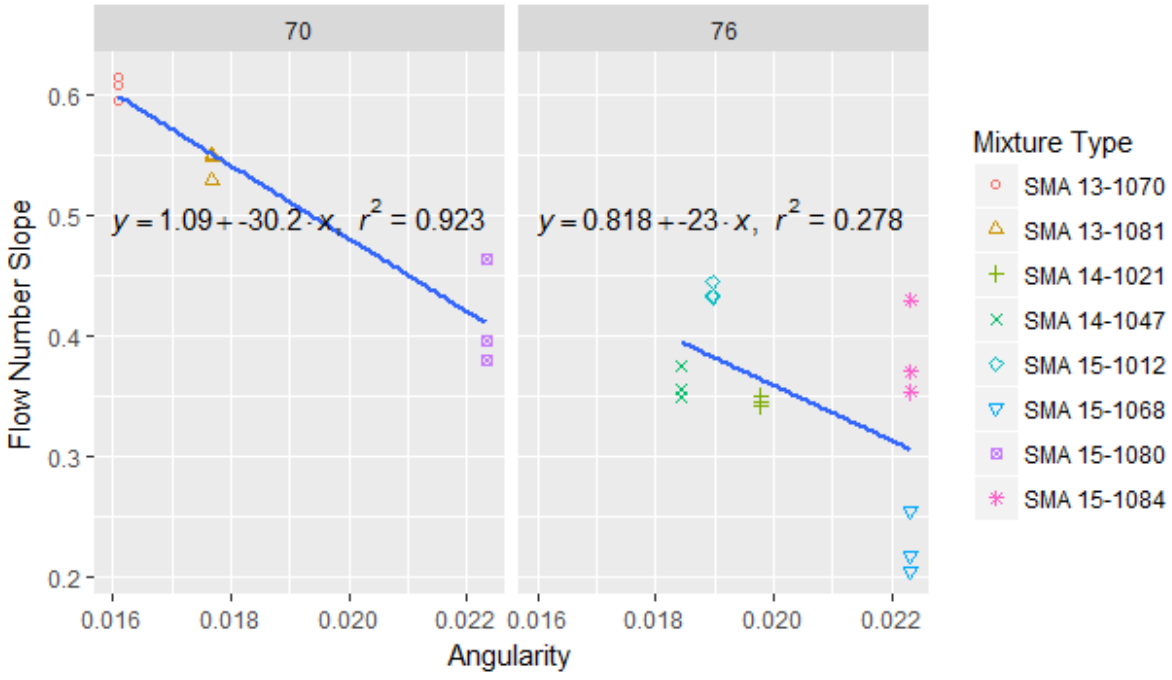

(b)

Figure 26. Angularity vs. FNS: (a) for SMA mixtures; (b) for SMA mixtures with PG 70-22 (*left*) and PG 76-22 (*right*) binder. FNS = flow number slope; SMA = stone matrix asphalt.

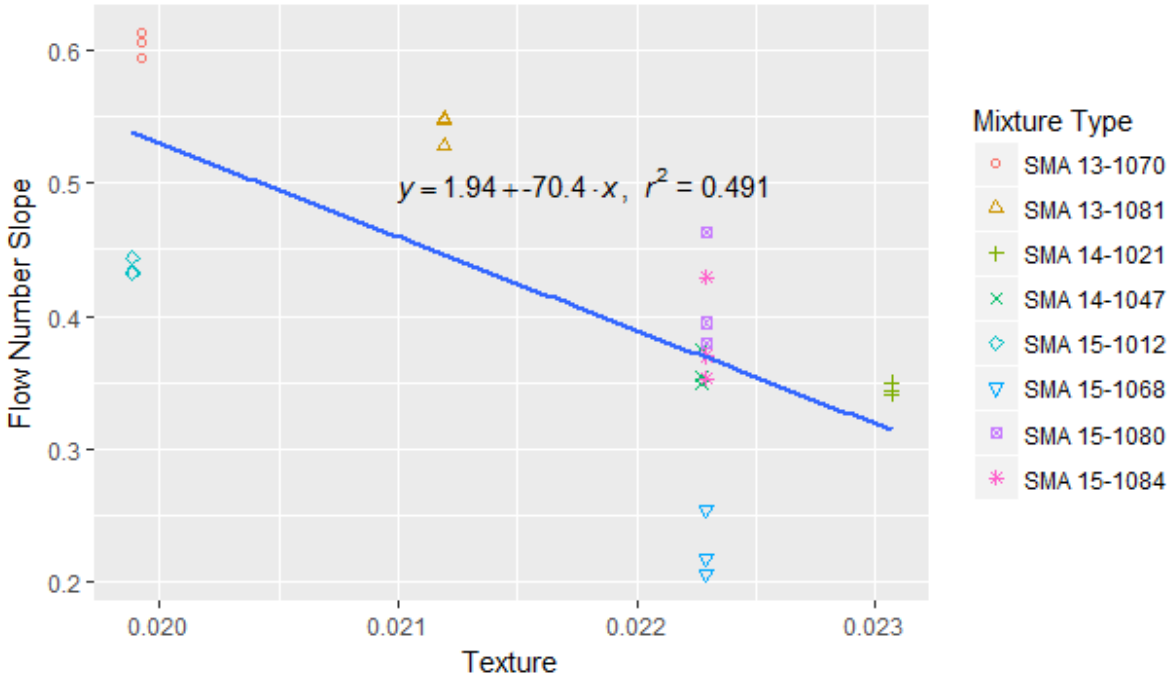

(a)

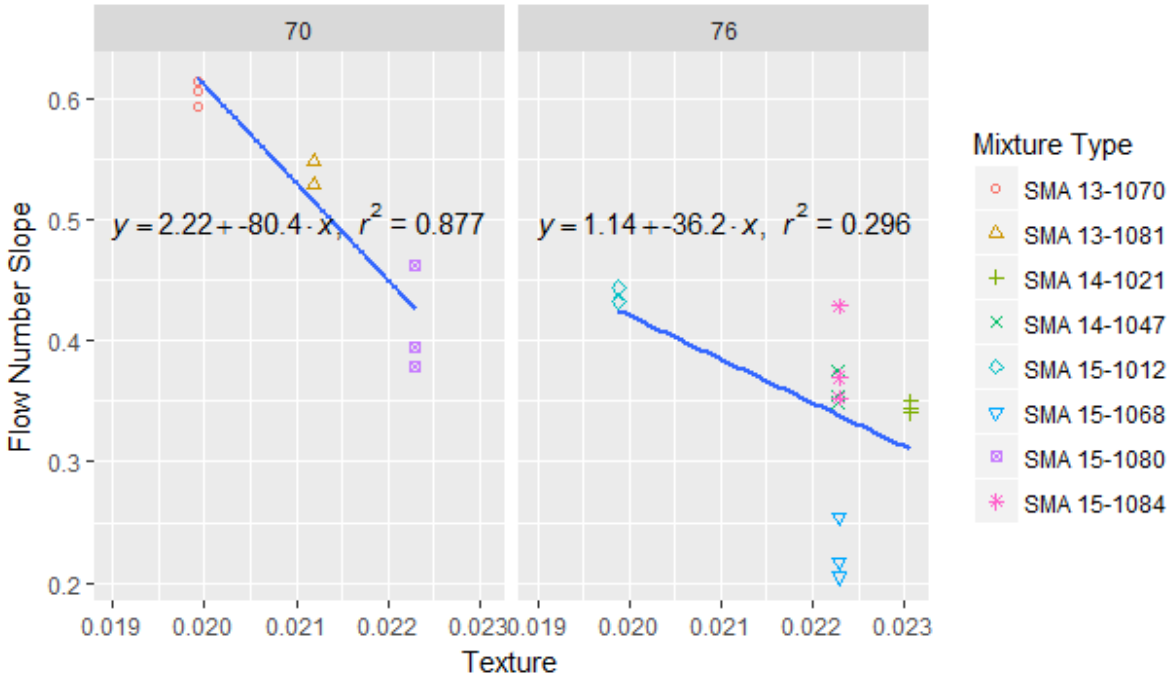

(b)

Figure 27. Texture vs. FNS: (a) for SMA mixtures; (b) for SMA mixtures with PG 70-22 (*left*) and PG 76-22 (*right*) binder. FNS = flow number slope; SMA = stone matrix asphalt.

Fatigue Performance of SMA Under Different Strain Levels Using the Beam Fatigue Test

The number of loading cycles to failure under three different strain levels obtained from beam fatigue tests was used as another important indicator to measure the fatigue performance of SMA mixtures. The statistical analyses were performed between the number of loading cycles to failure under three different strain levels and both the asphalt contents and performance grades of all the mixtures. The statistical results are shown in Table 26. As shown, the number of loading cycles and performance grade regression pairs under 300 and 600 microstrain show a p-value smaller than the significance level of 5%, indicating the asphalt binder performance grade can significantly affect the number of loading cycles to failure at 300 and 600 microstrain. Asphalt contents among different mixtures were similar and hence showed lower significance. Figure 28 shows that the stiffer the asphalt binder (through polymer modification), the more loading cycles the SMA mixtures can withstand until failure.

To interpret the beam fatigue test results better, the measured number of loading cycles to failure (NOC) under different strain levels were taken as logarithms for the studied eight types of SMA mixtures, each with three replicates. Regression analyses were performed between aggregate morphologies and Log(NOC). A total of 15 regression pairs between the five morphological characteristics and the Log(NOC) under three different strain levels were analyzed statistically.

The descriptive statistics of the aggregate morphological characteristics and the fatigue parameter (Log(NOC)) are listed in Table 27. The regression pairs that have a p-value greater than the specified significance level of 5% ($\alpha = 0.05$) were considered to have poor correlations between the dependent and independent variables. Regression analyses were performed only on the regression pairs in bold type, which had the p-values less than 5%.

Figure 29 shows the correlations of Log(NOC) with the weighted mean AF and TF values under 300 microstrain. Figure 30 shows the regression relationship between Log(NOC) and the weighted mean AF and TF values under 450 microstrain. Figure 31 shows the correlation of Log(NOC) with the weighted mean TF under 600 microstrain. As shown, Log(NOC) tended to increase as angularity and texture increased, indicating that SMA mixtures with more angular and rougher aggregates can withstand more loading cycles until failure and have a better fatigue life.

Table 26. Statistical Results of Regression Analyses Between Number of Loading Cycles to Failure and Asphalt Content and Performance Grade

Regression Pair	T Stat	p-value	R^2
NOC-AC (300 microstrain level)	-0.088	0.9307	0.0004325
NOC-PG (300 microstrain level)	5.674	**2.214e-05**	0.6414
NOC-AC (450 microstrain level)	1.144	0.2675	0.0678
NOC-PG (450 microstrain level)	2.101	0.05001	0.1969
NOC-AC (600 microstrain level)	1.251	0.2253	0.0726
NOC-PG (600 microstrain level)	2.671	**0.01469**	0.2629

Bold type indicates statistical significance. NOC = number of loading cycles to failure under different strain levels; AC = asphalt content; PG = performance grade.

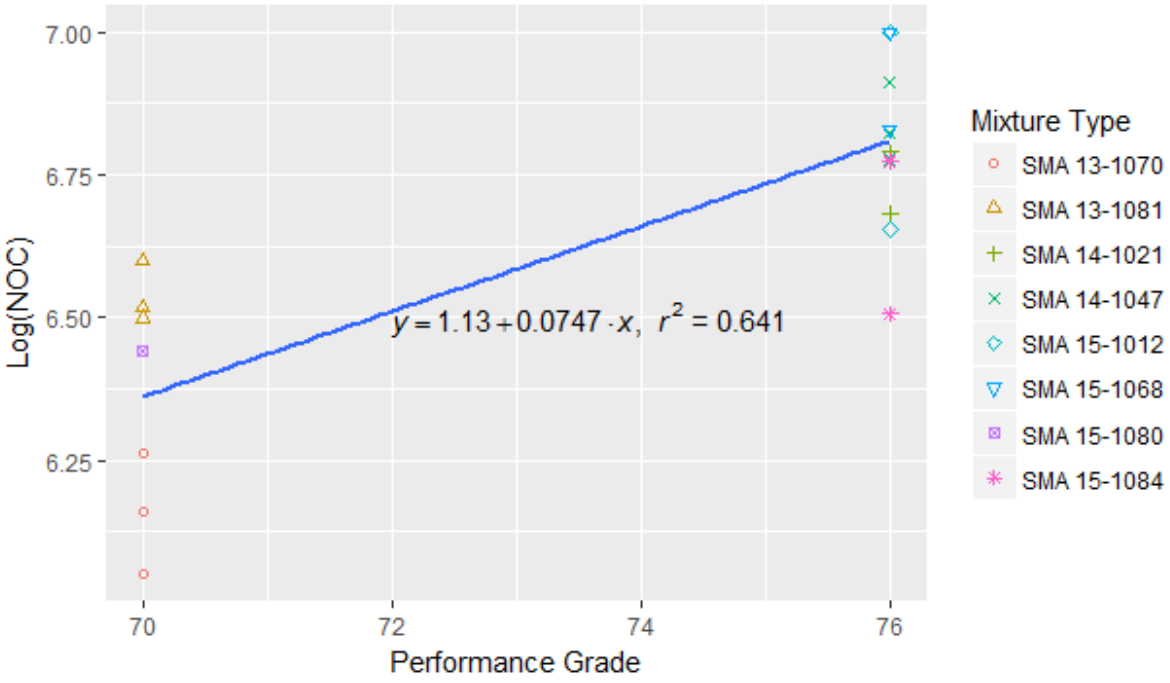

(a)

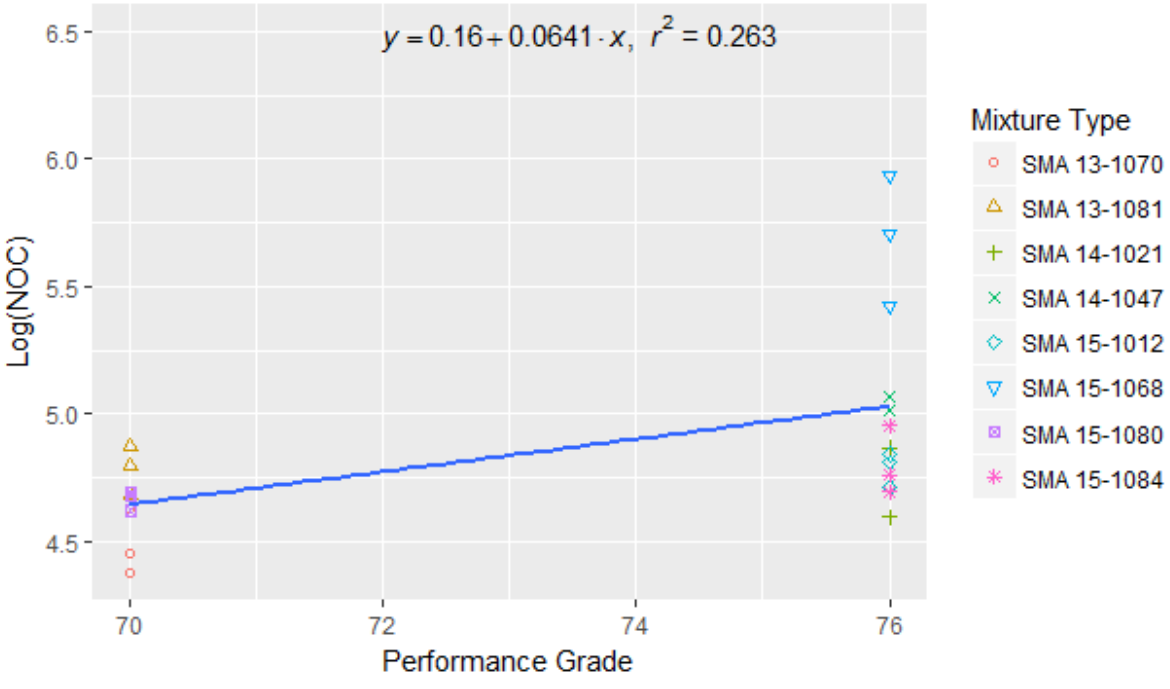

(b)

Figure 28. Performance Grade of Asphalt Binder vs. Number of Cycles to Failure: (a) under 300 microstrain level; (b) under 600 microstrain level. NOC = number of loading cycles to failure; SMA = stone matrix asphalt.

Table 27. Statistical Results of Regression Pairs Between Aggregate Morphologies and Number of Loading Cycles to Failure Under Different Strain Levels

Regression Pair	T Stat	p-value
Log(NOC)-S (300 microstrain level)	0.994	0.3333
Log(NOC)-FER (300 microstrain level)	-1.065	0.3009
Log(NOC)-AF (300 microstrain level)	3.031	**0.007185**
Log(NOC)-TF (300 microstrain level)	2.757	**0.01299**
Log(NOC)-S (450 microstrain level)	1.855	0.08
Log(NOC)-FER (450 microstrain level)	-1.839	0.08248
Log(NOC)-AF (450 microstrain level)	2.246	**0.03747**
Log(NOC)-TF (450 microstrain level)	2.268	**0.03585**
Log(NOC)-S (600 microstrain level)	1.402	0.1763
Log(NOC)-FER (600 microstrain level)	-1.336	0.1964
Log(NOC)-AF (600 microstrain level)	2.343	**0.02958**
Log(NOC)-TF (600 microstrain level)	1.833	0.08177

Bold type indicates statistical significance. NOC = number of loading cycles to failure under different strain levels; S = sphericity; FER = flat and elongated ratio; AF = angularity factor; TF = texture factor.

The fatigue properties of SMA mixtures could be greatly improved for aggregate blends with higher AF and TF indices. The effect of texture on the fatigue resistance of SMA mixtures was positive because rough-textured aggregates improved inter-particle contact and provided a better binder-aggregate interaction, which made the SMA mixtures more resistant to fatigue cracking. Fatigue cracking can be decreased by improving the aggregate-binder interactions through using aggregates with rougher texture. Thus, angular and rough-textured aggregates in SMA mixtures are crucial and desirable to obtain better fatigue performance. Little et al. (2003) also demonstrated that granite mixtures show better fatigue performance than limestone mixtures because the granite aggregates are rougher and more angular.

Uncompacted Void Content of Coarse Aggregates

Figure 32 presents the distributions of five morphological parameters for the first 16 aggregate fractions, including sphericity, flatness ratio, elongation ratio, angularity, and texture. Those aggregates were selected randomly without sieving. A total of 120 aggregates were selected for each type of aggregate. The figure shows the ranges and mean values of morphological characteristics for 16 types of aggregates.

The greatest sphericity was for 13-1073 Staunton #68, and the smallest was for 13-1073 Staunton #8. This difference is statistically significant, as determined by an analysis of variance (ANOVA) for all locations and a Tukey honest significant difference test between all pairs of locations. This may be because 13-1073 Staunton #68 was produced with an impact crusher, where particles impact each other, therefore producing more equant particles, whereas 13-1073 Staunton #8 was processed using a jaw crusher, which cannot produce particles as equant as the impact crusher. Further, it can be seen that the 13-1071 Bealeton aggregates have close mean values of sphericity, as do the 14-1019 Leesburg aggregates. This indicates that aggregates from the same origin might have similar morphological characteristics.

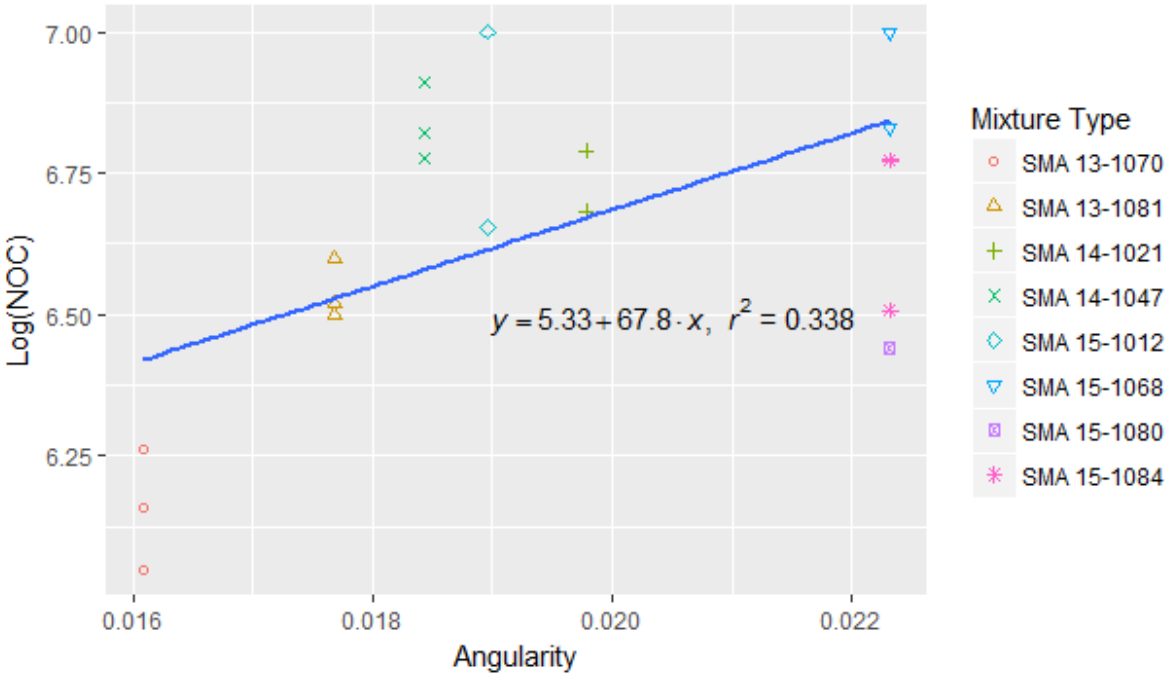

(a)

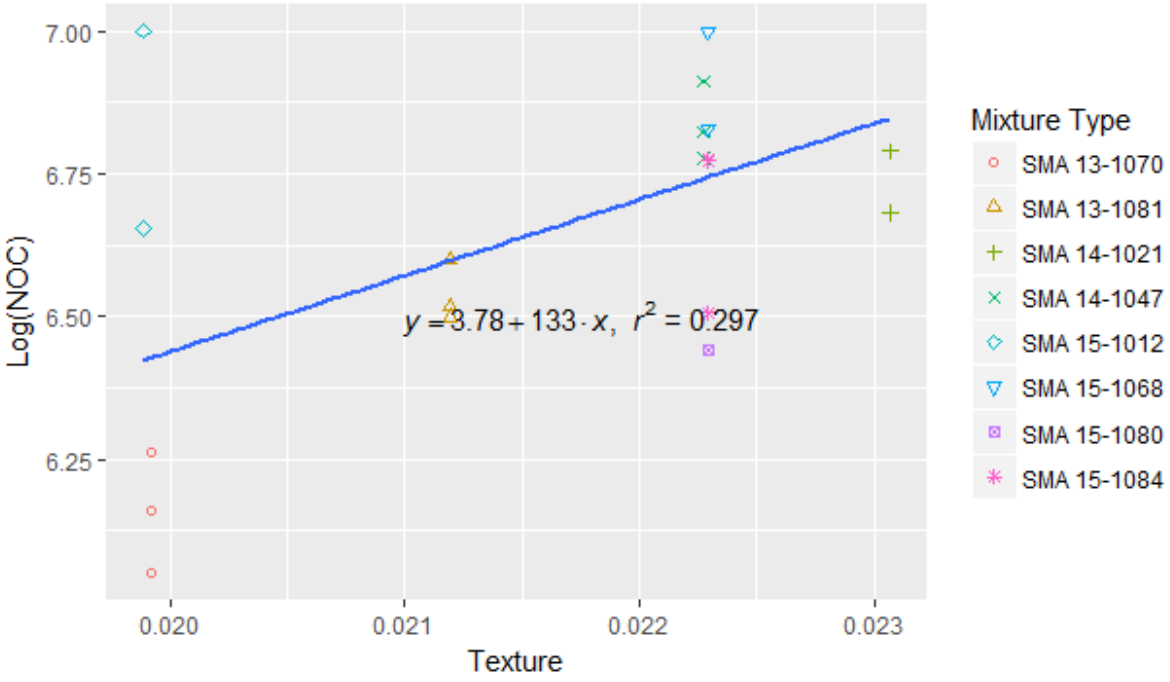

(b)

Figure 29. Angularity and Texture vs. Number of Cycles to Failure: (a) angularity vs. Log(NOC) for all SMA mixtures under 300 microstrain level; (b) texture vs. Log(NOC) for all SMA mixtures under 300 microstrain level. NOC = number of loading cycles to failure; SMA = stone matrix asphalt.

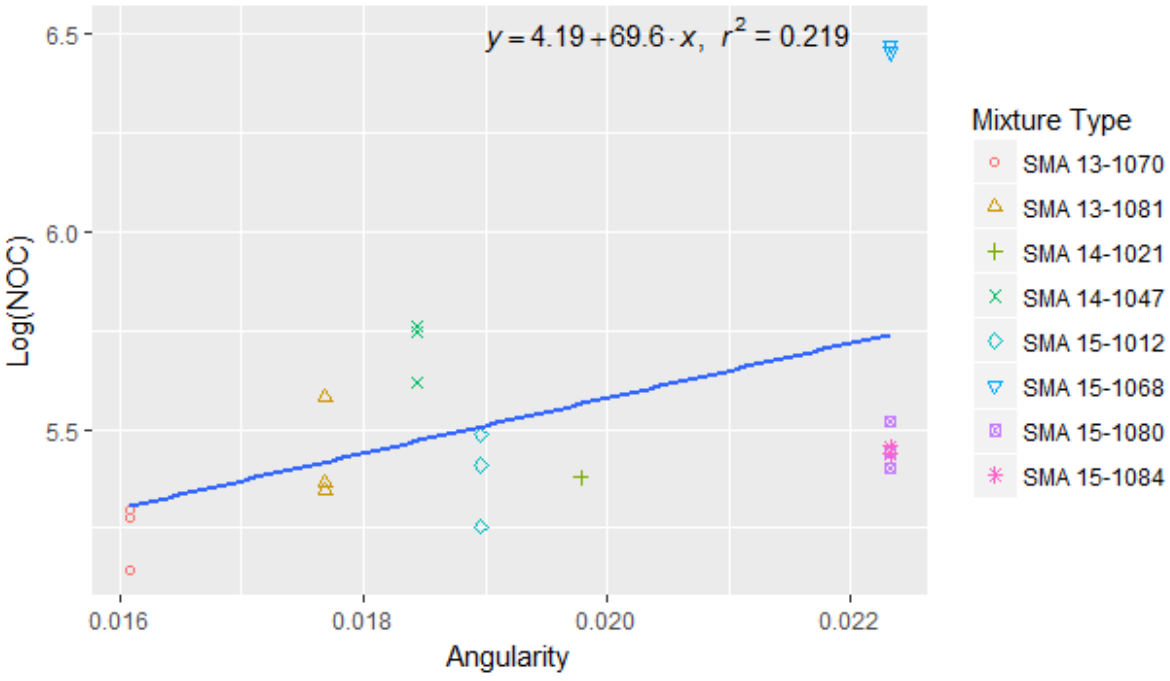

(a)

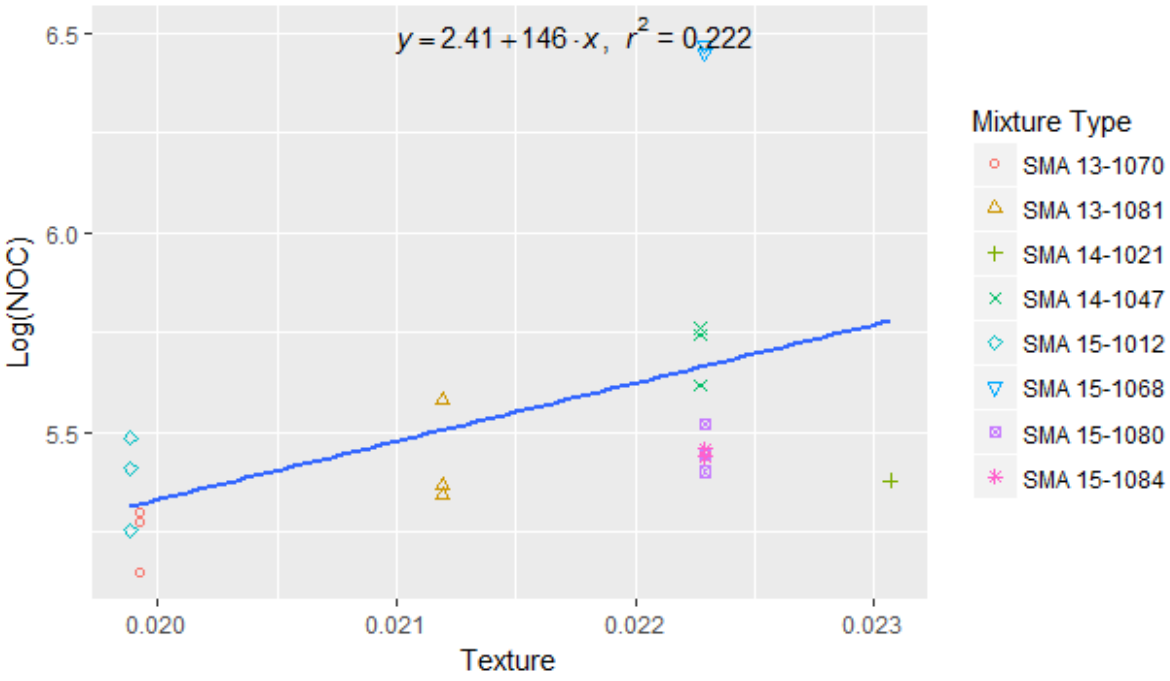

(b)

Figure 30. Angularity and Texture vs. Number of Cycles to Failure: (a) angularity vs. Log(NOC) for all SMA mixtures under 450 microstrain level; (b) texture vs. Log(NOC) for all SMA mixtures under 450 microstrain level. NOC = number of loading cycles to failure; SMA = stone matrix asphalt.

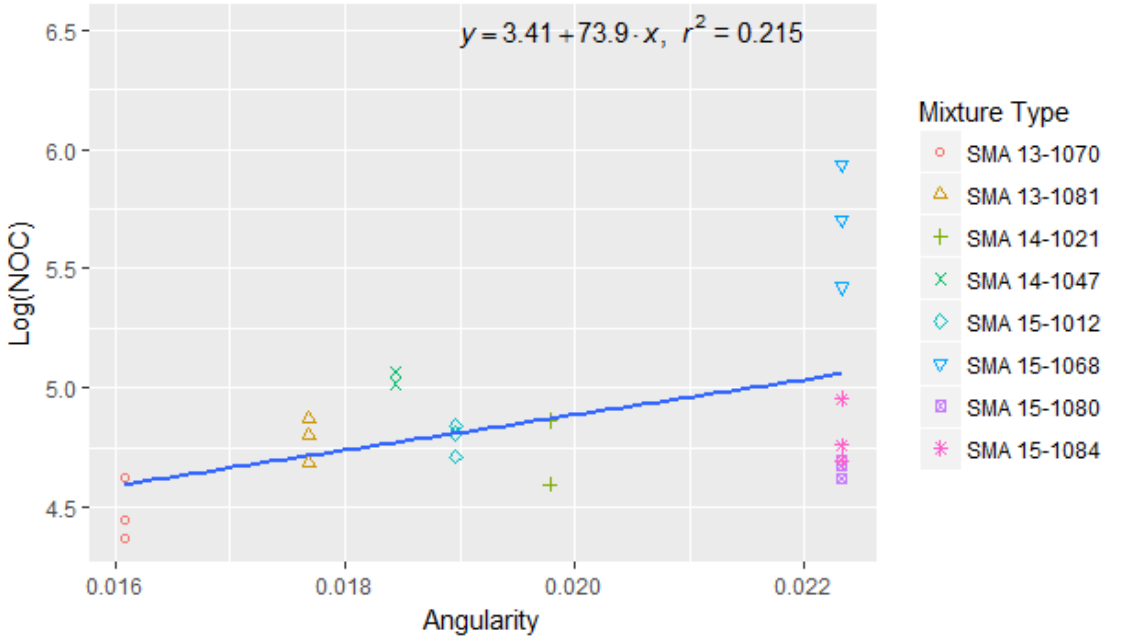

Figure 31. Angularity vs. Log(NOC) for All SMA Mixtures Under 600 Microstrain Level. NOC = number of loading cycles to failure; SMA = stone matrix asphalt.

The 13-1071 Bealeton aggregate fractions have a smaller flatness ratio than the other aggregate fractions, which implies that the 13-1071 Bealeton aggregates are the flattest. It is obvious that the 13-1073 Staunton aggregates, 13-1071 Bealeton aggregates, 14-1048 Bealeton aggregates, and 14-1019 Leesburg aggregates have different flatness ratio values, although they are all diabase. These differences are also statistically significant using the same ANOVA as before. One possible explanation is that aggregates with the same rock type but from different locations have different morphological characteristics because of difference in rock fabric and production and handling processes. It can be seen that 13-1073 Staunton #68 has the greatest elongation ratio and 13-1073 Staunton #8 has the smallest. This difference is statistically significant. This also might be due to the use of different crushers.

It can be seen that 14-1048 Bealeton #60 was the most angular aggregate, followed by 14-1019 Leesburg #78 and then 13-1073 Staunton #68, which are all coarse aggregates. The least angular was 3-1073 Staunton #10, which is fine aggregate. This indicates that coarse aggregates might have more angular particles than fine aggregates, which further implies that different sized aggregates might have different morphological characteristics.

It can be seen that 13-1071 Bealeton RAP, 14-1048 Bealeton RAP, and 14-1019 Leesburg RAP had the greatest texture. This might be due to the fact that RAP is a special material type, a mixture of aggregates and asphalt binder that have been pulled apart. The 13-1073 Staunton aggregates had different texture values; this might be because the Staunton aggregates consisted of a different set of rock types. All other types of aggregates tended to have very close texture values.

Overall, it can be concluded that aggregate morphological characteristics will be influenced by size, material type, origins, and production technology.

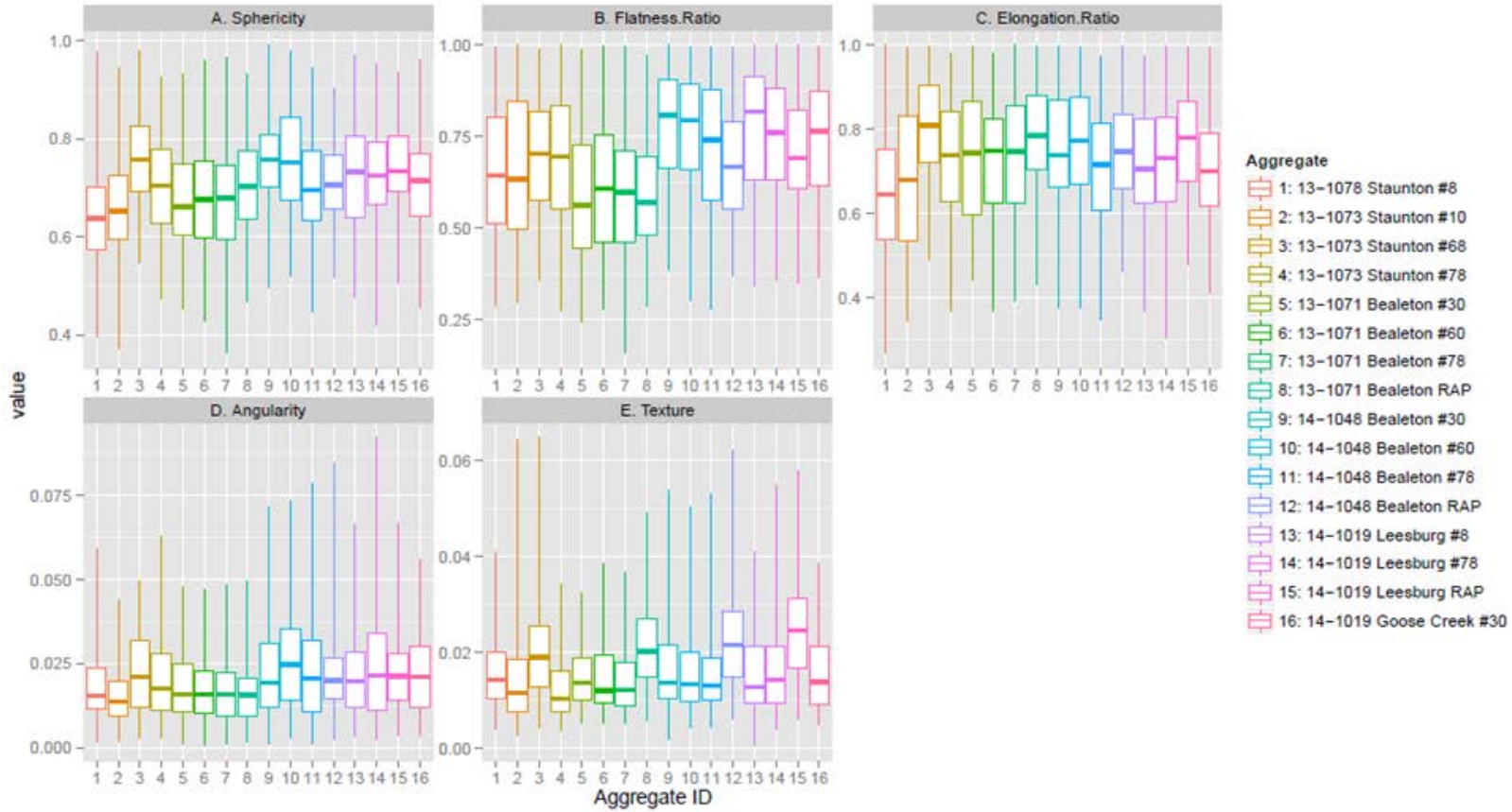

Figure 32. Improved FTI Morphological Characteristic Distributions of 16 Aggregate Fractions. FTI = Fourier transform interferometry; RAP = recycled asphalt pavement.

Aggregates with the size ranges of 4.75 to 9.5 mm and 9.5 to 12.5 mm were analyzed to evaluate the relationship between morphological characteristics and the uncompacted void content of coarse aggregates. To examine the effects of the morphological characteristics on the uncompacted void content of coarse aggregates, the void contents were measured for aggregates in two size ranges: 8 types of aggregates were measured for particles that pass the 9.5 mm sieve but are retained on the 4.75 mm sieve, and 11 types of aggregates were examined for particles that pass the 12.5 mm sieve but are retained on the 9.5 mm sieve. The morphological characteristics, including sphericity, flatness ratio, elongation ratio, angularity, and texture, of these aggregates were obtained using the improved FTI system. The effects of the morphological characteristics (the independent variables) described on the uncompacted void content (the dependent variable) were examined using linear regression analysis.

Table 28 presents the correlation matrix between average uncompacted void contents and mean values of five morphological characteristics for aggregates passing the 9.5 mm sieve and retained on the 4.75 mm sieve. As can be seen in Table 28, for coarse aggregates retained on the 4.75 mm sieve, angularity and texture are most strongly correlated; flatness ratio, elongation ratio, and texture have the strongest influence on uncompacted void content.

Table 29 presents the correlation matrix between average uncompacted void contents and mean values of five morphological characteristics for aggregates passing the 12.5 mm sieve and retained on the 9.5 mm sieve. For coarse aggregates retained on the 9.5 mm sieve, sphericity and elongation ratio have the strongest correlation. Elongation ratio and angularity have the highest correlation with uncompacted void content, although it is weak.

As shown in Figures 33 and 34, the coefficients of determination (R^2) for the 4.75 to 9.5 mm sieve size and the 9.5 to 12.5 mm sieve size were 0.99 and 0.75, respectively, after the outlier was removed. The outlier comprised the data from 13-1073 Staunton #8 in Figures 33 and 34. It is distinct because 13-1073 Staunton #8 aggregates were produced by a jaw crusher; the other aggregates were produced by cone and impact crushers. Regression analysis showed that those five morphological characteristics correlated well with the uncompacted void content of coarse aggregates measured for individual sieve sizes. The respective calculated regression equations are as follows:

For aggregates retained on the 4.75 mm sieve (4.75 to 9.5 mm):

Uncompacted void content (%) = 54.278 – 100.121 (Sphericity) + 26.026 (Flatness ratio) + 61.579 (Elongation ratio) – 46.896 (Angularity) + 180.147 (Texture).

For aggregates retained on the 9.5 mm sieve (9.5 to 12.5 mm):

Uncompacted void content (%) = 59.288 + 200.82 (Sphericity) – 59.16 (Flatness ratio) – 144.612 (Elongation ratio) – 288.913 (Angularity) – 63.763 (Texture).

Table 28. Summary Data and Correlation Matrix for the 4.75 mm Sieve Size

Aggregates	Uncompacted Void Content (%)	Sphericity	Flatness Ratio	Elongation Ratio	Angularity	Texture
13-1078 Staunton #8	54.4000	0.5932	0.7072	0.5689	0.0197	0.0157
13-1073 Staunton #68	48.7000	0.5526	0.5113	0.5745	0.0135	0.0092
13-1073 Staunton #78	48.3000	0.6280	0.6324	0.6444	0.0139	0.0079
13-1071 Bealeton #60	49.7000	0.5683	0.5867	0.5793	0.0166	0.0118
14-1048 Bealeton #60	51.0000	0.6624	0.7049	0.6591	0.0247	0.0147
14-1048 Bealeton #78	49.9000	0.5693	0.6018	0.5607	0.0163	0.0120
14-1019 Leesburg #8	48.8000	0.6033	0.6859	0.5823	0.0189	0.0129
14-1019 Leesburg #78	49.2000	0.6039	0.9064	0.4962	0.0204	0.0065
Correlation Matrix						
Void Content	1.0000	-0.0700	-0.4767	0.5676	0.0934	0.4780
Sphericity		1.0000	0.6675	0.4364	0.1872	0.3543
Flatness Ratio			1.0000	-0.3717	0.4649	0.4140
Elongation Ratio				1.0000	-0.2947	-0.0066
Angularity					1.0000	0.7656
Texture						1.0000

Table 29. Summary Data and Correlation Matrix for the 9.5 mm Sieve Size

Aggregates	Uncompacted Void Content (%)	Sphericity	Flatness Ratio	Elongation Ratio	Angularity	Texture
13-1078 Staunton #8	53.8000	0.6338	0.6559	0.6447	0.0178	0.0157
13-1073 Staunton #68	49.1000	0.7537	0.7071	0.7891	0.0145	0.0169
13-1073 Staunton #78	46.8000	0.6625	0.6565	0.6888	0.0193	0.0116
13-1071 Bealeton #30	49.6000	0.5925	0.5689	0.6207	0.0168	0.0122
13-1071 Bealeton #60	47.8000	0.6521	0.5715	0.7179	0.0145	0.0135
14-1048 Bealeton #30	49.2000	0.7040	0.7664	0.7006	0.0151	0.0141
14-1048 Bealeton #60	48.8000	0.7152	0.7515	0.7089	0.0247	0.0151
14-1048 Bealeton #78	47.5000	0.6642	0.6992	0.6658	0.0227	0.0151
14-1019 Leesburg #8	48.0000	0.7088	0.7788	0.6878	0.0227	0.0166
14-1019 Leesburg #78	47.2000	0.6620	0.6957	0.6656	0.0225	0.0144
14-1019 Goose Creek #30	49.4000	0.6092	0.6823	0.5848	0.0216	0.0133
Correlation Matrix						
Void Content	1.0000	-0.0594	0.0265	-0.1403	-0.3007	0.0872
Sphericity		1.0000	0.6949	0.8636	-0.0455	0.7678
Flatness Ratio			1.0000	0.2449	0.4434	0.6544
Elongation Ratio				1.0000	-0.3999	0.5457
Angularity					1.0000	0.1792
Texture						1.0000

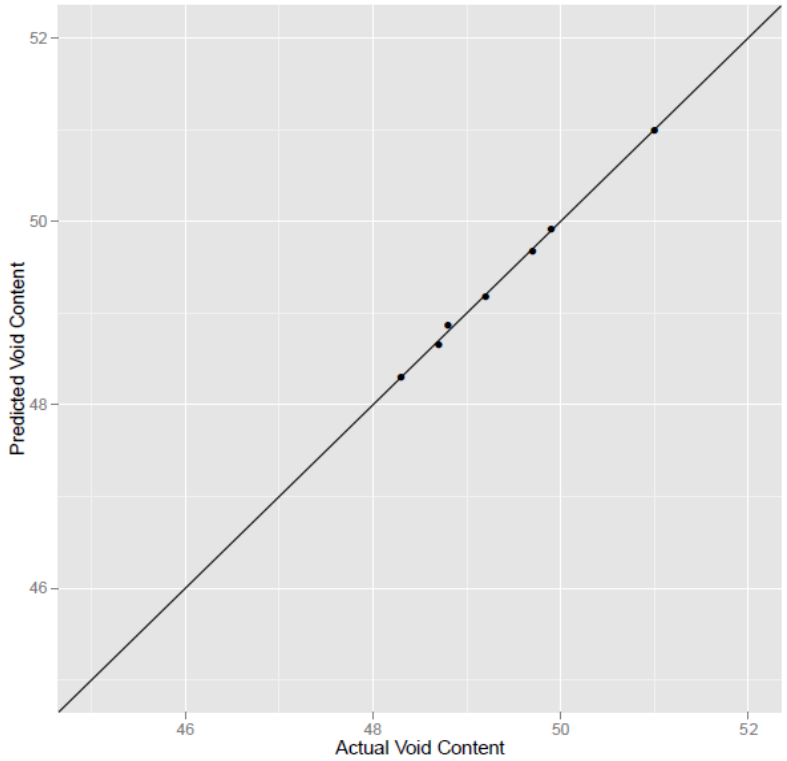

Figure 33. Actual vs. Predicted Uncompacted Void Content for Aggregates Passing the 9.75 mm Sieve and Retained on the 4.75 mm Sieve (R^2 = 0.99).

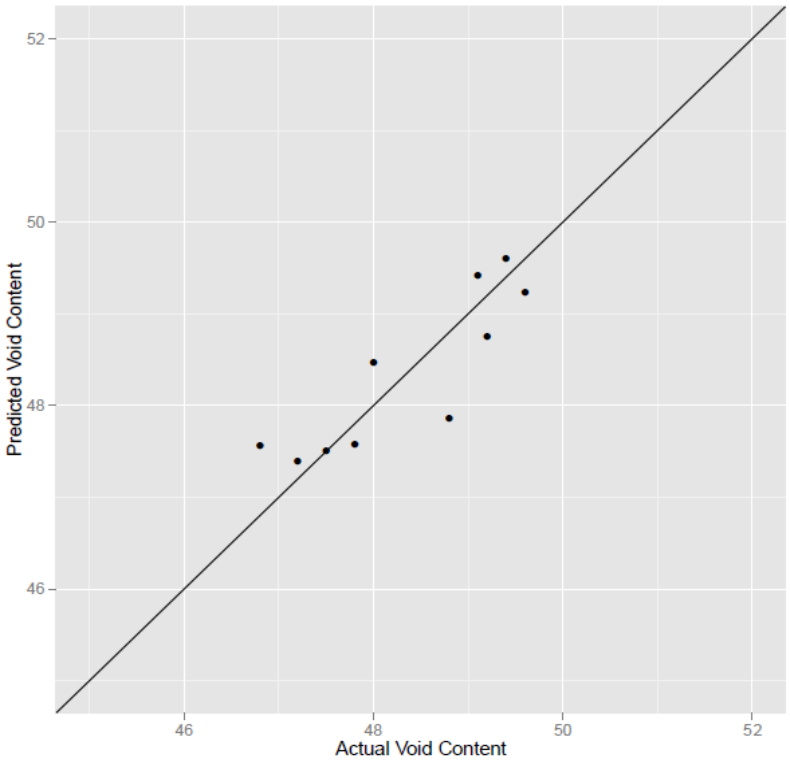

Figure 34. Actual vs. Predicted Voids for Aggregates Passing the 12.5 mm Sieve and Retained on the 9.5 mm Sieve (R^2 = 0.76).

For aggregates with the size range of 4.75 to 9.5 mm, the regression indicates that the predicted uncompacted void content increases with a decrease in sphericity and angularity and an increase in flatness ratio, elongation ratio, or texture. For aggregates with the size range of 9.5 to 12.5 mm, the regression indicates that the predicted uncompacted void content increases with an increase in sphericity and with a decrease in flatness ratio, elongation ratio, angularity, and texture. Both regressions indicate that the void content can vary with various morphological characteristics and increase with a decrease of sphericity and angularity for coarse aggregates of both size ranges. However, for fine aggregates, the uncompacted void content increases with an increase in angularity and roughness for two size ranges: No. 16 to No. 30, and No. 30 to No. 50 (Kuo and Freeman, 2000).

Overall, the regression models for coarse aggregates with size ranges of 4.75 to 9.5 mm and 9.5 to 12.5 mm indicate that morphological characteristics have a great impact on the uncompacted void content of coarse aggregates, as the coefficients of determination for the regression models were 0.99 and 0.76, respectively. Previous research on fine aggregates has been conducted on the relationship between shape characteristics and void content, which also validated such a finding (Dilek and Leming, 2004; Kuo and Freeman, 2000). However, this study investigated the relationship between morphological characteristics and uncompacted void contents of coarse aggregate for the first time. The effects of shape characteristics of different sized particles on uncompacted void content tend to be consistent for fine aggregates (Dilek and Leming, 2004; Kuo and Freeman, 2000), but it is a different case for the coarse aggregates included in this study. The regression models show that the effects of morphological characteristics of different sized coarse aggregates on the uncompacted void content vary greatly. Different imaging indices show different levels of impact on the uncompacted void content. For example, the uncompacted void content increases with a decrease of sphericity for aggregates with size range of 4.75 to 9.5 mm and increases with a decrease in angularity for aggregates with a size range of 9.5 to 12.5 mm. To understand better the relationship between morphological characteristics and the uncompacted void content of coarse aggregates, further research can be conducted by collecting a larger number of coarse aggregates from a wider range of origins with different rock types and produced by different crushing techniques.

Field Performance

The field performance of the SMA mixtures was extracted from VDOT's PMS and is shown in Table 30. All field sections showed excellent performance against rutting. Asphalt mixtures with PG 70-22 binder (Mixtures 13-1070 and 13-1081) also showed low field rutting values compared to those of mixtures that used polymer-modified binders. However, higher truck traffic levels occur on interstate routes, which used asphalt mixtures with polymer-modified binder.

Table 30. Field Performance Data From VDOT's Pavement Management System

Mix ID	Route Type	Route No.	VDOT District	County	Direction	MP From	MP to	Before Paving			After Paving		
								IRI (in/mi)	Rut Depth (in)	CCI (Year of Data Collection)	IRI (in/mi)	Rut Depth (in)	CCI (Year of Data Collection)
13-1070	US	15	Culpeper	Fauquier	SB	6.9	11.49	---	---	---	63 67 68	0.08 0.10 0.12	98 (2014) 97 (2015) 90 (2016)
13-1081	US	340	Staunton	Augusta	NB	17.94	19.72	---	---	---	103 108	0.08 0.08	94 (2015) 98 (2016)
	US	340	Staunton	Augusta	SB	17.94	19.72	---	---	---	100 108 106	0.08 0.07 0.09	100 (2014) 98 (2015) 98 (2016)
14-1047	IS	66	Culpeper	Fauquier	WB	19.44	20.64	95	0.11	56 (2014)	51 55 56	0.09 0.11 0.11	99 (2015) 95 (2016) 98 (2017)
15-1012	IS	495	NOVA	Fairfax	NB	13.29	15	88 160	0.19 0.18	74 (2014) 85 (2015)	62 69	0.12 0.15	98 (2016) 93 (2017)
15-1068	IS	95	NOVA	Prince William	SB	10.98	13.12	121	0.14	54 (2015)	66 71	0.11 0.11	97 (2016) 96 (2017)
15-1084	SR	123	NOVA	Fairfax	NB	0.061	2.136	95	0.20	78(2015)	81	0.08	98 (2016)

MP = milepost; IRI = International Roughness Index; CCI = Critical Condition Index; IS = interstate.

SUMMARY OF FINDINGS

- All SMA-9.5 mixtures examined in this study met the criterion of $VCA_{MIX} < VCA_{DRC}$ when a breakpoint sieve of 2.38 mm was used for calculation.

- Most of the SMA-9.5 mixtures also met VDOT's specification for the SMA-12.5 gradation requirement, which shows that using certain gradations, a producer can meet VDOT requirements for both SMA-9.5 and SMA-12.5 mixtures. Hence, VCA_{MIX} was calculated based on a 4.75 mm breakpoint sieve (breakpoint sieve for SMA-12.5 mixture). Three mixtures did not meet the criterion of $VCA_{MIX} < VCA_{DRC}$, indicating loss of stone-on-stone contact.

- The fineness modulus for the gradation (per ASTM C125) (ASTM, 2017) was determined for all mixtures and ranged from 5.08 (Mixture 13-1081) to 5.38 (Mixture 14-1021). Apeagyei et al. (2011) indicated that mixtures performed poorly in rutting when the fineness modulus was less than 5.0.

- Volumetric results showed that as the percent passing the 4.75 mm sieve increases, the VMA of the mix decreases and VCA_{MIX} increases.

- The shape factor results from the improved FTI system, including sphericity and flatness ratio, were in good agreement with manual measurements using a vernier caliper.

- Aggregates used in the mixtures included in this study were produced in quarries equipped with an array of crushing equipment including jaw, impact, cone, and gyratory crushers from a variety of rock types. The aggregates met the F&E requirement.

- Overall, there was no major difference in the dynamic modulus values between different mixtures.

- The flow number results under the unconfined condition varied greatly, indicating the different rutting resistance potentials of these SMA mixtures; flow numbers under the confined condition for all types of SMA mixtures were the same. In both the confined and unconfined flow number tests, polymer-modified binders showed a lower slope compared to PG 70-22 binders, indicating better rutting resistance.

- All mixtures showed lower rut values in the APA test than the criterion of 4.0 mm for Virginia's SMA.

- Based on beam fatigue testing, SMA mixtures with polymer-modified binder showed excellent fatigue performance.

- All mixtures showed a maximum number of cycles of 1,200 in the Texas overlay test, suggesting excellent reflection crack resistance of these mixtures.

- Polymer-modified asphalt showed low Jnr values in MSCR testing, indicating better performance of these binders with regard to rutting and the accommodation of temperature variations and extreme loading conditions.

- Statistical results showed that the flow number test parameter Log(FN) was correlated with the aggregate morphological characteristics (S, FER, AF, and TF).

- The linear regression analyses between the weighted mean morphological characteristics (S, FER, AF, and TF) and FNS of all SMA mixtures were performed with or without grouping FNS data based on performance grade. FNS increased with increased weighted mean FER values and decreased with increased weighted mean S, AF, and TF values. The lower the FNS, the better the rutting performance.

- Statistical results showed that the fatigue parameter Log(NOC) was correlated with the morphological characteristics (AF and TF).

- Linear regression analyses indicated that the morphological characteristics correlated well with the uncompacted void content of coarse aggregates with size ranges of 4.75 to 9.5 mm and 9.5 to 12.5 mm. Both regression models for these two aggregate size ranges showed that the uncompacted void content increased with a decrease in angularity for coarse aggregates.

CONCLUSIONS

- *Using the appropriate breakpoint sieve for the VCA_{MIX} calculation is important for assessing the presence of good stone-on-stone contact and a denser coarse aggregate fraction in SMA mixtures*. SMA requires good stone-on-stone contact of the coarse aggregate to be able to function as a durable and rut-resistant mixture. It is important to recognize a distinction between the breakpoint sieve established by the design procedure (Virginia Test Method 99) (VDOT, 2014) and what could be called the "effective" breakpoint sieve, the smallest sieve used in the VCA_{MIX} calculation, since the calculation includes only the established breakpoint and larger sieves on which 10% or more material is retained. For example, the established breakpoint sieve for the SMA-9.5 mixtures is the 2.36 mm sieve; however, for a gradation where <10% material is retained on the 2.36 mm sieve, the 4.5 mm sieve is the "effective" breakpoint sieve and the material retained on the 2.36 mm sieve is not included in the VCA_{MIX} calculation.

- *The improved FTI system can accurately quantify morphological characteristics of aggregates*. The technology is well suited for research work and should be used in studies where aggregate morphology is of interest. However, it is not commercially developed such that it could be implemented for routine practice.

- *SMA mixtures consisting of more spherical (equant), less flaky aggregates with more angular and rougher textured surfaces have better rutting resistance.*

- *SMA mixtures consisting of more angular and rougher textured aggregates have better fatigue characteristics*.

- *Among morphological characteristics, flatness ratio, elongation ratio, and texture have the greatest effect on uncompacted void content for coarse aggregates retained on the 4.75 mm sieve, whereas elongation ratio and angularity have the greatest effect on void content for coarse aggregates retained on the 9.5 mm sieve*.

- *Based on laboratory test results, with polymer-modified binder, better rutting resistance can be obtained even if the aggregate morphological characteristics are slightly less favorable*.

RECOMMENDATIONS

1. *VDOT's Materials Division should continue with the revised gradation changes for the SMA-9.5 mixture along with other specifications for aggregate and volumetric requirements. If the SMA-9.5 mixture also meets the gradation requirement for an SMA-12.5 mixture (i.e., a coarser SMA-9.5 mixture in which less than 10% material is retained on the 2.36 mm sieve), then the $VCA_{MIX} < VCA_{DRC}$ criterion should be checked using the 4.75 mm sieve as the breakpoint sieve to ensure stone-on-stone contact. For SMA-9.5 mixtures that are not coarse enough to be interchangeable with SMA-12.5 mixtures, the 2.36 mm sieve should be used as the breakpoint sieve.*

2. *VDOT's Materials Division should encourage the use of polymer-modified binders when the SMA-9.5 mixture is specified to increase fatigue life and reduce rutting.*

3. *VDOT's Materials Division and the Virginia Transportation Research Council (VTRC) should consider initiating an investigation to study the feasibility of using an upper limit on the uncompacted void content of aggregates in addition to or as an alternative to the F&E requirement.*

IMPLEMENTATION AND BENEFITS

Implementation

With regard to Recommendation 1, no change is needed as the current VDOT specification included the new gradation change. Selection of the breakpoint sieve is effectively controlled in Virginia Test Method 99, wherein the material on the breakpoint sieve is considered as coarse aggregate only if it exceeds 10% retained.

With regard to Recommendation 2, VDOT's Materials Division implemented this recommendation by making a note in the asphalt mix selection guidelines.

With regard to Recommendation 3, a research needs statement will be developed for VTRC's Asphalt Research Advisory Committee to consider at its Fall 2019 meeting.

Benefits

SMA is very sensitive to changes in the material passing the respective "breakpoint" sieve (2.38 mm breakpoint sieve for SMA 9.5-mm mixtures). Excessive material passing the breakpoint sieve (reduction in the coarse aggregate fraction) will cause the mixture to lose stone-on-stone contact.

Implementing Recommendation 1 will ensure stone-on-stone contact and reduce rutting. Implementing Recommendation 2 will contribute to increased fatigue and rutting resistance of SMA mixtures. The benefit of implementing Recommendation 3 is the possible adoption of a simpler method to avoid aggregates having excessive aspect ratios.

ACKNOWLEDGMENTS

The authors thank John Burch, Troy Deeds, Donnie Dodds, Ben Earl, Zachary Robb, and Jennifer Samuels of VTRC for their outstanding efforts in sample collection and testing. Appreciation is also extended to Linda Evans of VTRC for her editorial assistance. The authors also appreciate the project's technical review panel for their expertise and guidance: Bill Bailey, Rob Crandol, Sungho Kim, David Lee, and David Shiells of VDOT and Trenton Clark of the Virginia Asphalt Association.

REFERENCES

Akbuluta, S., Yenera, E., Arasan, S., Hinislioglua, S., and Hattatoglu, F. Correlation Between Shape of Aggregate and Mechanical Properties of Asphalt Concrete: Digital Image Processing Approach. *Road Materials and Pavement Design,* Vol. 12, No. 2, 2011, pp. 239-262.

Al-Rousan, T.M. *Characterization of Aggregate Shape Properties Using a Computer Automated System.* Doctoral Dissertation. Texas A&M University, College Station, 2005.

Al-Rousan, T., Tutumlmuer, E., and Pan, T. Evaluation of Image Analysis Techniques for Quantifying Aggregate Shape Characteristics. *Construction and Building Materials,* Vol. 21, 2006, pp. 978-990.

Al-Rousan, T., Masad, E., Tutumluer, E., and Pan, T. Evaluation of Image Analysis Techniques for Quantifying Aggregate Shape Characteristics. *Construction and Building Materials,* Vol. 21, No. 5, 2007, pp. 978-990.

American Association of State Highway and Transportation Officials. *AASHTO T 326: Standard Method of Test for Uncompacted Void Content of Coarse Aggregate (As Influenced by Particle Shape, Surface Texture, and Grading).* Washington, DC, 2005a.

American Association of State Highway and Transportation Officials. *AASHTO T 304: Standard Method of Test for Uncompacted Void Content of Fine Aggregate*. Washington, DC, 2005b.

American Association of State Highway and Transportation Officials. *AASHTO T 321: Standard Method of Test for Determining the Fatigue Life of Compacted Hot-Mix Asphalt (HMA) Subjected to Repeated Flexural Bending*. Washington, DC, 2007.

American Association of State Highway and Transportation Officials. *AASHTO T 342: Standard Method of Test for Determining Dynamic Modulus of Hot-Mix Asphalt Concrete Mixtures.* Washington, DC, 2014.

American Association of State Highway and Transportation Officials. *Standard Specifications for Transportation Materials and Methods of Sampling and Testing.* Washington, DC, 2017.

Anderson, M. Understanding the MSCR Test and Its Use in the PG Asphalt Binder Specification. 2011. http://www.asphaltinstitute.org/wp-content/uploads/public/asphalt_academy/webinars/pdfs/MSCR_Webinar_Aug2011.pdf. Accessed May 30, 2017.

Apeagyei, A.K., McGhee, K.K., and Clark, T. Influence of Aggregate Packing and Asphalt Binder Characteristics on Performance of Stone Matrix Asphalt. *Transportation Research Board 92nd Annual Meeting Compendium of Papers.* Transportation Research Board, Washington, DC, 2011.

Arago, F.T.S., Pazos, A.R.G., Motta, L.M.G., Kim, Y.R., Nascimento, L.A.H. Effects of Morphological Characteristics of Aggregate Particles on the Mechanical Behavior of Bituminous Paving Mixtures. *Construction and Building Materials,* Vol. 122, 2016, pp. 444-453.

ASTM International. *ASTM D3398: Standard Test Method for Index of Aggregate Shape and Texture.* West Conshohocken, PA, 2006.

ASTM International. *ASTM D4791: Standard Test Method for Flat Aggregates, Elongation Aggregates, or Flat and Elongated Aggregates in Coarse Aggregate.* West Conshohocken, PA, 2010.

ASTM International. *ASTM D5821: Standard Test Method for Determining the Percentage of Fractured Aggregates in Coarse Aggregate.* West Conshohocken, PA, 2013.

ASTM International. *ASTM C125: Standard Terminology Relating to Concrete and Concrete Aggregates.* West Conshohocken, PA, 2017.

Bessa, I., Branco, V., Soares, J., and Neto, J. Aggregate Shape Properties and Their Influence on the Behavior of Hot-Mix Asphalt. *ASCE Journal of Materials in Civil Engineering,* Vol. 27, No. 7, 2014.

Brandon, D., and Kaplan, W.D. *Microstructural Characterization of Materials.* Wiley, New York, 1999.

Brown, E.R., and Haddock, J.E. Method to Ensure Stone-on-Stone Contact in Stone Matrix Asphalt Paving Mixtures, *Transportation Research Record: Journal of the Transportation Research Board,* Vol 1583, Issue 1, 1997.

Brown, E.R., and Cooley, L.A., Jr. *NCHRP Report 425: Designing Stone Matrix Asphalt Mixtures for Rut Resistant Mixtures.* Transportation Research Board, Washington, DC, 1999.

Buchanan, M.S. *Evaluation of the Effects of the Flat and Elongated Particles on the Performance of Hot Asphalt Mixtures.* NCAT Report No. 2000-03, 18–21. Auburn University, Auburn, AL, 2000.

Celaya, B., and Haddock, J.E. *Investigation of Coarse Aggregate Strength for Use in Stone Matrix Asphalt.* FHWA/IN/JTRP-2006/4. Purdue University, West Lafayette, IN, 2006.

Chen, J.S., Chang, M.K., and Lin, K.Y. Influence of Coarse Aggregate Shape on the Strength of Asphalt Concrete Mixtures. *Journal of the Eastern Asia Society for Transportation Studies,* Vol. 6, 2005, pp. 1062-1075.

Chen, J., Hsieh, W., and Liao, M. Effect of Coarse Aggregate Shape on Engineering Properties of Stone Mastic Asphalt Applied to Airport Pavements. *International Journal of Pavement Research and Technology,* Vol. 6, No. 5, 2013, pp. 595-601.

Dilek, U., and Leming, M. Relationship Between Particle Shape and Void Content of Fine Aggregate. *Cement, Concrete, and Aggregates,* Vol. 26, No. 1, 2004, pp. 1-7.

Downs, R.T., and Hall-Wallace, M. The American Mineralogist Crystal Structure Database. *American Mineralogist,* Vol. 88, No. 1, 2003, pp. 247-250.

Fernlund, J.M.R. Image Analysis Method for Determining 3-D Shape of Coarse Aggregate. *Cement and Concrete Research,* Vol. 35, No. 8, 2005, pp. 1629-1637.

Fletcher, T., Chandan, C., Masad, E., and Sivakumar, K. Aggregate Imaging System for Characterizing the Shape of Fine and Coarse Aggregates. *Transportation Research Record: Journal of the Transportation Research Board,* No. 1832, 2003, pp. 67-77.

Ford, C. Understanding Q-Q Plots. 2015. University of Virginia Library. https://data.library.virginia.edu/understanding-q-q-plots/. Accessed May 30, 2017.

Huang, B., Chen, X., Shu, X., Masad, E., and Mahmoud, E. Effects of Coarse Aggregate Angularity and Asphalt Binder on Laboratory-Measured Permanent Deformation Properties of HMA. *International Journal of Pavement Engineering*, Vol. 10, No. 1, 2009, pp. 19-28.

Huang, Y., Hugo, F., Steyn, W., Xiong, H., and Wang, L. *Comparative Evaluation of Performance of Warm Mix RAP Asphalt Under Accelerated Unidirectional Wheel Load Trafficking.* Accelerated Pavement Testing International Conference, San José, Costa Rica, 2016.

Janoo, V.C. *Quantification of Shape, Angularity, and Surface Texture of Base Course Materials.* Special Report 98-1. USA Cold Regions Research and Engineering Laboratory, Hanover, NH, 1998.

Jurado, M., Gibson, N., Celaya, M., and Nazarian, S. Evaluation of Asphalt Damage and Cracking Development With Seismic Pavement Analyzer. *Transportation Research Record: Journal of the Transportation Research Board*, No. 2204, 2012, pp. 47-54.

Kandhal, P.S., and Parker, F. *NCHRP Report 405: Aggregate Tests Related to Asphalt Concrete Performance in Pavements.* Transportation Research Board, Washington, DC, 1998.

Kim, Y.R., and Souza, L.T. *Effects of Aggregate Angularity on Mix Design Characteristics and Pavement Performance.* Technical Report MPM-10. Department of Civil Engineering, University of Nebraska-Lincoln, 2009.

Krumbein, W.C. Measurement and Geological Significance of Shape and Roundness of Sedimentary Aggregates. *Journal of Sedimentary Petrology*, Vol. 11, 1941, pp. 64-72.

Kuo, C., and Freeman, R. Imaging Indices for Quantification of Shape, Angularity, and Surface Texture of Aggregates. *Transportation Research Record: Journal of the Transportation Research Board*, No. 1721, 2000, pp. 57-65.

Lally, E.M. *Fourier Transform Interferometry for 3D Mapping of Rough and Discontinuous Surfaces.* Doctoral Dissertation. Virginia Polytechnic Institute and State University, Blacksburg, 2010.

Lally, E.M., Gong, J., and Wang A. Method of Multiple References for 3D Imaging With Fourier Transform Interferometry. *Optic Express*, Vol. 18, No. 17, 2010, pp. 17591-17596.

Little, D., Button, J., Jayawickrama, P., Solaimanian, M., and Hudson, B. Quantify Shape, Angularity and Surface Texture of Aggregates Using Image Analysis and Study Their

Effect on Performance. Report No. 0-1707-4. Texas Department of Transportation, Austin, 2003.

Liu, Y., Sun, W., Nair, H., Lane, S., and Wang, L. Quantification of Aggregate Morphological Characteristics as Related to Mechanical Properties of Asphalt Concrete With Improved FTI System. *Journal of Materials in Civil Engineering,* Vol. 28, No. 8, 2016.

Mahmoud, E., and Ortiz, E. *Implementation of AIMS in Measuring Aggregate Resistance to Polishing, Abrasion, Breakage.* FHWA-ICT-14-014. Illinois Center for Transportation, Rantoul, 2014.

Masad, E. *NCHRP-IDEA Project 77: The Development of a Computer Controlled Image Analysis System for Measuring Aggregate Shape Properties.* Transportation Research Board, Washington, DC, 2003.

Masad, E., and Button, J.W. Unified Imaging Approach for Measuring Aggregate Angularity and Texture. *Computer Aided Civil Infrastructure Engineering,* Vol. 15, No. 4, 2000, pp. 273-280.

Masad, E., Olcott, D., White, T., and Tashman, L. Correlation of Fine Aggregate Imaging Shape Indices With Asphalt Mixture Performance. *Transportation Research Record: Journal of the Transportation Research Board,* No. 1757, 2001, pp. 148-156.

McGhee, K., Clark, T.M., and Rorrer, T.M. Stone Matrix Asphalt in Virginia: A Ten-Year Performance Review. *Transportation Research Board 91st Annual Meeting Compendium of Papers.* Transportation Research Board, Washington DC, 2010.

Meininger, R.C. *NCHRP Report 281: Aggregate Test Related to Performance of Portland Cement Concrete Pavement.* Transportation Research Board, Washington, DC, 1998.

Mohammad, L., Zahang, H., Haung, B., and Tan, Z. Laboratory Performance Evaluation SMA, CMHB and Dense Graded Asphalt Mixtures. *Journal of the Association of Asphalt Paving Technologists,* Vol. 68, 1999, pp. 252-280.

Naidu, G., and Adiseshu, S. Influence of Coarse Aggregate Shape Factors on Bituminous Mixtures. *International Journal of Engineering Research and Applications,* Vol. 1, Issue 4, 2011, pp. 2013-2024.

Pan, T., Tutumluer, E., and Carpenter, S. Effect of Coarse Aggregate Morphology on the Resilient Modulus of Hot-Mix Asphalt. *Transportation Research Record: Journal of the Transportation Research Board,* No. 1929, 2005, pp. 1-9.

Pan, T., Tutumluer, E., and Carpenter, S.H. Effect of Coarse Aggregate Morphology on Permanent Deformation Behavior of Hot Mix Asphalt. *Journal of Transportation Engineering,* Vol. 132, No. 7, 2006, pp. 580-589.

Prowell, B.D., Cooley, L.A., Jr., and Schreck, R.J. Virginia's Experience With 9.5 mm NMAS SMA. *Transportation Research Record: Journal of the Transportation Research Board,* No. 1813, 2002.

Prowell, B.D., Watson, D.E., Hurley, G.C., and Brown, E.R. *Evaluation of Stone Matrix Asphalt (SMA) for Airfield Pavements.* Final Report 04-04. National Center for Asphalt Technology, Auburn, AL, 2009.

Rao, C., and Tutumluer, E. Determination of Volume of Aggregates: New Image Analysis Approach. *Transportation Research Record: Journal of the Transportation Research Board,* No. 1721, 2000, pp. 73-80.

Rao, C., Tutumluer, E., and Stefanski, J.A. Flat and Elongated Ratios and Gradation of Coarse Aggregates Using a New Image Analyzer. *ASTM Journal Testing and Evaluation,* Vol. 29, No. 5, 2001, pp. 79-89.

Rao, C., Tutumluer, E., and Kim, I.T. Quantification of Coarse Aggregate Angularity Based on Image Analysis. *Transportation Research Record: Journal of the Transportation Research Board,* No. 1787, 2002, pp. 117-124.

Roy, N., Veeraragavan, A., and Krishnan, J. Interpretation of Flow Number Test Data for Asphalt Mixtures. *Proceedings of the Institution of Civil Engineers-Transport,* Vol. 168, No. 3, 2015, pp. 191-199.

Saeed, A., Hall, J.W., and Barker, W.R. *NCHRP Report 453: Performance-Related Tests of Aggregates for Use In Unbound Pavement Layers.* Transportation Research Board, Washington, DC, 2001.

Shu, X., Huang, B, and Vukosavljevic, D. Laboratory Evaluation of Fatigue Characteristics of Recycled Asphalt Mixture. *Construction and Building Materials,* Vol. 22, Vol. 7, 2008, pp. 1323-1330.

Sime, L.C., and Ferguson, R.I. Information on Grain Sizes in Gravel-Bed Rivers by Automated Image Analysis. *Journal of Sedimentary Research,* Vol. 73, No. 4, 2003, pp. 630-636.

Smith, M.R., and Collis, L. *Aggregates: Sand, Gravel and Crushed Rock Aggregates for Construction Purposes,* Second Edition. Geological Society, London, 1993.

Souza, L.T. *Investigation of Aggregate Angularity Effects on Asphalt Concrete Mixture Performance Using Experimental and Virtual Asphalt Samples.* Masters Thesis. University of Nebraska, Lincoln, 2009.

Stiady, J., Hand, A., and White, T. *ASTM STP 1412: Quantifying Contribution of Aggregate Characteristics to HMA Performance Using PURWheel Laboratory Tracking Device.* ASTM International, West Conshohocken, PA, 2001.

Sun, W., Wang, L., and Tutumluer, E. Image Analysis Technique for Aggregate Morphology Analysis With Two-Dimensional Fourier Transform Method. *Transportation Research Record: Journal of the Transportation Research Board,* No. 2267, 2012, pp. 3-13.

Tafesse S., Robison Fernlund, J.M., Sun, W., and Bergholm, F. Evaluation of Image Analysis Methods Used for Quantification of Aggregate Angularity. *Sedimentology,* Vol. 60, No. 4, 2013, pp. 1100-1110.

Texas Department of Transportation. *Test Procedure for Overlay Test: Tex-248-F.* 2009. http://ftp.dot.state.tx.us/pub/txdot-info/cst/TMS/200-F_series/archives/248-0109.pdf. Accessed January 2, 2017.

Tutumluer, E., Pan, T., and Carpenter, S.H. *Investigation of Aggregate Shape Effects on Hot Mix Performance Using an Image Analysis Approach.* UILU-ENG-2005-2003. University of Illinois at Urbana-Champaign, 2005.

Unal, H., and Mimaroglu, A. Evaluation of Morphologic Characteristics and Mechanical Performance of Rockforce Mineral Fiber- and Glass Fiber-Reinforced Polyamide-6 Composites. *Science and Engineering of Composite Materials,* Vol. 21, No. 3, 2014, pp. 323-328.

Virginia Department of Transportation. *Virginia Test Method 121: Sample Preparation and Calculations for Flat and Elongated Testing by ASTM D4791 – (Asphalt Lab).* Richmond, 2007.

Virginia Department of Transportation. *Virginia Test Method 110: Determining Rutting Susceptibility Using the Asphalt Pavement Analyzer.* Richmond, 2009.

Virginia Department of Transportation. *Virginia Test Methods.* 2014. http://www.virginiadot.org/business/resources/Materials/bu-mat-VTMs.pdf. Accessed May 19, 2015.

Virginia Department of Transportation. *Road and Bridge Specifications, 2016.* http://www.virginiadot.org/business/resources/const/VDOT_2016_RB_Specs.pdf. Accessed May 19, 2017.

Walubita, L.F., Hugo, F., and Epps, A.L. *Performance of Rehabilitated Lightweight Aggregate Asphalt Concrete Pavements Under Wet and Heated Model Mobile Load Simulator Trafficking: A Comparative Study With the Txmls.* FHWA/TX-00/0-1814-3. Center for Transportation Research, Bureau of Engineering Research, University of Texas at Austin, 2000.

Wang, R.Y. Two-dimensional Fourier Transform. 2007. http://fourier.eng.hmc.edu/e101/lectures/Image_Processing/node6.html. Accessed May 30, 2017.

Wang, H., Bu, Y., Wang, Y., Yang, X., and You, Z. The Effect of Morphological Characteristic of Coarse Aggregates Measured With Fractal Dimension on Asphalt Mixture's High-Temperature Performance. *Advances in Materials Science and Engineering,* Vol. 2016, 2016, pp. 1-9.

Wang, L., Wang, X., Mohammad, L., and Abadie C. Unified Method to Quantify Aggregates Shape Angularity and Texture Using Fourier Analysis. *Journal of Materials in Civil Engineering*, Vol. 17, No. 5, 2005, pp. 498-504.

Wang, L., Sun, W., Lally, E.M., Wang, A., Druta, C., and Tutumluer, E. *NCHRP Report 724: Application of LADAR in the Analysis of Aggregate Characteristics.* Transportation Research Board, Washington, DC, 2012.

Watson, D.E., and Julian, E. *Effect of Flat and Elongated Aggregate on Stone Matrix Asphalt Performance.* NCAT Report 17-03. Auburn University, Auburn, AL, 2017.